Die approbierte Originalversion dieser Dissertation ist an der Hauptbibliothek der Technischen Universität Wien aufgestellt (http://www.ub.tuwien.ac.at).

The approved original version of this thesis is available at the main library of the Vienna University of Technology (http://www.ub.tuwien.ac.at/englweb/).

Dissertation

Scientific Satellite Ground Station at 2 GHz in Urban Environment

ausgeführt zum Zwecke der Erlangung des akademischen Grades eines Doktors der technischen Wissenschaften unter Leitung von

Arpad L. Scholtz
E389
Institut für Nachrichtentechnik und Hochfrequenztechnik

eingereicht an der Technischen Universität Wien
Fakultät für Elektrotechnik und Informationstechnik

von

Dipl.-Ing. Werner KEIM
Matrikelnummer 9425243
Obere Hauptstraße 23, 2305 Eckartsau

Wien, im November 2004

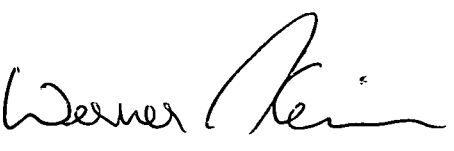

Abstract

The aim of this work was to demonstrate that an autonomous and reliably working satellite ground station in urban area can be designed, built, and operated at costs affordable for Universities. This was shown by participating in a Canadian based project called MOST (Microvariability and Oscillations of STars). MOST is a microsatellite space telescope mission to analyze the inner structure of stars by asteroseismological methods, to find Exoplanets, and to set a lower limit for the age of the Universe. The microsatellite carries a Rumak-Maksutov telescope with an aperture of 15 cm. The size of the satellite is 65 cm x 65 cm x 30 cm and the mass is about 65 kg. The Austrian part of this project was funded by ASA (Austrian Space Agency).

For ease of maintenance the ground station is located at the Institute for Astronomy of the University of Vienna. Therefore interference from sources in the urban environment had to be considered. In course of this work it was shown that interference from intermodulation products originating from mobile radio are present but do not hinder or influence the communication with the satellite. Also it was shown that there is man made noise interference at low elevation angles. Man made noise corrupts communication with the satellite at very low elevation angles only. The ground station built operates in an unmanned autonomous mode as default. However, remote access via Internet has been provided for operating convenience.

Since September 2003 the ground station is working. Up to now there were about 3000 passes of the satellite over Vienna. From all satellite passes with an elevation angle above 4 ° successful communication was established with a reliability of 98 %. Since January 2004 the station is working in unmanned autonomous mode.

Contents

Introduction 1

1 The Project MOST 3
- 1.1 MOST Satellite . . . 4
  - 1.1.1 The Telescope . . . 6
- 1.2 MOST Orbit . . . 8
- 1.3 MOST Satellite Design . . . 9

2 MOST Vienna Ground Station 12
- 2.1 Requirements due to the Orbit of MOST . . . 12
  - 2.1.1 MOST Period Calculation . . . 12
  - 2.1.2 Satellite Range Calculation . . . 15
  - 2.1.3 Maximum Contact Time . . . 15
  - 2.1.4 Doppler Shift . . . 17
- 2.2 Ground Station Concept . . . 19
  - 2.2.1 RF - Communication System . . . 19
  - 2.2.2 Safety System . . . 20
  - 2.2.3 Theoretical Radio Horizon . . . 21
- 2.3 Link Budget . . . 22
  - 2.3.1 Satellite Parameters . . . 23
  - 2.3.2 Ground Station Component Parameters . . . 23
  - 2.3.3 Propagation Loss . . . 27
  - 2.3.4 System Noise Temperature . . . 36
  - 2.3.5 Link Budget Calculation . . . 37
- 2.4 Ground Station Subsystem and Integration . . . 43
  - 2.4.1 Isolation . . . 45
  - 2.4.2 Antenna Stacking Distance . . . 46
  - 2.4.3 Integration . . . 47

3 System Performance Verification 51
- 3.1 Figure of Merit G/T_S . . . 51
- 3.2 Intermodulation . . . 57
- 3.3 Desensibilization . . . 63
- 3.4 RSSI/Uplink Performance . . . 64
- 3.5 Downlink Signal . . . 66

3.6 Antenna Characteristic 67
3.7 Man Made Noise 69
3.8 Radio Horizon 73
3.9 Ground Station Performance 74
3.10 Reliability 77

4 Ground Station Operation **81**
4.1 Principle of Operation Strategy 81
4.2 Operation 81

Conclusion **90**

A Mobile Radio Frequencies **91**

B NASA Two-Line Element Set **95**

Bibliography **98**

Abbreviations

Constants and Variables

a	length of semimajor axis
A	total absorption due to rain and gaseous attenuation
A_e	effective antenna area
β	angle between satellite at horizon and ground station
B	bandwidth
c	speed of light
$C(D)$	effective cross attenuation of a drop
d	distance ground station to satellite
D	Diameter of parabolic antenna
d_{max}	maximum distance ground station to satellite
d_{opt}	distance between Yagi antennas
e	eccentricity
E_b	energy per bit
f	frequency
F	noise figure
F_C	centrifugal force
f_Δ	Doppler shift
$f_{\Delta D}$	Doppler shift downlink
$f_{\Delta U}$	Doppler shift uplink
f_d	downlink frequency
F_G	force of universal gravity
f_r	receive frequency
F_{sun}	solar flux density
f_t	transmit frequency
f_u	uplink frequency
γ	specific rain attenuation

G	gravitational constant
G_A	antenna gain
G_{Ar}	antenna gain receive antenna
G_{ASD}	antenna gain of downlink satellite antenna
G/T_S	figure of merit
h_R	rain height above mean sea level
h_S	station height above mean sea level
i	inclination
k	Boltzmann constant
λ	wavelength
L_B	beamsize correction factor
L_{FSL}	free space loss
L_{FSLD}	free space loss at downlink
L_{FSLU}	free space loss at uplink
l_{PL}	maximum path length of satellite over ground station
L_R	rain attenuation
M	mass of Earth
M_D	downlink margin
M_U	uplink margin
$N(D)$	number of drops of diameter D per meter
N_0	spectral noise density
Ω	rectascension of the ascending node
Φ	latitude
P_{cold}	noise power of cold temperature source
$P_{coldsky}$	noise power of cold sky
P_e	perigee
P_{hot}	noise power of hot temperature source
P_{sun}	noise power of Sun
ppm	part per million
R	rainfall rate
r_E	mean radius of Earth
r_r	length of communication path through rain
r_S	distance mid point Earth to satellite
s	rain path reduction factor

θ	elevation angle
θ_{sun}	diameter of sun in degree seen from Earth
θ_A	3 dB beam width of receive antenna
T	power flux density
t_0	initial epoch
T_A	antenna noise temperature
T_{comp}	composite noise temperature
T_{cold}	temperature of cold noise source
T_{DUT}	temperature of device under test
T_{hot}	temperature of hot noise source
t_{max}	maximum visibility duration of satellite above ground station
t_P	period
T_S	system noise temperature
v_k	satellite velocity
v_S	satellite speed in ground station direction
Y	Y-factor

Text

ASA	Austrian Space Agency
BPSK	Binary Phase Shift Keying
CCD	Charged Coupled Device
DECT	Digital Enhanced Cordless Telephone system
DUT	Device Under Test
EIRP	Effective Isotropic Radiated Power
ESA	European Space Agency
F	Focal length
FDD	Frequency Division Duplex
FEC	Forward Error Correction
FM	Frequency Modulation
GFSK	Gaussian Frequency Shift Keying
GSM	Global System for Mobile communication
ITU	International Telecommunication Union
LEO	Low Earth Orbit
MOST	Microvariability and Oscillations of STars
NASA	North American Space Agency
NORAD	North American Aerospace Defense Command
PC	Personal Computer
ppm	parts per million
RBW	Resolution Bandwidth
RF	Radio Frequency
SAA	South Atlantic Anomaly
SNR	Signal-to-Noise Ratio
SWP	Sweep Time
TNC	Terminal Node Controller
UMTS	Universal Mobile Telecommunication System

UPS	Uninterruptible Power Supply
USAF	United States Air Force
VBW	Video Bandwidth

Introduction

Space research with satellites usually is an expensive task performed by big organizations like ESA (European Space Agency) and NASA (National Aeronautics and Space Administration). A novel approach for Universities, which have a limited budget only, is to contribute to space research by means of small satellites and "low-cost" ground stations. The aim of this work was to participate on such a demonstration by contributing to the Canadian based project MOST (Microvariability and Oscillations of Stars).

The project "MOST" is a microsatellite space telescope mission [Grocott 03]. The Institute for Astronomy of the University of Vienna in cooperation with the Institute of Communications and Radio-Frequency Engineering of the Vienna University of Technology are the only partners of the project outside Canada. The Austrian contribution is to design, set up, and operate an autonomous ground station in the 18th district of Vienna [Keim 04].

Due to the urban location of the ground station interference with man made noise, and intermodulation by mobile radio services has to be considered. Also natural barriers in certain directions hinder communication down to the horizon.

Chapter 1 describes the MOST mission and the MOST satellite. The mission goals are listed, and a description of the satellite and its subsystems is given. Also the orbit of the MOST satellite is explained.

Starting from the information about the satellite the ground station design is described in Chapter 2. Starting with an analysis of the impact of the atmosphere on the communication link, and a description of the ground station equipment, the link budgets for uplink and downlink were calculated.

Chapter 3 presents the measurements which were done to evaluate the performance of the ground station. Measurements without the satellite include the figure of merit, intermodulation, desensibilization, man made noise, and antenna characteristic. For a description of the performance measurements with the satellite were done which include RSSI/uplink performance, downlink signal, radio horizon, ground station performance, and reliability.

Chapter 4 explains the operation of the satellite ground station. Also computer programs which facilitate communication with the satellite are shown. Examples for the data downloaded from the satellite and also a short explanation of the data analysis is given.

Chapter 1

The Project MOST

Can we understand our Sun in the context of other stars? By putting a birthdate on the oldest stars in the solar neighborhood, can we set a limit on the age of the Universe? How do strong magnetic fields affect the physics of other stars and our own Sun? What are mysterious planets around other stars really like? These and other questions will be addressed by the Project MOST (Microvariability and Oscillations of STars).

The MOST astronomy mission is Canada's first space telescope [Zee 02]. The mission of MOST is to perform high-precision photometry of Sun-like and magnetic stars from space, as well as to study microvariability in Wolf-Rayet winds and other targets. The major goals of the mission are to set a lower limit on the age of several nearby stars which allow a lower limit to be set on the age of the Universe and second the search for Exoplanets.

The reason to go to space is that photometry is scintillation noise limited for ground based observations, but only photon noise limited in space. Scintillation is a rapid variation in the light of a celestial body caused by turbulence in the Earth's atmosphere; a twinkling. The MOST mission uses a telescope with 15 cm diameter for photometric observation. This telescope in space will achieve a noise level of only 1 ppm (part per million) for solar type stars as faint as V=3 mag for a continuous observing run of 55 days. This level of photometric accuracy can be obtained from ground only if a network of 8 m-size telescopes is available continuously for at least one month. Another reason is that from space long photometric data sets without interruption (the day on Earth) are possible. The MOST satellite can observe a target star up to seven weeks without interruption.

With the MOST telescope periodic luminosity changes down to 4 ppm can be measured. To bring an example for the sensitivity of MOST: if a streetlamp is 1 km away and then the eye is moved 0.5 mm closer to it, the streetlamp is now about 1 ppm brighter to the eye. This accuracy will allow the MOST team to translate subtle surface vibrations of nearby Sun-like stars into information about

their internal structure and age, with a technique known as stellar seismology.

The main parts of the MOST project are the MOST satellite and the MOST ground stations. There are three ground stations for the MOST project, two in Canada (Toronto and Vancouver) and one in Austria (Vienna), see Figure 1.1.

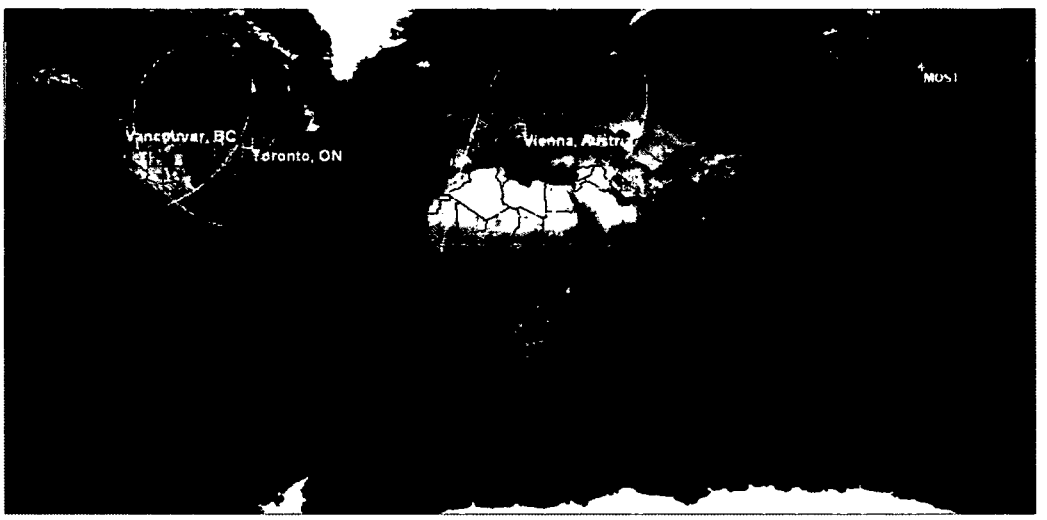

Figure 1.1: Geographical location of the three ground stations. Two stations in Canada (Toronto and Vancouver) and one ground station in Austria (Vienna) are available. The emphasized parts of the map are the visibility range of the ground station. The Austrian station nearly doubles the data transfer capacity.

The emphasized parts of the map around the ground stations in Figure 1.1 are the visibility ranges of each ground station. Communication with the satellite is possible only when the sub satellite point is within the emphasized areas. The sub satellite point is the point where the line between the satellite and the mid point of Earth crosses the surface of the Earth. Figure 1.1 shows that the visibility range of Toronto and the visibility range of Vancouver overlap. Within the overlap regions of the ground stations the best download performance is reached if only one station has contact to the satellite such avoiding cross interference between the stations. From the Vienna ground station the satellite can be seen when it is not visible from Toronto or Vancouver. This nearly doubles the observation data download capacity of the MOST project, which in turn nearly doubles the scientific output of MOST.

1.1 MOST Satellite

The satellite MOST is a microsatellite and has the size of a small traveller suitcase (65 cm x 65 cm x 30 cm). MOST has a mass of 54 kg and carries equipment

designed to probe stars and extrasolar planets by measuring tiny light variations. To obtain these measurements, MOST uses a small (15 cm aperture) high precision photometric optical telescope. Figure 1.2 shows the MOST satellite in the clean room at the launch site in Plesetsk, Russia. The satellite is in a rack which protects it during transportation. On the upper left of the satellite the telescope can be seen. The telescope door, which protects the telescope from damage in case of tumbling of the satellite, is open, and the periscope mirror can be seen. On the upper right the heater for the satellite can be seen, which ensures that the temperature of the satellite is within predefined values. The lower half shows two backup solar panels which supply the satellite with power in case of tumbling.

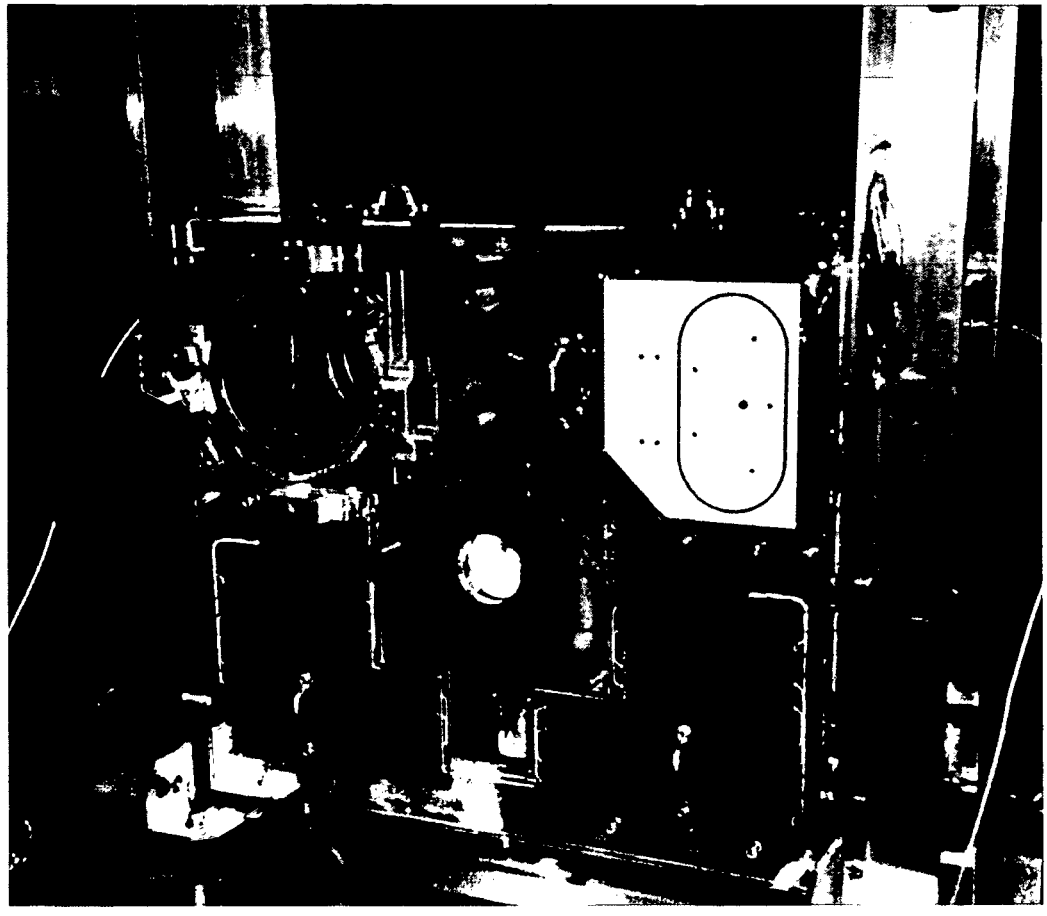

Figure 1.2: MOST satellite in a transportation rack. On the upper left the telescope, and on the upper right the heater can be seen. Also backup solar panels are shown [UBC].

Figure 1.3 shows the satellite mounted at the upper stage of the rocket. The mounting position of the satellite is upside down. On the top side only a solar panel is fixed. On the back side are the main solar panels and Sun sensors. The Sun sensors coarsely detect the position of the satellite with respect to the Sun.

If the Sun sensors detect that the satellite is strongly mispointing, the telescope door will be closed to protect the telescope from damage. On the left side a solar panel and one transmit antenna and one receive antenna can be seen. Further two magnetorquers which are fixed on the bottom side of the satellite can be seen.

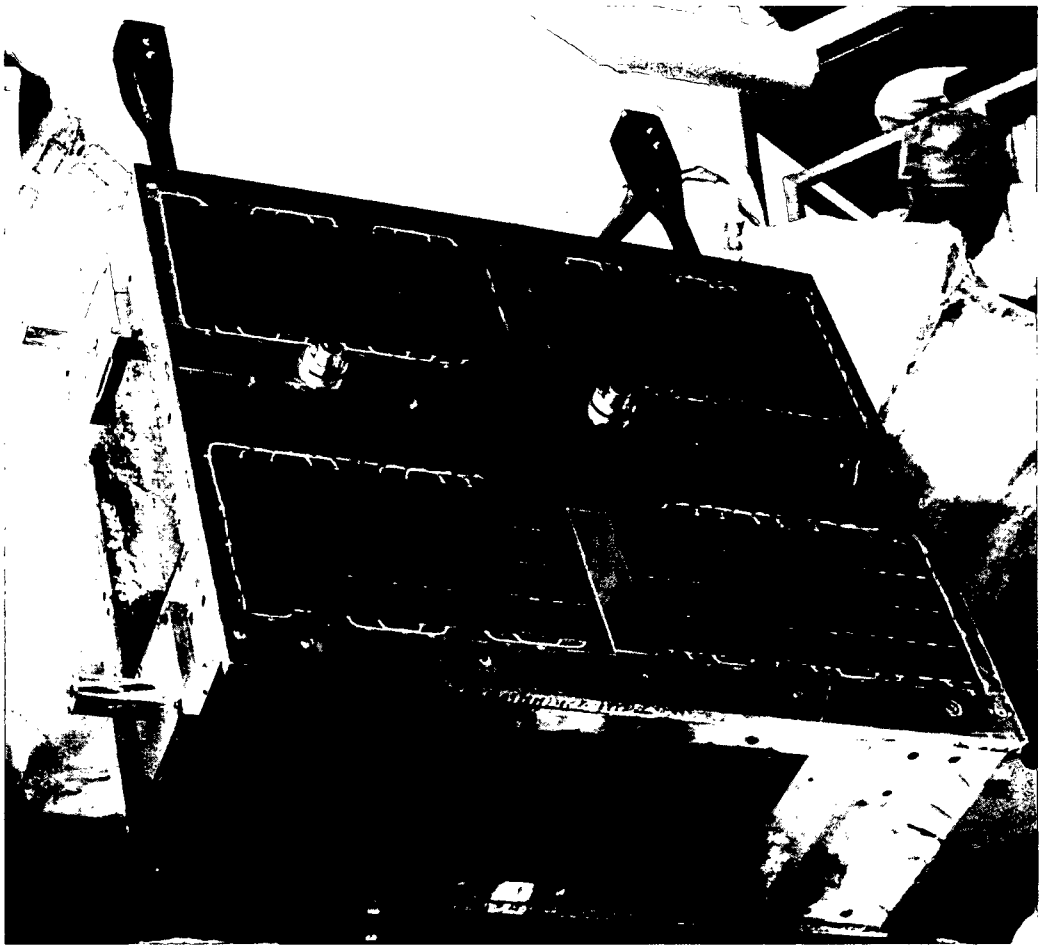

Figure 1.3: MOST satellite mounted on upper stage of the rocket. The satellite is mounted upside down. The main solar panel and Sun sensors can be seen on the back side of the satellite. On the left are the receive and transmit antennas [Eurockot 03].

1.1.1 The Telescope

The telescope is a F/6 Rumak-Maksutov with the addition of a field flattener close to the focal plane. Figure 1.4 shows an outline of the Rumak-Maksutov telescope.

The light of the observed star is passing through the aperture at the front of the satellite. The telescope with an aperture of 150 mm is fed by a 45° diagonal

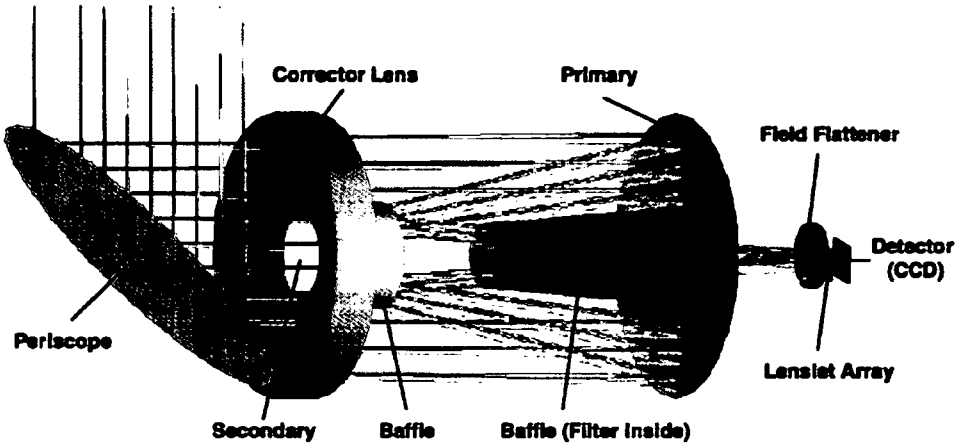

Figure 1.4: Schematic of MOST telescope [Walker 03]. The telescope is fed by a periscope mirror. A Fabry lens array spreads the star light over a larger number of pixels on the CCD to accommodate expected image wander due to the attitude control jitter.

periscope mirror. The light of the stars reflected by the periscope mirror passes through a meniscus lens called corrector, which corrects the spherical abberation. Then the light is reflected from the main mirror to the secondary mirror. From the secondary mirror the light passes through a hole in the main mirror to a Fabry-lens array and is received by a CCD (Charged Coupled Device) detector. Stray light reaching the focal plane from out of the field sources must be reduced by a factor of 10^{-5} to attenuate Earthshine and light from other bright objects. This is reached by the use of several baffles.

A scheme of the CCD detector field can be seen in Figure 1.5. There are two CCD detectors onboard the satellite, a science detector and a tracking detector. Both detectors are fed by the telescope. The stars detected by the tracking detector, marked with green color in Figure 1.5, are compared to a star map onboard on the satellite to keep the satellite in position. The so called guide stars are marked with orange color in Figure 1.5. The science detector is marked with red color. To achieve the necessary photometric precision, an array of 6 x 6 microlenses (Fabry lenses) is introduced in front of a part of the science detector (turquoise color). Fabry lenses image the entrance aperture onto the CCD detector. The imaging via the Fabry lenses minimize the impact of CCD detector pixel to pixel response variations, eliminate the problem of subpixel sensitivity, and eliminate image wandering caused by the tracking jitter. Further the photoelectron storage per exposure is greatly increased. The satellite is aligned such that the primary target will lie at the center of one of the Fabry-lenses. The remaining part of the science detector is used for observation of secondary targets. Due to limited

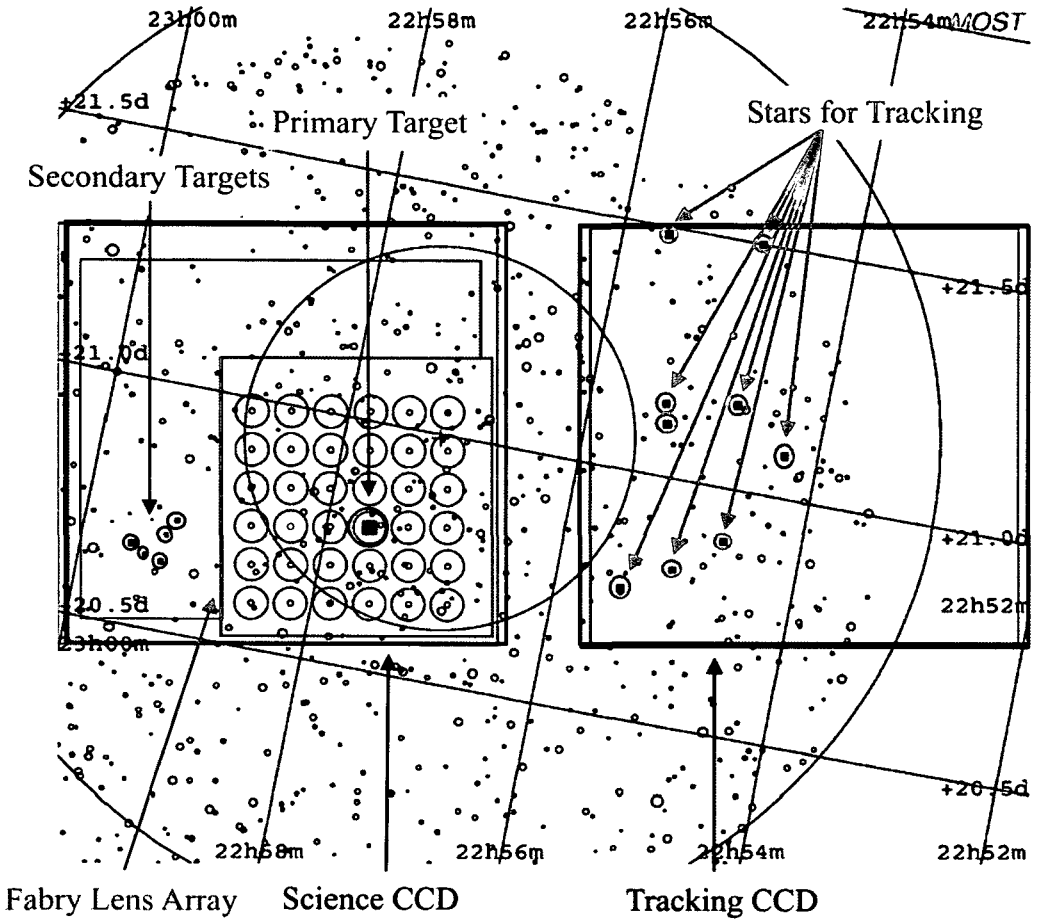

Figure 1.5: CCD detector field of the satellite [Walker 03]. On the left side the science CCD detector with the Farby lens array and on the right side the tracking CCD detector are shown.

memory capacity only a horizontal strip around the primary target of the science CCD is read. To further reduce the size of the collected data just a small square around the primary and secondary targets are stored in the memory. The secondary targets in the example shown in Figure 1.5 are marked with violet color.

1.2 MOST Orbit

The orbit of the MOST satellite was chosen to achieve more then 90 % duty cycle for continuous observation of a target for several weeks [Grocott 03]. This means that solar eclipse by the Earth's limb and passage through the South-Atlantic-Anomaly (SAA) must inhibit less than 10 % of observations. During solar eclipses the satellite must be powered by batteries. Also the solar eclipse leads to a loss of

solar sensing as well as thermal shocks to the satellite. To maintain enough power for the satellite the perpendicular axis to the rear solar panel must lie within 30° of the direction to the Sun.

The "blackout" time through the SAA increases with altitude. On the other hand, the higher the orbit, the less the limb of the Earth cuts into the observation and the shorter are the solar eclipses. For the MOST orbit an altitude of 830 km was chosen. A three-stage Russian SS-19 rocket, modified for carrying satellites, injected MOST into a near-polar orbit inclined at 98.7° to the equator. The satellite was launched from Plesetsk in northern Russia on 30 June 2003.

Figure 1.6 shows the orbit of the MOST satellite. It is a polar sun synchronous orbit over the terminator. Due to this orbit the satellite can be seen from each ground station at dawn and dusk.

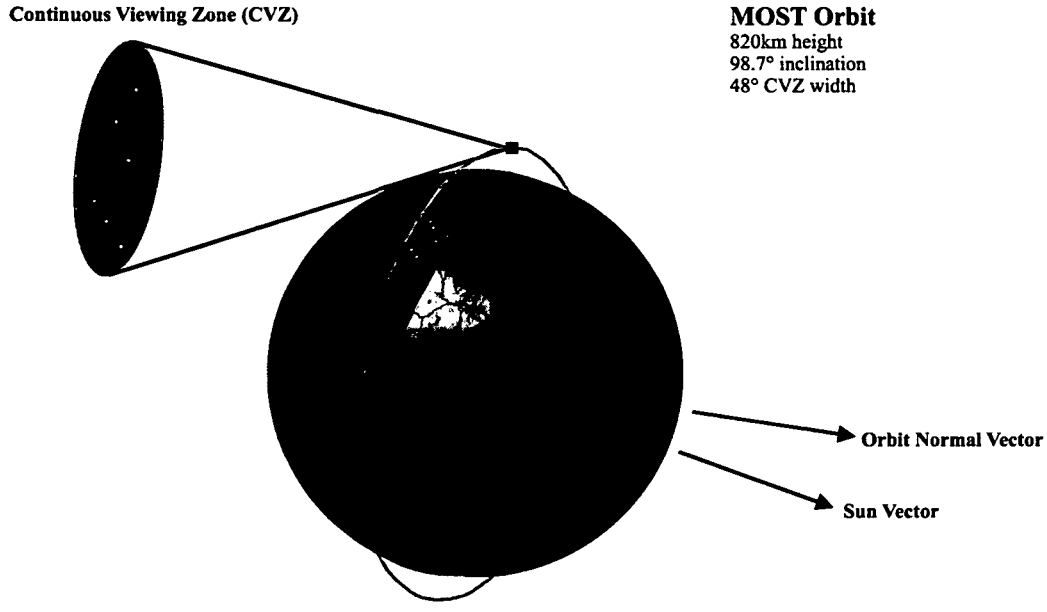

Figure 1.6: The MOST satellite has a polar sun synchronous low earth orbit in 830 km height. The front side of the satellite points to the observed star and the back side to the Sun.

1.3 MOST Satellite Design

The following section gives a short description of the satellite design [Zee 02]. The structure of the satellite consists of aluminium trays that house the satellite's electronic, battery, and communication equipment. The trays are stacked such that they form the structural backbone of the satellite. To this backbone

the science instrument, a Rumak-Maksutov telescope with an aperture of 15 cm is mounted. Six aluminium honeycomb panels, acting as substrates for solar cells and carriers for attitude sensors, enclose the tray stack and telescope assembly, forming a box. An actuated telescope door protects the telescope in case of tumbling of the satellite.

Figure 1.7 shows the system architecture of the MOST satellite.

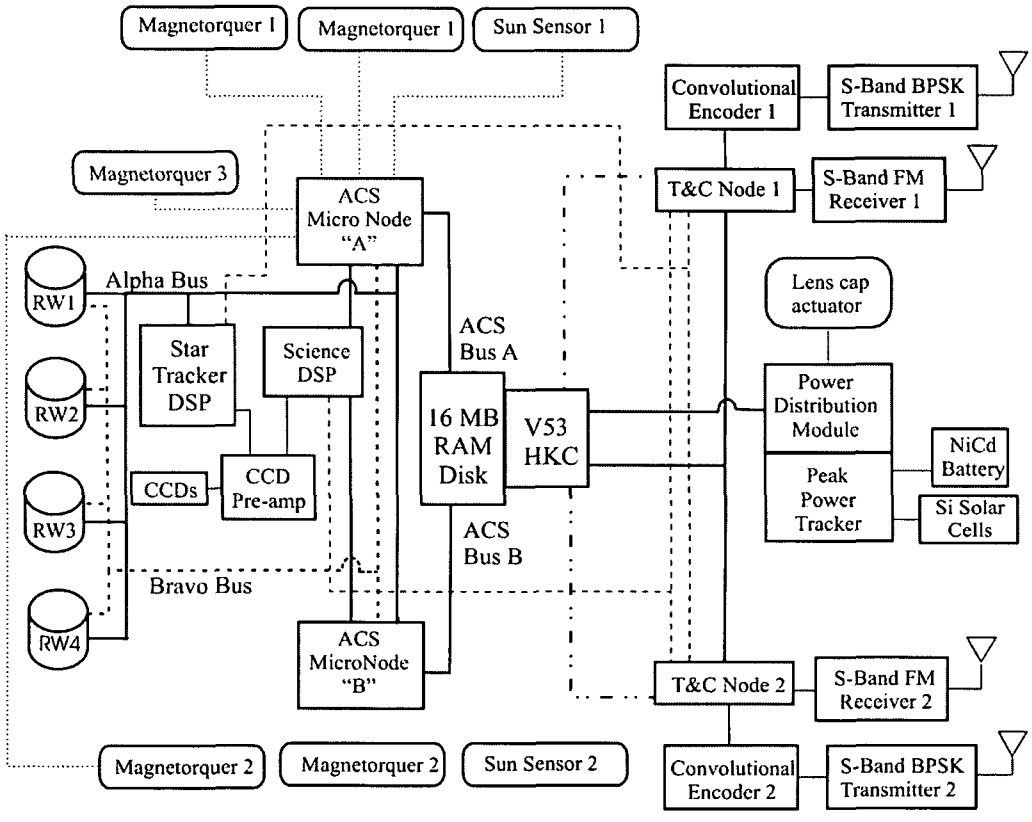

Figure 1.7: The MOST system architecture [Zee 02] is shown. There are five computers on board for housekeeping, attitude control, instrument control and data control. Silicon solar cells provide the satellite with energy. Two FM receivers and two BPSK transmitters are for communication with the ground stations.

There are five computers on board of the MOST satellite for housekeeping, attitude control, instrument control and data processing. The housekeeping computer's main tasks include receiving, executing, distributing commands and/or files uploaded from the ground, and collecting and transmitting engineering and science data to the ground. Two attitude control computers process sensor information and send commands to actuators. One of the attitude control computers is a cold spare. The two remaining computers are for instrument control and data

processing. All computers have error detection and correction hardware and software to correct bit errors induced by the South Atlantic Anomaly.

High efficiency silicon solar cells at all sides of the satellite provide power for operation. During eclipses a NiCd battery provides energy. The battery is charged via the solar cells.

The attitude control system consists of actuators, attitude control computer and sensors. The actuators consist of magnetorquers and reaction wheels, while sensors include magnetometers, sun sensors, and rate sensors. The solar arrays also contribute to coarse sun sensing.

To ensure that components within the satellite operate at suitable temperatures, a combination of passive surface treatments is used. In the event that the satellite enters a cold state, resistive heaters are used to keep the battery and trays sufficiently warm.

MOST employs two BPSK (Binary Phase Shift Keying) transmitters and two FM (Frequency Modulation) receivers to communicate with the ground stations. All radios work in the S-band frequency range (1.6 GHz ...3.6 GHz). The data rate for the uplink is 9.6 kbit/s and for the downlink 38.4 kbit/s. Sufficient downlink margin is maintained by a FEC (forward error correction) scheme. For the forward error correction half rate convolution coding is used. To maintain omnidirectional coverage, one transmitter/receiver pair is located on either side of the satellite. Each transmitter and each receiver is connected to a quadrifilar helix antenna. To ensure that the two antenna pairs do not interfere with each other, different frequencies are used for channel A and channel B. Dependent on the attitude of the satellite either channel A or channel B or both channels can be used. As transmission protocol a packet oriented protocol similar to the X.25 protocol is used.

Chapter 2

MOST Vienna Ground Station

In Chapter 1 the MOST mission and the MOST satellite was described. Outgoing from this information the concept of the Vienna ground station was developed. This chapter describes the design and set up of the Vienna ground station starting from the satellite communication system parameters and the orbit parameters.

2.1 Requirements due to the Orbit of MOST

To establish a communication channel to a satellite knowledge about the position and velocity of the satellite is necessary. The requirements on the ground station equipment and the antenna structure are dependent on the satellite orbit.

MOST has a polar sun synchronous low earth orbit (LEO) at a mean height of 830 km above the surface of the Earth with an inclination of 98.7°. Polar means that the satellite passes nearly over the poles of the Earth. Due to the Sun synchronous orbit MOST is flying always along the terminator. A schematic of the MOST satellite orbit was shown in Figure 1.6 in Section 1.2.

In the following, the orbit period and the average speed of the satellite will be calculated. The orbit period is necessary to know how fast the antenna must track the satellite and for how long it is possible to communicate with the satellite. This is important for the antenna rotator requirements. The speed of the satellite is needed to calculate the frequency range of the Doppler correction. The transmitter and the receiver must be able to compensate the Doppler shift.

2.1.1 MOST Period Calculation

To establish a communication link with a satellite the current position of the satellite must be known. Fundamental for the understanding of the satellite orbit and his regularity are the laws of Johannes Kepler:

1. The orbit of a planet about a star is an ellipse with the star at one focus.

2. A line joining a planet and its star sweeps equal areas during equal intervals of time.

3. The square of the sidereal period of an orbiting planet is directly proportional to the cube of the orbit's semimajor axis.

Isaac Newton has verified these laws with his laws of motion and universal gravity.

MOST has a polar sun-synchronous low earth orbit. This type of orbit can only be reached for a specific set of inclination angles. Due to the flattening of the Earth at the poles the orbital plane rotates. The change of the orbital plane is

$$\frac{\Delta\Omega}{Day} = -\frac{9.98^\circ}{\left(\frac{a}{r_E}\right)^{7/2}(1-e^3)^2}\cos i, \tag{2.1}$$

where a is the semimajor axis, r_E is the mean radius of Earth and i is the inclination. For a sun-synchronous orbit this change must be 360° in one year.

However, for the calculation of the satellite period we assume that the Earth is a point mass and the only force which takes effect to the satellite is the gravity of Earth [Bohrmann 66]. The position of the orbit plane will be defined against the equatorial plane through two parameters, inclination i and rectascension Ω of the intersection line of the two planes.

The orbit ellipse is characterized by the length of the semimajor axis a, and the eccentricity e. The position of the ellipse in the orbital plane is defined by the angle ω between the direction to the rising node showing into the direction in which the satellites crosses the equator from south to north, and the direction to the perigee P_e (nearest point to earth) of the ellipse, the so called argument of the perigee. Apart from these five orbit elements a definite point in time (epoch), like the time at a perigee crossing, or node crossing, or the mean anomaly for a initial epoch t_0, is needed to determine the definite motion of the satellite.

The period time t_P is not an independent orbit element, because of the correlation with the semimajor axis due to the third Keplerian law (t_P^2 proportional to a^3). The proportionality constant can be derived considering the special case of a circular orbit $r_S = a$. On a circular orbit gravitational force and centrifugal force must be equal. Newton's law of universal gravity is

$$F_G = \frac{Gm_1m_2}{r^2}, \tag{2.2}$$

where $G = 6.67 \cdot 10^{-11} Nm^2kg^{-2}$ is the universal constant of gravitation, m_1 is the

mass of the first object, m_2 is the mass of the second object and r is the distance between the objects. The centrifugal force is

$$F_C = \frac{mv^2}{r}, \tag{2.3}$$

where m is the mass of the object, v the velocity of the object and r the radius of its path. If the centrifugal force and the gravitational force are equal and with the mass of the Earth $M = 6 \cdot 10^{24}\,kg$ and the mass of the satellite we get

$$\frac{m_s {v_S}^2}{r_S} = \frac{GMm_S}{{r_S}^2}. \tag{2.4}$$

Using this equality, the satellite velocity can be computed to be

$$v_S = \sqrt{\frac{GM}{r_S}}. \tag{2.5}$$

The velocity of the satellite can also be written as

$$v_S = \frac{2\pi r_S}{t_P}, \tag{2.6}$$

where t_P is the orbit period. Finally with this equation and Equation (2.5) the orbit period of the satellite is

$$t_P = 2\pi\sqrt{\frac{{r_S}^3}{GM}}. \tag{2.7}$$

With the distance $r_S = 7202\,km$, which is the sum of the mean radius of Earth and the mean height of the satellite above the Earth surface and Equation (2.7), the orbit period for MOST is

$$t_P = 101\,min\,10\,sec. \tag{2.8}$$

From Equation (2.5) the velocity of the MOST satellite is

$$v_S = 7.45\,km/s. \tag{2.9}$$

2.1.2 Satellite Range Calculation

For calculation of the free space loss the distance between the ground station and the satellite is needed. Figure 2.1 shows a schematic of the geometric relation between the satellite and the ground station, where r_E is the radius of Earth, r_S is the distance from the center of the Earth to the satellite, d is the distance between the ground station and the satellite, and θ is the elevation angle.

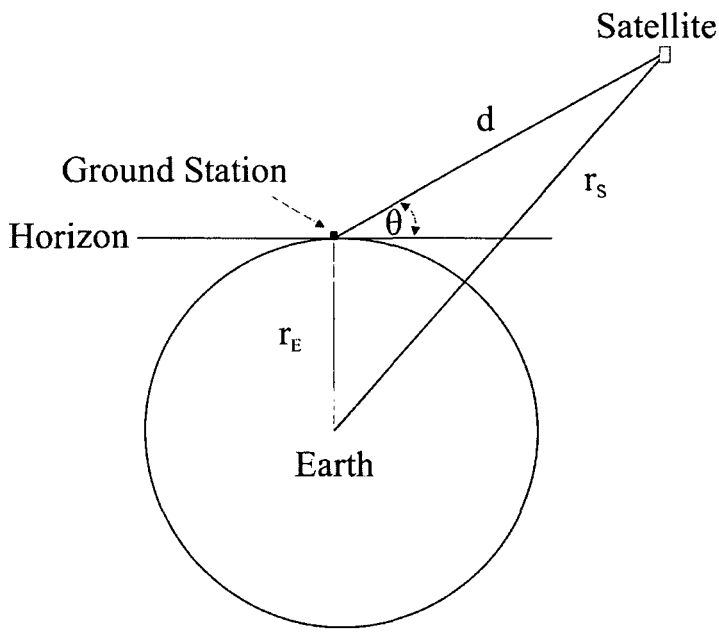

Figure 2.1: Geometric relation between ground station and satellite

With the cosine law we get

$$r_S^2 = d^2 + r_E^2 - 2dr_E \cos(\theta + \pi/2). \tag{2.10}$$

If we solve Equation 2.10 such that we get a relation for the distance between the ground station and the satellite in dependence of the elevation angle we come to

$$d = -r_E \sin(\theta) + \sqrt{r_E^2 \sin(\theta)^2 + r_S^2 - r_E^2} \tag{2.11}$$

2.1.3 Maximum Contact Time

The maximum contact time to the satellite will be if the satellite moves directly above the ground station. For the calculation of the maximum contact time the path length from rising of the satellite to its setting is needed.

Figure 2.2 shows the geometric relation for the calculation of the maximum contact time.

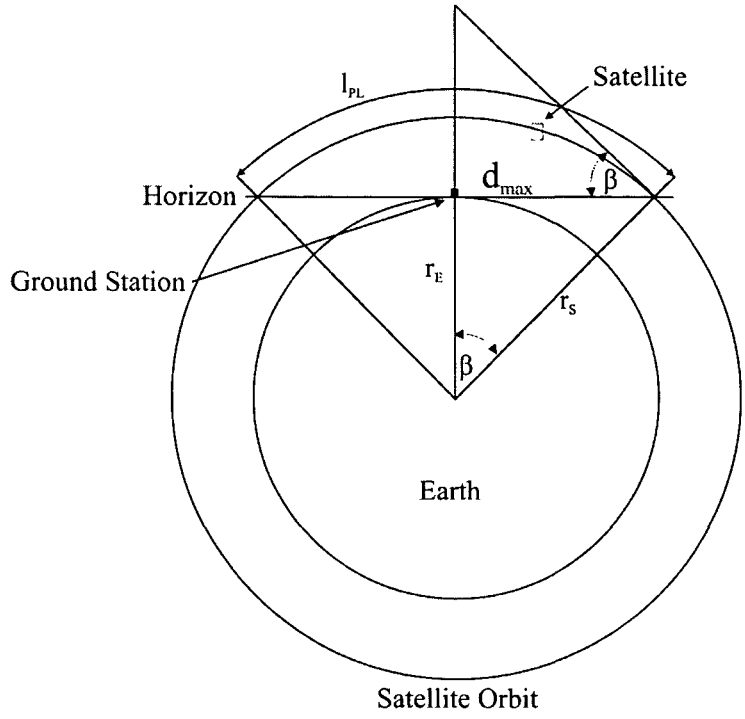

Figure 2.2: Geometric relation for the calculation of the maximum contact time and the Doppler shift.

At first the angle between the points where the satellite rises above the horizon and set below the horizon have to be calculated. With Equation 2.11, the mean radius of earth of $r_E = 6372\,km$, the height of the satellite of $h_S = 830\,km$ above the surface of the Earth, and an elevation angle of $\theta = 0\,°$ the maximum distance of the ground station to the point where the satellite rises above the horizon is

$$d_{max} = 3356.6\,km. \tag{2.12}$$

The angle between the satellite at horizon and the ground station location is

$$\beta = \arctan \frac{d_{max}}{r_E}. \tag{2.13}$$

Equation 2.12 leads to an angle of

$$\beta = 27.8\,°. \tag{2.14}$$

The path length of the satellite is

$$l_{PL} = 2\frac{\pi}{180}\beta r_S. \tag{2.15}$$

With Equation (2.14) and the distance of the satellite to the center of the Earth of $r_S = 7202\,km$ the path length is

$$l_{PL} = 6989\,km. \tag{2.16}$$

The maximum contact time is the relation of path length to the velocity of the satellite

$$t_{max} = \frac{l_{PL}}{v_S}. \tag{2.17}$$

With Equation (2.9) and Equation (2.16) the maximum contact time to the satellite is

$$t_{max} = 15\,min\,38\,sec. \tag{2.18}$$

The satellite can be seen at the Vienna ground station 3 to 4 times at dawn and 3 to 4 times at dusk. The maximum contact time per day will be around 120 minutes.

2.1.4 Doppler Shift

Due to the movement of the satellite relative to the ground station a Doppler shift at the transmit and receive frequencies has to be considered. The Doppler shift must be compensated by the transmitter and the receiver to guarantee communication with the satellite.

For the calculation of the maximum velocity component in direction to the ground station the angle between the tangent of the satellite orbit at the point where the satellite rises above the horizon has to be calculated. From Figure 2.2 it can be seen that this angle is equal the angle between of the satellite at horizon and the ground station location β (see Equation (2.13)).

The speed in the direction of the satellite is then calculated by

$$v_{Sr} = v_S \cos\beta, \tag{2.19}$$

where v_k is the velocity of the satellite. With Equation (2.9) and Equation (2.14) the maximum speed of the satellite in the direction of the ground station is

$$v_{Sr} = 6.6\,km/s. \tag{2.20}$$

The Doppler shifted receive frequency when the satellite approaches is

$$f_{rD} = f_t[1 + \frac{v_{Sr}}{c}], \tag{2.21}$$

and when the satellite leaves

$$f_{rD} = f_t[1 - \frac{v_{Sr}}{c}], \tag{2.22}$$

where f_t is the transmit frequency, v_Sr is the velocity of the satellite in the direction to the ground station and c is the velocity of light. The Doppler shift is then calculated by

$$f_\Delta = \pm f\frac{v_{Sr}}{c} \tag{2.23}$$

where f is the nominal frequency. With the uplink frequency $f_U = 2055\,MHz$, the velocity of propagation $c = 3 \cdot 10^8\,m/s$ and Equation (2.20) the maximum Doppler shift at the uplink is

$$f_{\Delta U} = \pm 45.2\,kHz. \tag{2.24}$$

With the downlink frequency of $f_D = 2232\,MHz$ the maximum Doppler shift at the downlink is

$$f_{\Delta D} = \pm 49.1\,kHz. \tag{2.25}$$

2.2 Ground Station Concept

2.2.1 RF - Communication System

Commercial ground stations e.g. Aflenz use a single antenna for uplink and downlink. The uplink and downlink signals are separated by means of a frequency selective frequency combiner. Unlike commercial ground stations the MOST ground station is optimized for best downlink performance. To avoid combiner loss separate antennas are used for uplink and downlink. The concept of the satellite ground station in Vienna is shown in Figure 2.3.

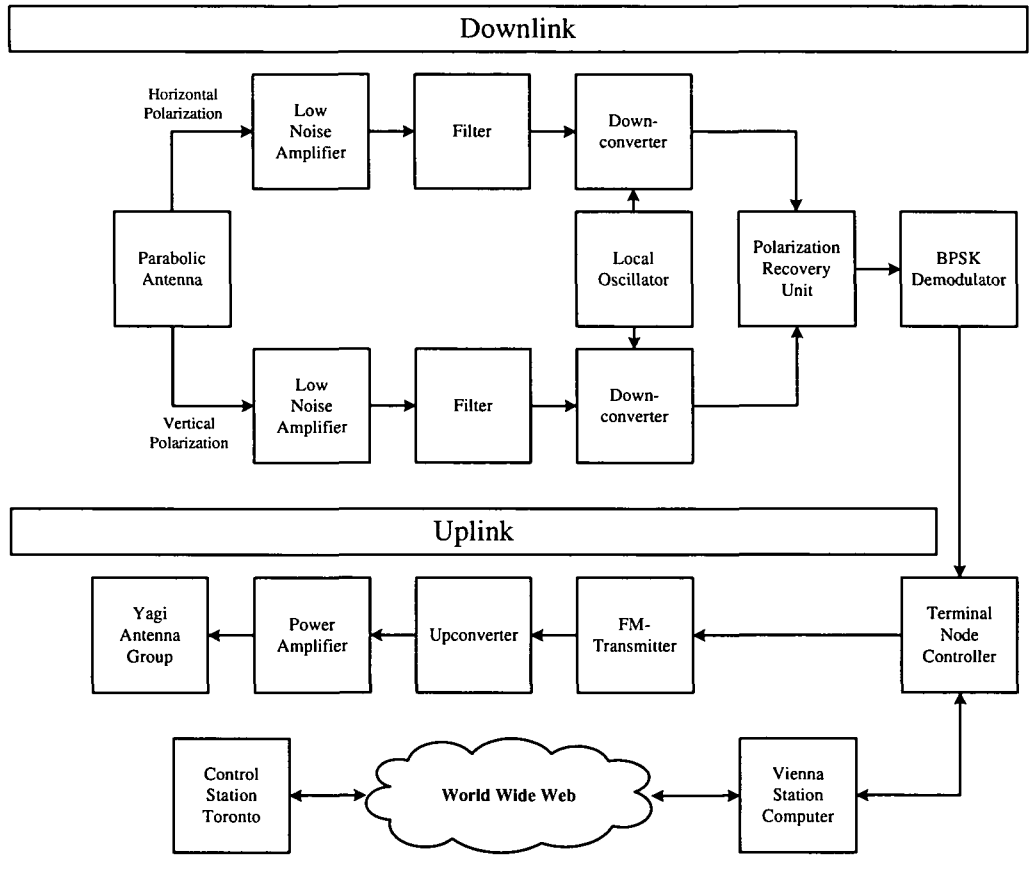

Figure 2.3: Block diagram of the ground station

At the downlink, a parabolic dish with a diameter of 3 m, a ratio of $F/D = 0.4$ (where F is the focal length and D is the diameter of the antenna) and a feed which receives two orthogonal states of linear polarization is used. Receive signals at 2232 MHz are fed into two identical preamplifiers directly attached to the antenna feed. Filters suppress the permanently present uplink spill-over to avoid blocking of the downconverters. The downconverters that follow are sharing one local oscillator to preserve relative phases and convert the signal from the receive frequency of 2232 MHz to the intermediate frequency of 140 MHz. A polarization

recovery unit combines the downconverter output signals in an optimum way. A BPSK (Binary Phase Shift Keying) demodulator incorporating FEC (Forward Error Correction) hardware completes the receiver.

A separate Yagi antenna group consisting of four Yagi antennas supports the uplink. The uplink signal is generated by means of a 435 MHz FM (Frequency Modulation) transmitter and is then converted to 2055 MHz by the upconverter. A 50 W power amplifier is placed near the antenna to avoid cable loss. The uplink signal is fed to the Yagi antenna group by a passive quarter-wavelength power divider.

Transmission protocols are taken care of by a terminal node controller connected to the Vienna station computer. This computer also acts as bridge to the Internet for data retrieval from Toronto.

2.2.2 Safety System

A safety system is necessary to allow for unattended automatic operation of the ground station. The safety system monitors the whole ground station equipment and sets the station into a safe mode in case of a failure. Figure 2.4 shows the block diagram of the safety system.

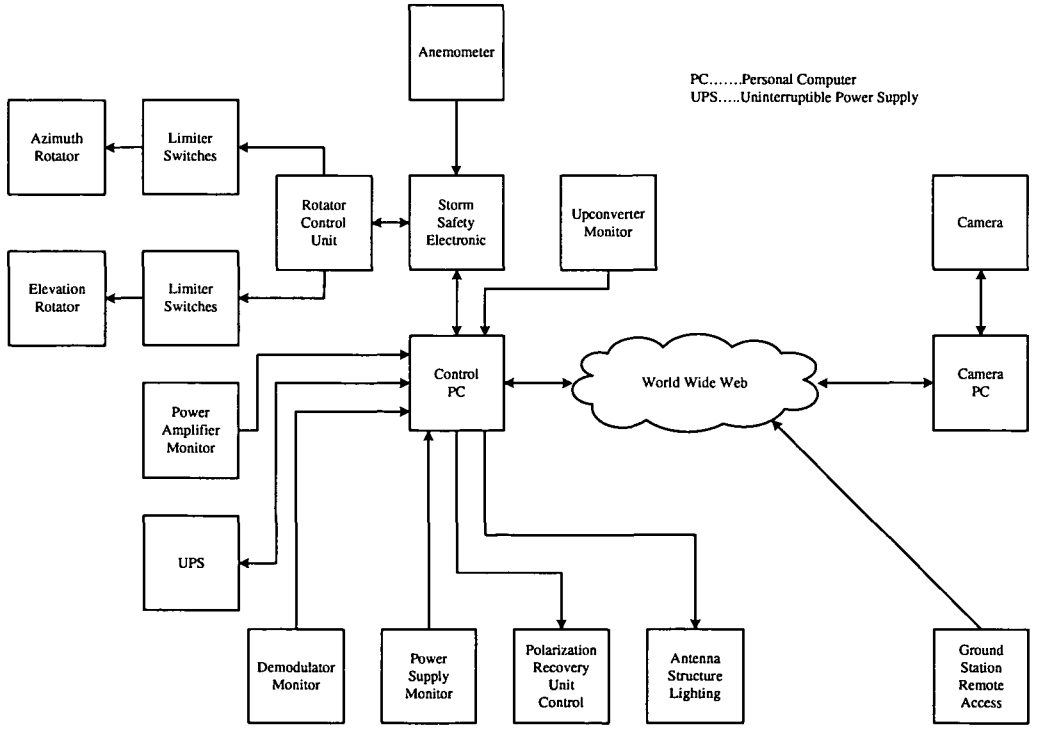

Figure 2.4: Block diagram of the ground station

The control computer is connected to the whole communication equipment and is also responsible for tracking the antenna. To ensure that the control computer is always running, an uninterruptible power supply (UPS) is needed. All other components of the station are also connected to the UPS in order to bring the station into a safe position if the main power for the station fails.

The pointing position of the antenna is determined by counting pulses. If an error occurs the real pointing position of the antenna differs from the value reported by the rotator controller, and the calibration of the rotator controller is lost. Limiter switches are needed to ensure that in case of loss of the calibration of the rotator controller unit the movement of the antenna is stopped.

The storm safety electronic protects the antenna structure from damage in case of strong winds. The storm safety electronic [Rieger 02] is connected to an anemometer, which measures the current wind speed. Also the communication between the control PC and the rotator controller unit is controlled by the storm safety electronic. If a predefined wind speed is exceeded, the storm safety electronic interrupts tracking of the satellite by interrupting the communication between the PC and the rotator controller unit, and moving the antenna into a safe parking position. To avoid that the antenna will be permanently moved between tracking and parking position, a defined hold time of the parking position and a wind speed hysteresis is defined.

To allow the administrator and the operators to see the station remotely, two cameras are installed. One camera shows the status of the antenna structure, the other camera shows the status of the communication equipment. This is important in case of a failure to check if the problem can be solved remotely.

The status of the station itself is also monitored. The monitor equipment reports the status of any individual station component to the control computer. If one of the parameters of any component is outside of the nominal range the computer can change parameters or shutdown the component.

Remote control operation of the station is possible. For remote control operation the desktop of the ground station computer can be displayed on each computer which has access to the ground station computer.

2.2.3 Theoretical Radio Horizon

The location of the ground station is at the Institute for Astronomy in the 18th district of Vienna at a height of 265 m above the sea level. Figure 2.5 shows an estimation of the theoretical radio horizon of the Vienna ground station, determined from a topographic map.

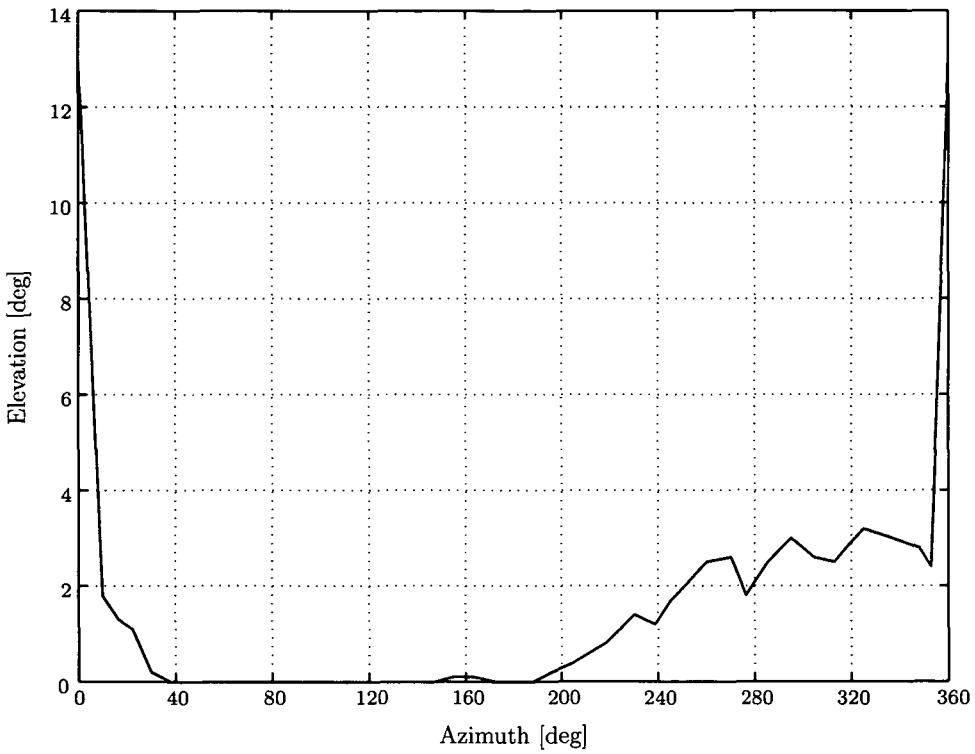

Figure 2.5: Theoretical radio horizon determined from a topographic map. Below the solid line natural barriers hinder the communication to the satellite.

The cardinal point North is at an azimuth angle of 0°. In the north the dome of the Institute for Astronomy hinders communication below 12°. Beside the dome towards east the Nussberg hinders communication below 1.5°. From the northeast to the southeast the horizon appears totaly flat to the station. From the southwest until the dome of the Institute for astronomy natural barriers hinders communication down to an elevation of 0°. Examples for the natural barriers from south to north are: Wiener Blick, Satzberg, Jubilaeumswarte, Heuberg, Hochbruckenberg, and Exelberg.

2.3 Link Budget

At the beginning of a planning process requirements are defined which the communication system has to fulfill. The link budget is a balance sheet of gains and losses, it outlines the detailed participation of transmission and reception resources, noise sources and all effects throughout the link. The link budget includes both, uplink and downlink. The uplink includes the Earth station transmitter and the satellite receiver. The downlink includes the satellite transmitter and the Earth station receiver. The primary goal for a link budget is to determine the actual system performance and this has to be compared with the requirements.

To reach this goal all parameters of the communication link have to be calculated.

2.3.1 Satellite Parameters

While the parameters of the ground stations can be chosen independently the parameters of the satellite are given by the Canadian satellite team. Table 2.1 shows the downlink parameters and Table 2.2 shows the uplink parameters of the MOST satellite provided by the Canadian MOST team.

Transmit power	0.5 W	27 dBm
Loss		2 dB
Antenna gain		0 dBi

Table 2.1: MOST satellite downlink parameters

Due to limited available power generated by the solar panels the transmit power of the satellite is 0.5 W. Between transmitter and antennas is an unavoidable loss of 2 dB. The satellite has on two of the small sides a pair of antennas, one for transmit and one for receive. Due to the small size of the satellite a omnidirectional antenna characteristic is nearly reached with this configuration. Therefore the antenna gain of the satellite is 0 dBi.

System noise temperature	2400 K	33.8 dBK
Receiver bandwidth	110 kHz	50.4 dBHz
min. required SNR		5.0 dB

Table 2.2: MOST satellite uplink parameters

The antennas of the satellite communication system see the "hot" Earth. Therefore the system noise temperature of the satellite receiving system is 2400 K. The receiving bandwidth is 110 kHz. Due to the spreading of the signal a signal to noise ratio of 5.0 dB is needed for a bit error ration of 10^{-5}.

2.3.2 Ground Station Component Parameters

In this subsection the parameters of the components used for uplink and downlink are listed. The goal was to build the ground station with a given budget of around 50.000 Euro. To reach this goal semi-professional equipment adapted for our purpose was used. The design process of the ground station was iterative. The parameters of the selected semi-professional equipment were taken and inserted in the link budget calculation to check if the selected components fulfill the requirements or if an improved equipment is necessary. Following the parameters of the equipment used are presented.

Downlink Antenna

The frequency dependent values of the antenna (e.g. antenna gain) are listed for the receive frequency of about 2232 MHz.

Type:	Parabolic antenna
Diameter	3.0 m
Focal length	120.0 cm
F/D ratio[1]	0.40
Gain	34.9 dBi
Beam Width	3.2 °

The larger the diameter of the receiving antenna the higher the antenna gain. The size of the receiving antenna is limited by the static of the antenna structure and the torque to the antenna rotator due to winds. In the case of the Vienna ground station the antenna rotator was the limiting factor of the antenna size. The used antenna size is the maximum for available low-cost antenna rotators.

With the diameter of the parabolic antenna and the receive frequency of 2232 MHz the 3 dB beamwidth was calculated with the empirical relation [Rothammel 03]

$$\Delta\phi = \Delta\vartheta = \frac{21.3}{Df} \tag{2.26}$$

With Equation (2.27) the full width half maximum beamwidth of the antenna is

$$\Delta\phi = \Delta\vartheta = 3.2\,^{\circ}. \tag{2.27}$$

Feed

Polarization	Dual Linear
Frequency Range	1.7 ... 2.3 GHz
F/D ratio	0.35 ... 0.42

It was expected that arbitrary states of polarization are to be received. Each polarization state can be recovered by a combination of two orthogonal linear polarization states. Therefore a feed which can receive two orthogonal linear polarization states is used.

[1] F/D ratio is the ratio of focal length to antenna diameter.

Low Noise Amplifier

Noise Figure	0.65 dB
Gain	41.0 dB
Operating Voltage	9 ... 20 V DC
Current typ.	30 mA

The low noise amplifier used has a noise figure of 0.65 dB. Low noise amplifiers with a smaller noise figure are available but more expensive.

Downconverter

Input Frequency	2232 MHz
Output Frequency	140 MHz
Local Oscillator Frequency	2372 MHz
Noise Figure	0.8 dB
Gain	32.0 dB
Operating Voltage	13.8 V DC
Current typ.	120 mA

The downconverter converts the receive signal from receive frequency to the intermediate frequency of 140 MHz. For each received linear state of polarization a downconverter is used. The downconverters share a common local oscillator to preserve relative phases.

Downlink Cable

Type	H2000
Loss at 2232 MHz	0.213 dB/m

Demodulator

Modulation Format	BPSK
Required SNR for BER = 10^{-5}	4.9 dB
FEC	1/2 Convolutional Coding
Data Rate	38.4 kBit/s

A BPSK demodulator with integrated convolutional decoder is used at the downlink. The demodulator can be remote controlled via a PC.

Modulator

Modulation Format	GFSK
Modulation Index	3
Data Rate	9.6 kbit/s

A FM modulator is used at the uplink. In combination with the TNC a GFSK modulated output signal is generated. The parameter of the modulator can be changed remotely via a PC.

Upconverter

Input Frequency	435 MHz
Output Frequency	2055 MHz
Local Oscillator Frequency	2490 MHz
Noise Figure	0.8 dB
Gain	32.0 dB
Operating Voltage	13.8 V DC
Current typ.	120 mA

The upconverter converts the signal generated from the modulator at 435 MHz to the transmit frequency of 2055 MHz.

Power Amplifier

Operating Frequency	2050 ... 2060 MHz
Power Output	50 W
Spurious Signals typ.	-70 dBc
Operating Voltage	26 ... 30 V DC
Current typ.	7.9 A

Above 50 W the cost of a power amplifier will increase rapidly. Therefore it was tried to gain as much as possible in the uplink to reduce the costs of the power amplifier. This was reached by using an uplink antenna group. As amplifier a GSM power amplifier for the North American market was retuned to our transmit frequency.

Uplink Cable

Type	Ecoflex 15
Loss at 2055 MHz	0.1493 dB/m

Uplink Antenna

Type:	Yagi Antenna Group
Gain	25.0 dBi
Beam Width	6.5 °

To reduce the costs for the power amplifier an antenna group consisting of four Yagi-antennas is used. The single Yagi antenna has an antenna gain of 20 dBi.

2.3.3 Propagation Loss

The propagation loss is divided into the following parts:

- Free Space Loss
- Atmospheric Loss
- Pointing Loss.

Free Space Loss

The dominant component of propagation loss is the free space loss. Although it is called free space loss it is no attenuation of signal but a spreading of signal over space.

A transmitter with an isotropic antenna characteristic radiates the transmit power P_t uniformly into space, so that the power flux density through an imaginary sphere with the radius d around the isotropic radiator will be constant over the whole surface of a sphere. The radial outward power flux density is

$$T = \frac{P_t}{4\pi d^2} \tag{2.28}$$

where d is the distance between the transmitter and the receiver. If this power flux density is received with an aperture A_r then the receive power P_r is the product of power flux density and receive antenna aperture,

$$P_r = \frac{P_t A_r}{4\pi d^2}. \tag{2.29}$$

The aperture of an antenna is

$$A_e = \frac{\lambda^2}{4\pi} G_A, \tag{2.30}$$

where G_A is the gain of the antenna with respect to an isotropic radiator and λ is the wavelength of the signal. With Equation (2.29) and Equation (2.30) we get

$$P_r = \frac{P_t G_{Ar} \lambda^2}{(4\pi d)^2} \tag{2.31}$$

where G_{Ar} is the gain of the receive antenna. From Equation (2.31) we can calculate the free space loss to

$$L_{FSL} = \frac{(4\pi d)^2}{\lambda^2}. \tag{2.32}$$

The free space loss can also be expressed as

$$L_{FSL} = \frac{(4\pi df)^2}{c^2}, \tag{2.33}$$

where c is the speed of light and f is the frequency of the signal. It can be seen from Equation (2.33) that the free space loss increases with frequency and also with distance.

Atmospheric Loss

The atmospheric loss can be divided into three components, as listed below [Saunders 99]:

- Ionospheric effects, involving interactions between the layers of charged particles around the Earth, the Earth's magnetic field and the radio waves.
- Tropospheric effects, involving interactions between the waves and the lower layer of the Earth's atmosphere, including the effects of the gases and hydrometeors such as rain.
- Local effects, involving interactions between the waves and features of the environment in the vicinity of the earth station such as terrain, trees and buildings. These effects are most important in mobile satellite systems, where the direct path may frequently be wholly or partially obscured.

When the ground station receive antenna is pointing to the sky it receives noise from various sources. This noise is added to the internal noise of the receiver and degrades the receiver performance. These effects will be considered by calculating an effective noise temperature of the antenna and combine it with the system noise temperature of the receiver to get an overall system noise temperature.

Ionospheric Effects The ionosphere is a region of ionized plasma which surrounds the Earth at a distance ranging from 50 km to 2000 km above its surface. The key parameter relating the structure of the ionosphere to its effect on radio communications is the electron concentration. Following a short description of the ionospheric effects and their influence on the MOST communication system is presented [Saunders 99]:

Faraday Rotation The polarization of a linearly polarized wave is rotated during its passage through the ionosphere due to the combined effects of the free electrons and the Earth's magnetic field. The angle associated with its rotation depends on the frequency and the total number of electrons encountered along the path. If linearly polarized waves are used, extra path loss will result due to polarization mismatch between the antennas.

The transmit and receive antennas at the MOST satellite are circularly polarized. Due to the use of circularly polarization and the optimum combiner unit at the ground station the extra path loss through the Faraday rotation is negligible.

Ionospheric Scintillation There is a wind present in the ionosphere which causes rapid variations in the local electron density, particulary close to sunset. These density variations cause changes in refraction of an Earth-satellite wave and hence of signal levels. Portions of the ionosphere then act like lenses, cause focusing and divergence of the wave and hence lead to signal level variations.

Tropospheric Effects

Attenuation The troposphere consists of a mixture of pixels, from the molecules in atmospheric gases to raindrops and hail. The loss resulting from a radio wave passing through the troposphere is composed of two contributions, from absorption and from scattering.

Absorption is the result of conversion from radio frequency energy to thermal energy within an attenuating particle.

Scattering results from redirection of the radio waves into various directions, so that only a fraction of the energy is transmitted into the direction of the receiver.

The main scattering particles to satellite systems are hydrometeors (raindrops, fog, clouds). In this case the scattering component of attenuation is only significant when the operating frequency is above 10 GHz. The absorption component also rises with frequency, although not so rapidly as the scattering component.

Rain Attenuation Effects due to rain are the most important in determining the system reliability of a satellite system. Therefore the hydrometeor effects

are limited to rain. The attenuation of a wave due to rain increases with the number of raindrops along the path. It also increases with the size of the drops and the length of the path through the rain r_R. If the density and the shape of the raindrops is constant in a given region, then the received power P_r is found to diminish exponentially with the distance r_R

$$P_r(r) = P_r(0)e^{-\alpha r_R} \tag{2.34}$$

where α is the reciprocal of the distance required for the power to drop by a factor e^{-1}. The rain attenuation expressed in decibel gives

$$L_R = 10\log_{10}\frac{P_t}{P_r} = 4.343\alpha r_R \tag{2.35}$$

where L_R is the rain attenuation and P_t is the transmit power. It is usual to calculate the total loss through rain via the specific attenuation in decibel per meter

$$\gamma = \frac{L_R}{r_R} = 4.343\alpha \tag{2.36}$$

The value of alpha is given by the following relationship

$$\alpha = \int_{D=0}^{\infty} N(D) \cdot C(D)dD \tag{2.37}$$

where $N(D)$ is the number of drops of diameter D per meter of path length and $C(D)$ is the effective attenuation cross-section of a drop. How Equation (2.37) can be solved in principle is shown in [Saunders 99]. A more practical approach is to use an empirical model, where it is assumed that the specific attenuation γ only depends on the rain rate R. The specific attenuation is obtained from the rain rate using

$$\gamma = aR^b \tag{2.38}$$

where a and b are frequency-dependent coefficients. Table 2.3 shows values of a and b at various frequencies for horizontal and vertical polarization [ITU P.838 92].

f/GHz	a_H	a_V	b_H	b_V
1	0.0000387	0.0000352	0.912	0.880
2	0.000154	0.000138	0.963	0.923
4	0.000650	0.000591	1.121	1.075
6	0.00175	0.00155	1.308	1.265

Table 2.3: Empirical rain attenuation model coefficients for horizontal (H) and vertical (V) polarization.

For linear and circular polarization, and for all path geometries, the coefficients in Equation (2.38) can be calculated from the values in Table 2.3 using the following equations [ITU P.838 92]:

$$a = \frac{a_H + a_V + (a_H - a_V)\cos^2\theta\cos 2\tau}{2} \tag{2.39}$$

$$b = \frac{a_H b_H + a_V b_V + (a_H b_H - a_V b_V)\cos^2\theta\cos 2\tau}{2a} \tag{2.40}$$

where θ is the elevation angle and τ is the polarization tilt angle relative to the horizontal ($\tau = 45\,^\circ$ for circular polarization).

With Equation (2.36) and Equation (2.38) the rain attenuation results in

$$L_R = r_R a R^b, \tag{2.41}$$

where r_R is the rain path length. To solve Equation (2.41) the path length through rain must be calculated. Figure 2.6 shows the geometry for the rain path length calculation.
All heights in Figure 2.6 are measured above the sea level, where h_R is the effective rain height and h_S is the height of the ground station antenna. Representative values for the effective rain height vary according to the latitude Φ of the ground station [ITU P.618 97]. The latitude of Vienna is approximately 48°. For a latitude $\Phi > 23°$ at the northern hemisphere the rain height in kilometer is

$$h_R = 5 - 0.075(\Phi - 23). \tag{2.42}$$

With the value for the latitude for Vienna the rain height is

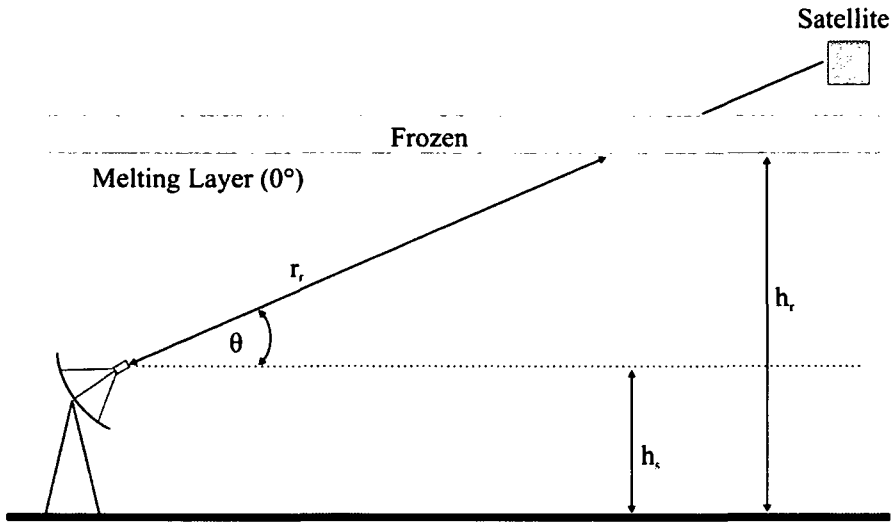

Figure 2.6: Geometric relation for the calculation of the rain path length of the communication link. h_R is the effective rain height and h_S is the height of the ground station antenna.

$$h_R = 3.125km. \tag{2.43}$$

The rain path length for elevation angles higher or equal than 5° can be calculated as

$$r_r = \frac{h_R - h_S}{\sin\theta} \tag{2.44}$$

where θ is the elevation angle. For elevation angles less than 5°, a more accurate path length estimate can be made using [Dissanayake 02]

$$r_r = \frac{2(h_R - h_S)}{\left[\sin^2\theta + \frac{2(h_R - h_S)}{R_e}\right]^{1/2} + \sin\theta}, \tag{2.45}$$

where R_e is the effective earth radius ($R_e = 8500\,\text{km}$). For paths in which the elevation angle is significantly less than 90°, it is necessary to account for the variation of the rain in horizontal direction. This will tend to reduce the rain attenuation due to the finite size of the rain cells. This effect can be treated by a reduction factor s so that the rain attenuation for low elevation angles is

$$L_R = r_r s a R^b \tag{2.46}$$

For the reduction factor s following in the case that the rain attenuation does not exceed 0.01% of the time in an average year the following relation is used [Saunders 99]

$$s_{0.01} = \frac{1}{1 + \frac{rsin\theta}{35e^{-0.015R_{0.01}}}}. \tag{2.47}$$

To show the impact of different rainfall rates to the rain attenuation Figure 2.7 shows the rain attenuation for different rainfall rates versus the elevation angle for Vienna is shown.

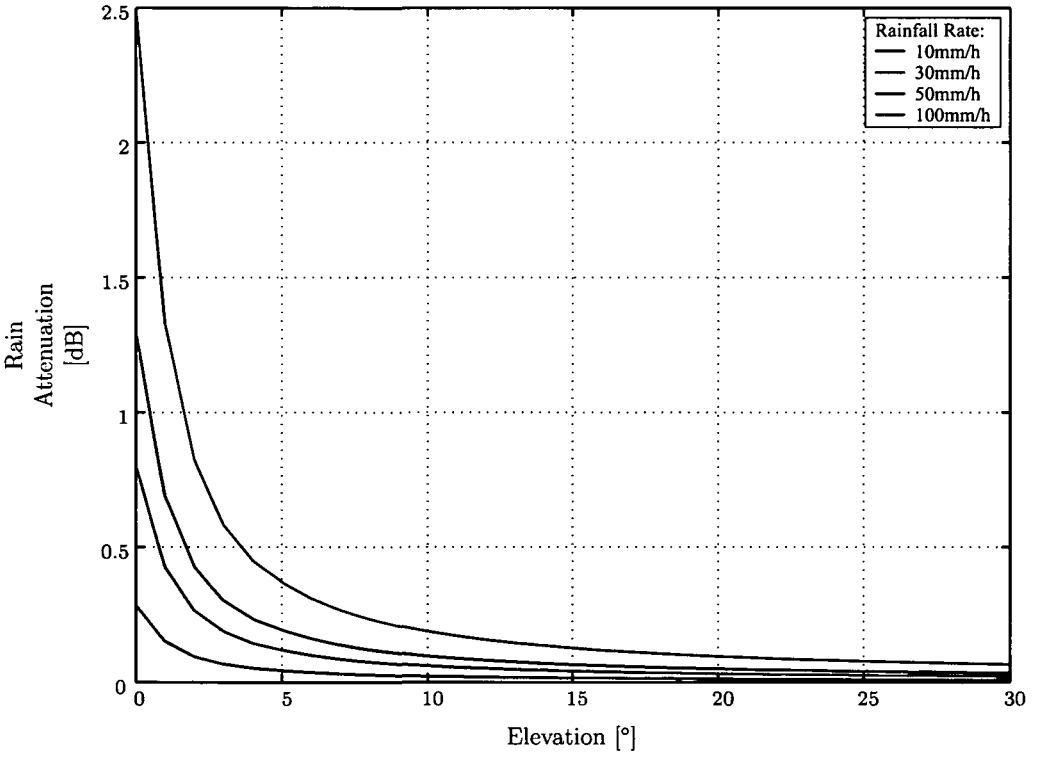

Figure 2.7: Rain attenuation at 2.232 GHz for different rainfall rates.

Gaseous Absorption Gaseous molecules found in the atmosphere may absorb energy from radio waves passing through the atmosphere and thereby causing attenuation. In normal atmospheric conditions, only oxygen and water vapor contribute significantly to absorption. Other atmospheric gases may be significant in very dry air at above 70 GHz. Figure 2.8 shows the specific attenuation of water vapor and oxygen [FCC 97].

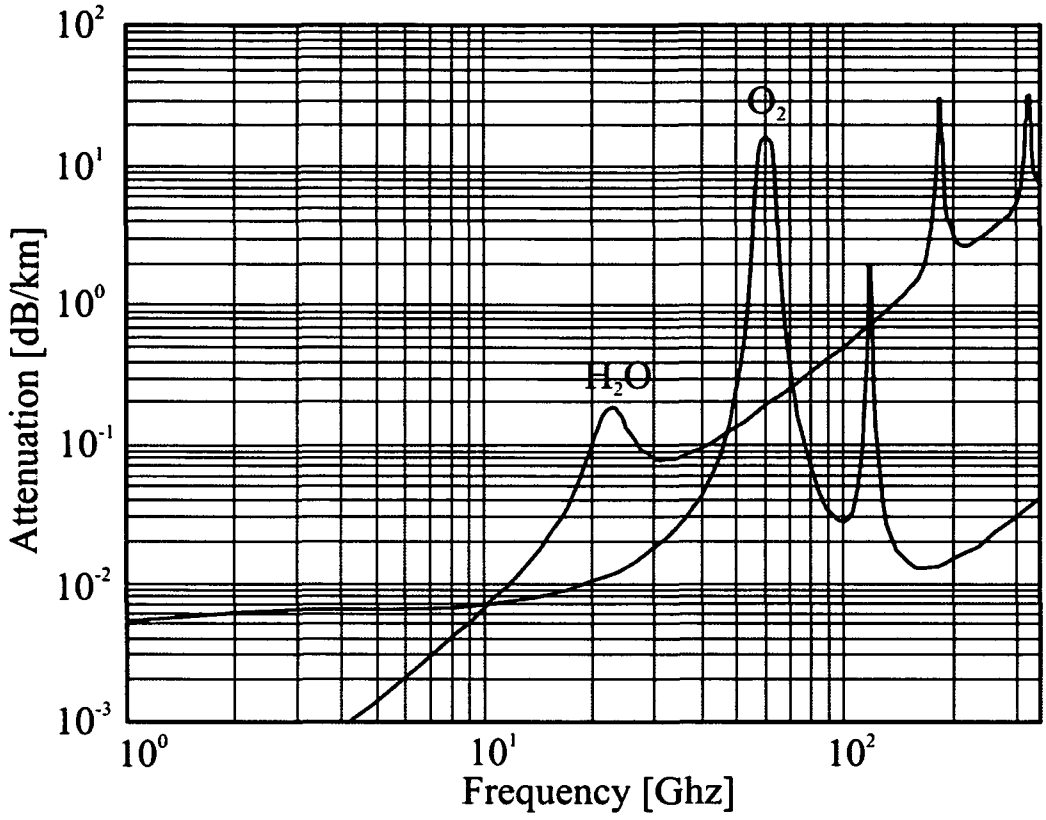

Figure 2.8: Specific attenuation of water vapor and oxygen.

At about 2 GHz the specific attenuation of oxygen is from Figure 2.8 about $6 \cdot 10^{-3}$ dB/km. The specific attenuation of water vapor at 2 GHz is significantly smaller than the specific attenuation of oxygen and can be neglected.

Depolarization The polarization state of an electromagnetic wave passing through an anisotropic medium (e.g. a rain cloud) is altered such that a vertical polarized wave may emerge with some horizontal components or a right hand circular polarized (RHCP) wave may emerge with some left hand circular polarized (LHCP) component. The depolarization may be measured in cross polar discrimination (XPD). XPD expresses how much of a signal in a given polarization is scattered into the opposite polarization.

Raindrops are the major source of tropospheric depolarization. In still air the drops tend to fall with their major axis parallel to the ground. In case of a wind the major axis of the drops will have an axis tilt. A wave passing through such raindrops will tend to have the component of the electric field parallel to the major axis attenuated more than the orthogonal polarization. The wave will emerge depolarized.

Depolarization is strongly correlated with the rain attenuation. For prediction of XPD this fact is used in the standard models.

Sky Noise The sky background appears as a combination of galactic effects and atmospheric effects. The galactic effects decrease with frequency. Atmospheric effects becomes significant at 10 GHz and increase with frequency.

The galactic effect is a combination of the cosmic background radiation, and the galactic noise temperature of radio stars and nebulas. The cosmic background radiation is independent of the frequency everywhere in the sky at a temperature of 2.7 K. The galactic noise temperature of radio stars and nebulas varies across the sky and decreases rapidly with frequency. Figure 2.9 illustrates the sky temperature, as measured from the Earth, due to both these effects [Sklar 01].

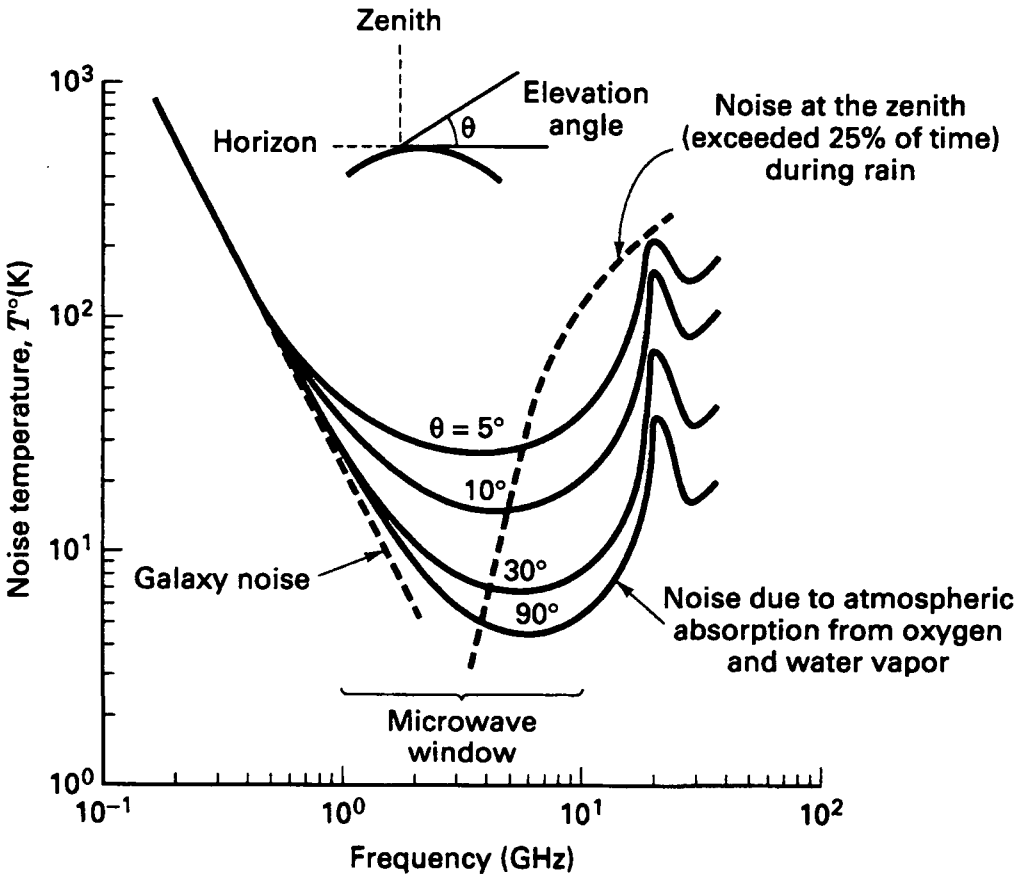

Figure 2.9: Sky noise temperature for different elevation angles.

There is a region between 1 GHz and 10 GHz where the sky noise temperature is

lowest. This region, known as microwave window or space window, is particulary useful for satellite communication. A good estimate for the temperature of the cold sky, the combination of cosmic and galactic noise temperature, at 2 GHz is 10 K.

2.3.4 System Noise Temperature

Figure 2.10 shows the ground station receiver path.

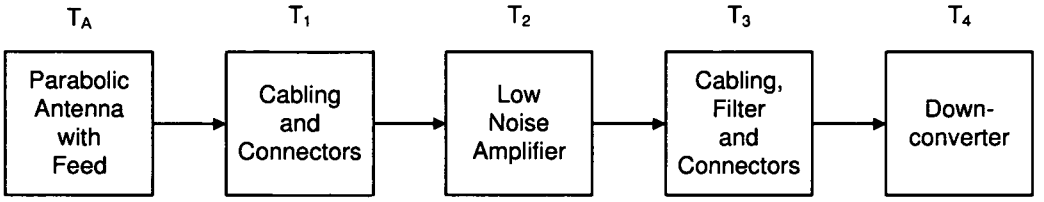

Figure 2.10: Ground station receiver path. The noise contribution of each component can be expressed as an equivalent noise temperature.

In case of an atmospheric absorption process the effective noise temperature is increased according to the total absorption. The overall antenna noise temperature can be calculated as

$$T_A = T_m(1 - 10^{-A/10}) + T_c \cdot 10^{-A/10} \tag{2.48}$$

where A is the total absorption due to rain and gaseous attenuation, T_m is the temperature of the rain medium and T_c is the temperature of the cold sky. The temperature of the rain medium is 280 K for clouds and 260 K for rain.

For the receive system a composite noise temperature can be calculated by the formula of Friis. The composite temperature of the receiving system is

$$T_{comp} = T_1 + \frac{T_2}{G_1} + \frac{T_3}{G_1 G_2} + \frac{T_4}{G_1 G_2 G_3} \tag{2.49}$$

where T_1 to T_4 are the effective temperatures, and G_1 to G_4 are the gains of the components. The system noise temperature T_S is the sum of the antenna noise temperature and the composite noise temperature

$$T_S = T_A + T_{comp}. \tag{2.50}$$

The components shown in Figure 2.10 are characterized in Section 2.3.2 with their noise figure given for a reference temperature of 290 K. If Equation (2.49) is used, the effective noise temperature of each component has to be calculated. The effective noise temperature is calculated by

$$T_N = (F - 1)T_0 \tag{2.51}$$

where T_N is the effective noise temperature of the network or component, F is the noise figure, and T_0 is the reference temperature.

2.3.5 Link Budget Calculation

In the sections above the theoretical background for the calculation of the link budget was given. Following the link budget calculation for uplink and downlink is shown.

Downlink

In Section 2.3.1 the parameters for the transmitter of the satellite are listed. With this parameters we can calculate the EIRP (Effective Isotropically Radiated Power). In the following logarithmic units are used with a reference power level of 1 mW.

$$EIRP = P_t - L - G_{ASD} \tag{2.52}$$

where P_t is the transmit power of the satellite transmitter, L are the losses, and G_{ASD} is the antenna gain of the downlink transmit antenna of the satellite. When we use the satellite parameters from Section 2.3.1 we get an EIRP of

$$EIRP = 27\,dBm - 2\,dB - 0\,dBi = 25\,dBm$$

The next step is the calculation of the propagation loss. The free space loss is the dominant factor of the propagation loss. For the calculation of the free space loss the maximum communication distance between satellite and ground station is needed. With Equation (2.11) the maximum distance is calculated. A realistic assumption for the communication with the satellite is that communication is possible at an elevation angle of $\theta = 2°$ or higher. Below 2° elevation man made noise or buildings will hinder communication. With the mean radius of the earth $r_E = 6372\,km$, and and the distance of the satellite from the mid point of Earth $r_S = 830\,km + 6372\,km = 7202\,km$, the maximum distance between the ground

station and the satellite is

$$d_{max} = 3130\,km.$$

The free space loss is

$$L_{FSL} = \frac{(4\pi df)^2}{c^2} \tag{2.53}$$

where $c = 3 \cdot 10^8 m/s$ is the speed of light, f the frequency, and d the distance between transmitter and receiver. With the downlink frequency of $f_D = 2232\,MHz$ and the maximum distance between satellite and ground station, the free space loss in decibel for the downlink is

$$L_{FSLD} = 10\lg \frac{(4\pi \cdot 3130 \cdot 10^3\,m \cdot 2232\,MHz)^2}{(3 \cdot 10^8\,m/s)^2} = 169.4dB.$$

Figure 2.11 shows the free space loss for uplink and downlink from the maximum to the minimum communication distance. It can be seen that the difference in the free space loss between maximum and minimum distance is about 12 dB.

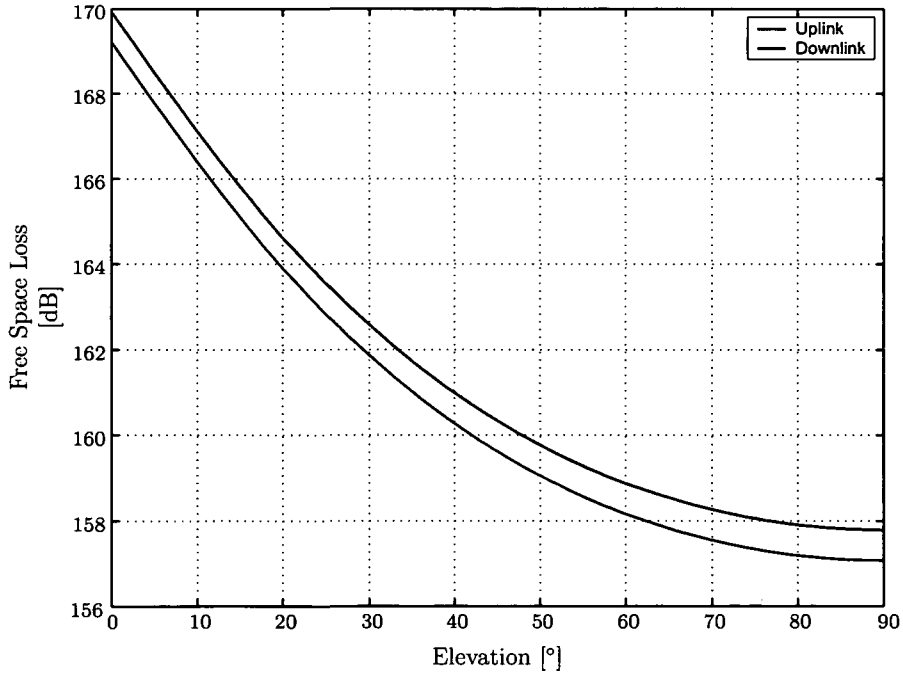

Figure 2.11: Free space loss for uplink and downlink from the maximum to the minimum communication distance. The difference between maximum and minimum free space loss is about 12 dB.

Another part of the propagation loss is the atmospheric loss. The dominant part of the atmospheric loss are the rain loss and the loss due to gaseous absorption.

For calculation of the rain loss at an elevation angle of $\theta = 2°$ the reduction factor and the length of the rain path have to be calculated. The rain path length is calculated with Equation (2.45). With the effective rain height of $h_R = 3.125\,km$, the height of the Earth station of $h_S = 265\,m$, and the elevation angle of $\theta = 2°$ the rain path length is

$$r_r = \frac{2(3125\,m - 265\,m)}{\left[\sin^2(2\,°) + \frac{2(3125\,m-265\,m)}{8500 \cdot 10^3\,m}\right]^{1/2} + \sin 2\,°} = 73\,km.$$

The reduction factor is calculated with Equation (2.47). With the rain fall rate for most of Europe (except for some Mediterranean regions) of $R_{0.01} = 30\,mm/h$ the reduction factor is

$$s = 0.886.$$

The satellite signal is circularly polarized. Therefore $\tau = 45°$ for calculation of the coefficients for the empirical rain model. With Table 2.3 and an elevation angle of $\theta = 2°$, the coefficients are

$$a = 0.000146$$

and

$$b = 0.944.$$

With Equation (2.38) the specific attenuation is

$$\gamma = 0.00362\,dB/km.$$

With the reduction factor, the specific attenuation, Equation (2.44), and Equation (2.46) the attenuation due to rain is

$$L_R = 0.24\,dB.$$

For the gaseous loss we get with the specific attenuation of oxygen of $6 \cdot 10^{-3}\,dB/km$, the path length of 4 km at the zenith and the elevation angle

$$L_G = 0.68\,dB.$$

If we combine the rain loss and the gaseous loss we get a total atmospheric loss of about

$$L_A = L_R + L_G = 0.94\,dB.$$

For the calculation of the link budget a value for $L_A = 1\,dB$ for the atmospheric loss is used.

The MOST satellite transmits a right hand circularly polarized signal. The ground station receives signals in two linear orthogonal polarization states. If a circular polarized signal is received with a linear polarized antenna then a polarization loss of 3 dB occurs. Due to the optimum combiner the polarization loss should be negligible. To be on the safe side the calculation of the link budget was done with the worst case of receiving with only one polarization state which leads to a polarization loss of

$$L_{Polarization} = 3\,dB.$$

Optimally the ground station antennas will track the satellite perfectly. Realistically there could be a slight misalignment in pointing of the antennas to the satellite. Therefore a pointing mismatch loss of

$$L_{Pointing} = 1\,dB$$

is considered. The total propagation loss in decibel is the sum of free space loss, atmospheric loss, polarization loss and pointing loss

$$L_D = L_{FSLD} + L_A + L_{Polarization} + L_{Pointing} = 174.4\,dB.$$

Under the assumption that the receive antenna has an isotropic antenna characteristic the received power is

$$P_{ri} = EIRP - L_D = -149.4\,dBm.$$

A value for the quality of the receiver is the figure of merit G/T_S. The higher the figure of merit the higher the performance of the receiver. The antenna gain of the 3 m parabolic dish is $G_{AP} = 34.9\,dBi$. The system noise temperature is calculated by Equation (2.50). Before the system noise temperature can be calculated the composite temperature of the receiver system and the antenna noise temperature must be calculated. Equation (2.48), the temperatures for the rain medium of $T_m = 280\,K$ and the cold sky $T_c = 10\,K$, and the absorption due to

rain and gaseous attenuation of $L_A = 1\,dB$ lead to an antenna temperature of

$$T_A = 280\,K(1 - 10^{-1/10}) + 10\,K \cdot 10^{-1/10} = 63\,K.$$

In order to calculate the composite temperature of the receiver the effective noise temperatures of the components have to be calculated.

The attenuation by short cables and connectors between the feed and the low noise amplifier is assumed as 0.5 dB. The attenuation of the cables and the filter between the low noise amplifier and the downconverter is 4 dB. With Equation (2.51) and a reference temperature of $T_0 = 290\,K$ the effective temperatures of the receiving system components are as follows:

$$\begin{aligned} T_1 &= 35\,\mathrm{K} \\ T_2 &= 43\,\mathrm{K} \\ T_3 &= 438\,\mathrm{K} \\ T_4 &= 59\,\mathrm{K} \end{aligned}$$

$T_1 = 35\,K$ is the effective temperature of the cables and connectors between feed and low noise amplifier. $T_2 = 43\,K$ is the effective temperature of the low noise amplifier. $T_3 = 438\,K$ is the effective temperature of the cabling and filter between low noise amplifier and downconverter. $T_4 = 59\,K$ is the effective temperature of the downconverter. With this result and Equation (2.49) the composite temperature is

$$T_{comp} = 83\,K.$$

The composite noise temperature and the antenna noise temperature leads, according to Equation (2.50), to a system noise temperature of

$$T_S = T_A + T_{comp} = 146\,K.$$

With this result and the antenna gain the G/T_S is

$$G/T_S = 13.3\,dB/K.$$

The ratio received power to noise spectral density is calculated with

$$\frac{P_r}{N_0} = \frac{G_{AD} P_{ri}}{k T_S} \tag{2.54}$$

where N_0 is the noise spectral density and $k = 13.81 \cdot 10^{-24}\,J/K$ is the Boltzmann

constant. With the values calculated above the receive power to noise spectral density is

$$\frac{P_r}{N_0} = 62.5\,dBm/Hz$$

The E_b/N_0 ratio is calculated with Equation (2.54) divided by the data rate. The date rate of the downlink is 38.4 kBit/s. Due to the use of a one half rate convolutional coding forward error correction the bit rate at the demodulator is doubled. The bit rate used for calculation of the E_b/N_0 is 76.8 kbit/s, which leads to

$$\frac{E_b}{N_0} = 13.6\,dB.$$

With the required signal to noise ratio of 4.9 dB for a bit error probability of 10^{-5} the downlink margin is

$$M_D = 8.7\,dB$$

Uplink

The transmit power of the power amplifier at the uplink is $P_t = 47\,dBm$. The cabling between the power amplifier and the Yagi antenna group has a loss of $L_{UC} = 2.5\,dB$. With the antenna gain $G_{AU} = 25\,dBi$ the EIRP at the uplink is

$$EIRP_U = 69.5\,dBm.$$

The uplink frequency is 2055 MHz. Free space loss at the uplink is

$$L_{FSLU} = 10\lg\frac{(4\pi \cdot 3130 \cdot 10^3\,m \cdot 2055\,MHz)^2}{(3 \cdot 10^8\,m/s)^2} = 168.6dB$$

The difference in frequency between uplink and downlink is not so high that there are essential changes at the atmospheric loss. Therefore the atmospheric loss is the same as at the downlink. Also a pointing mismatch loss of 1 dB is assumed for the uplink. Due to the reason that the transmit antennas are linearly polarized and the receive antenna is circularly polarized the polarization mismatch loss is

$$L_{PolarizationU} = 3\,dB.$$

With these results the total propagation loss of the uplink is

$$L_U = 173.6\,dB.$$

In the virtual case of a receive antenna with an isotropic antenna characteristic the received isotropic power is

$$P_{riu} = EIRP - L_U = -104.1\,dBm.$$

With the parameters from Table 2.2 the G/T_S of the satellite receiving system is

$$\frac{G}{T_S} = -33.8\,dB/K. \tag{2.55}$$

The carrier to noise spectral density ratio at the satellite is

$$\frac{P_r}{N_0} = 60.7\,dBm/Hz.$$

Under the use of the receiver bandwidth of the satellite from Table 2.2 the carrier to noise ratio is

$$\frac{E_b}{N_0} = 10.3\,dB \tag{2.56}$$

The required signal to noise ratio for a bit error probability of 10^{-5} is 5 dB. With this value the uplink margin is

$$M_U = 5.3\,dB. \tag{2.57}$$

Link Budget Table

Below the link budget is presented in tabular form.

It shows that the margins are low but sufficient for a stable communication with the satellite MOST.

2.4 Ground Station Subsystem and Integration

In this section the calculation of the stacking distance of the Yagi antenna group is done. Also an experiment to check the isolation between uplink and downlink antenna is shown. Further a brief overview about the integration of the ground station is given.

Uplink				
Frequency	2055	MHz		
Transmit Power	50	W	47.0	dBm
Line Loss			2.5	dB
Antenna Gain			25.0	dBi
EIRP			69.5	dBm
max. Distance	3130	km		
Free Space Loss	168.6	dB		
Polarization Loss	3.0	dB		
Atmospheric Losses	1.0	dB		
Pointing Loss	1.0	dB		
Total Propagation Loss			173.6	dB
Received Isotropic Power			-104.1	dBm
G/T_s			-33.8	dB/K
P_r/N_0			60.7	dB
Receive Bandwidth	76.8	kHz	50.4	dBHz
E_b/N_0			10.3	dB
min. required SNR			5.0	dB
Margin			5.3	dB

Table 2.4: Link budget table for uplink.

Downlink				
Frequency	2232	MHz		
Transmit Power	0.5	W	27.0	dBm
Line Loss			2.0	dB
Antenna Gain			0.0	dBi
EIRP			25.0	dBm
max. Distance	3130	km		
Free Space Loss	169.4	dB		
Polarization Loss	3.0	dB		
Atmospheric Losses	1.0	dB		
Pointing Loss	1.0	dB		
Total Propagation Loss			174.4	dB
Received Isotropic Power			-149.4	dBm
G/T_s			13.3	dB/K
P_r/N_0			62.5	dB
Receive Bandwidth	110.0	kHz	48.9	dBHz
E_b/N_0			13.6	dB
min. required SNR			4.9	dB
Margin			8.7	dB

Table 2.5: Link budget table for downlink.

2.4.1 Isolation

As mentioned in Section 2.2.1 a two antenna system is used for the ground station. To check if with this design the isolation between transmit path and receive path is in order of a duplexer of around 70 dB a measurement was performed.

Figure 2.12 shows a block diagram of the measurement setup.

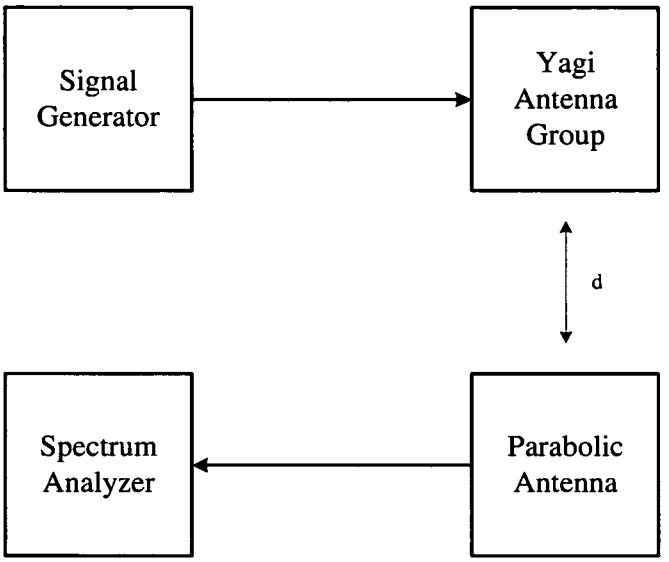

Figure 2.12: Isolation measurement setup. A defined signal was transmitted via the Yagi antenna group. The distance between Yagi antenna group and the parabolic dish was varied. The coupled transmit signal received by the parabolic dish was measured by a spectrum analyzer.

The transmit signal was generated by a signal generator and transmitted via the Yagi antenna group. The Yagi antenna group transmits horizontal linear polarized signals (see Figure 2.14). The signal received by the parabolic antenna was measured by a spectrum analyzer. With a switch it was possible to chose either the horizontal or vertical port of the antenna feed. Figure 2.13 shows the result of the measurement.

The distance in Figure 2.13 is the distance between the mid point of the Yagi antenna group and the edge of the parabolic dish. As it can be seen in Figure 2.13 the isolation between the transmit and receive path is higher than 90 dB. The distance between the transmit antenna and the receive antenna was set to 0.96 m to reach a good compromise for both polarization states.

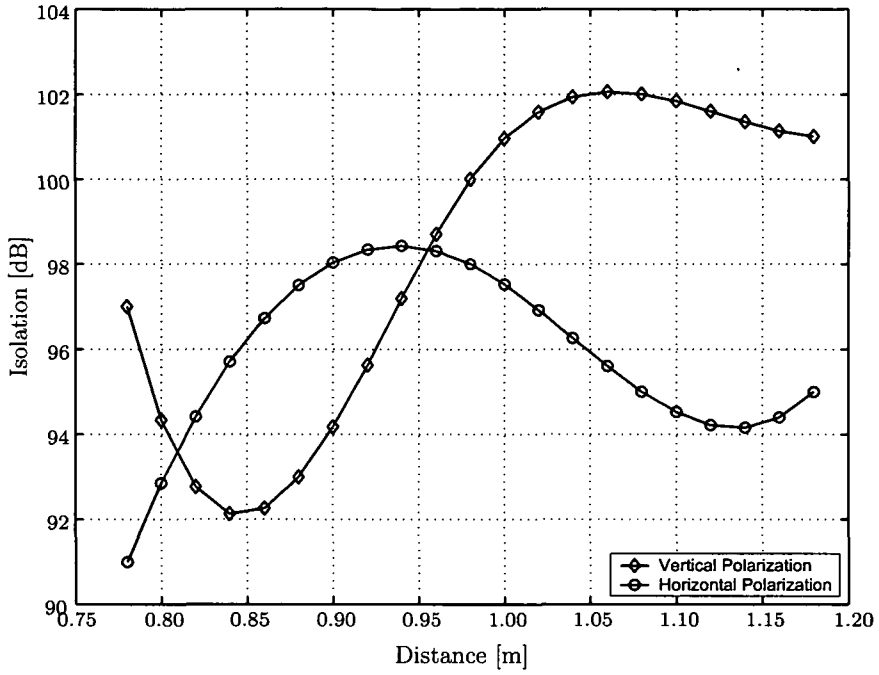

Figure 2.13: Isolation between mid point of transmit antenna group and edge of the receive antenna. The isolation between transmit and receive antenna is at least 90 dB. The distance between the antennas was chosen to reach good compromise for both polarization states.

2.4.2 Antenna Stacking Distance

For the uplink a Yagi antenna group consisting of four Yagi antennas is used. The stacking distance of the Yagi antennas is calculated by using the antennas effective aperture. The antennas are stacked such that the borders of the effective apertures are in touch with each other. The aperture of a single Yagi antenna is

$$A_e = \frac{\lambda^2}{4\pi} G \tag{2.58}$$

where λ is the wavelength and G is the antenna gain with respect to an isotropic radiator. The aperture of the single Yagi antenna can be approximated by a circle. The distance between two Yagi antennas will be two times the radius of the aperture of a single Yagi antenna

$$d_{opt} = 2\sqrt{\frac{A_w}{\pi}}. \tag{2.59}$$

With Equation (2.58) the distance between two Yagi antennas is

$$d_{opt} = 2\sqrt{\frac{\lambda^2 G_A}{4\pi^2}}. \tag{2.60}$$

By using the antenna gain of a single Yagi antenna from Section 2.3.2 of $G_A = 21\,dBi$ and the transmit frequency of $f_t = 2055\,MHz$ the distance between two Yagi antennas is

$$d_{opt} = 0.465\,m. \tag{2.61}$$

A picture of the final assembled Yagi antenna group is shown in Figure 2.14. This distance proved as good compromise in practice between an increase of sidelobes and an increase of gain.

2.4.3 Integration

In order to get permission for the setting up of a ground station at the Institute for Astronomy, which is classified as historical building, the design of the ground station had to be verified by a structural engineer. By getting the permission to set up the ground station of the "Bundesdenkmalamt" the integration of the ground station started. All mechanical parts of the ground station antenna structure were manufactured at the mechanical work shop of the Institute of Communications and Radio-Frequency Engineering. Also a permission for the setting up and operating of the ground station by the "Fernmeldebehörde" was granted. After one year of integration the ground station setting up was finished and the ground station was ready to start operation. In Figure 2.14 the antenna structure of the ground station can be seen.

The parabolic antenna with a diameter of 3 m is the receive antenna. The four Yagi antennas combined to a group are used for uplink. Further the rotators for azimuth and elevation can be seen.

Figure 2.15 shows the main part of the Vienna ground station equipment.

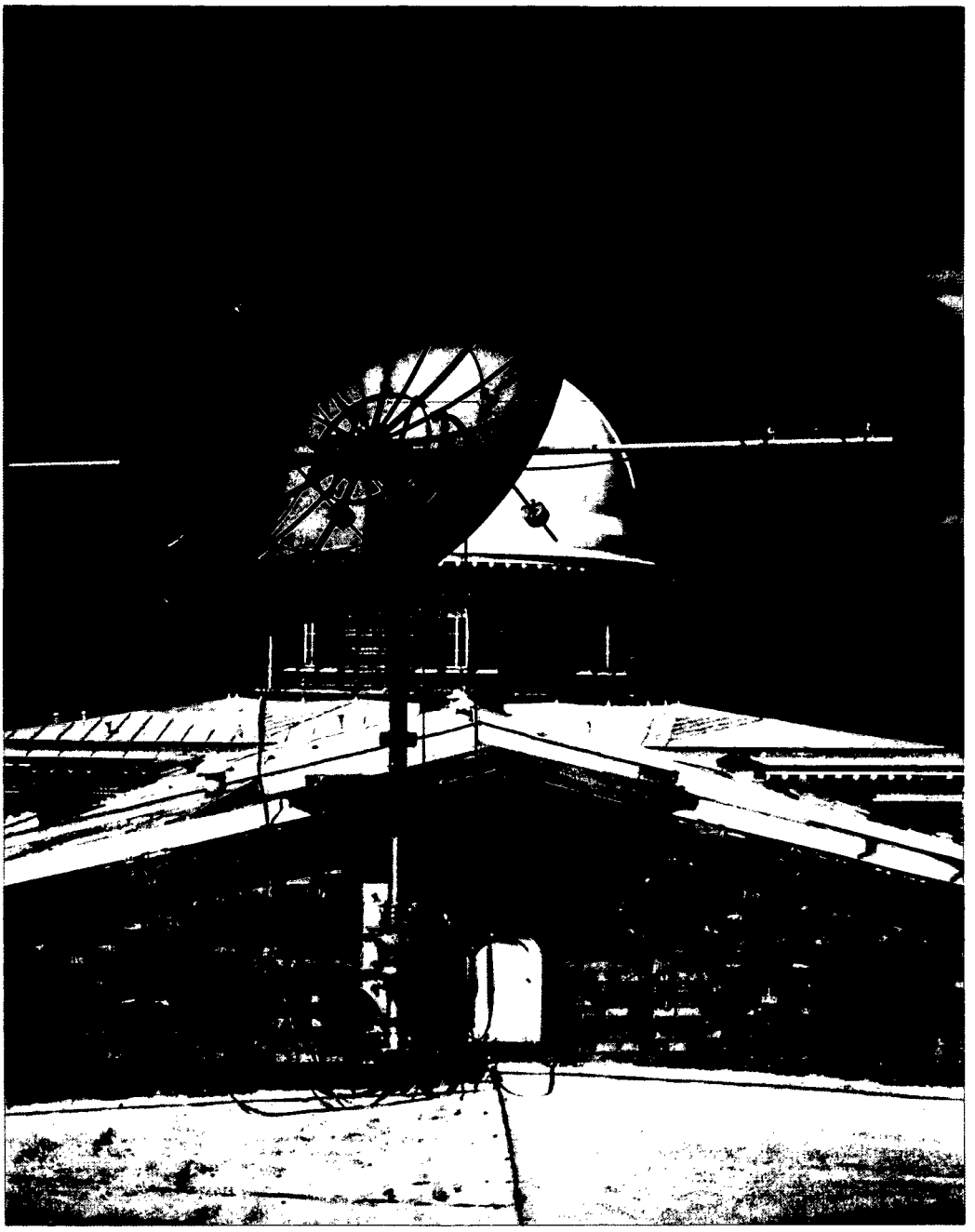

Figure 2.14: Vienna ground station antenna structure. The structure consists of a main rod and a rotating rod. On the upper left the receive antenna, a parabolic dish with a diameter of 3 m can be seen. On the upper right is the transmit antenna, a Yagi antenna group consisting of four single Yagi antennas. Also the rotators for azimuth and elevation can be seen.

Figure 2.15: Vienna ground station equipment. On the left the air condition system of the operation room can be seen. The main part of the equipment is in the 19" rack on the right. From top to bottom are following components: FM modulator and upconverter, downconverters and filters, BPSK demodulator, TNC and power amplifier safety equipment, control PC, storm safety electronic, power supply, power amplifier power supply and lighting, time switches, UPS.

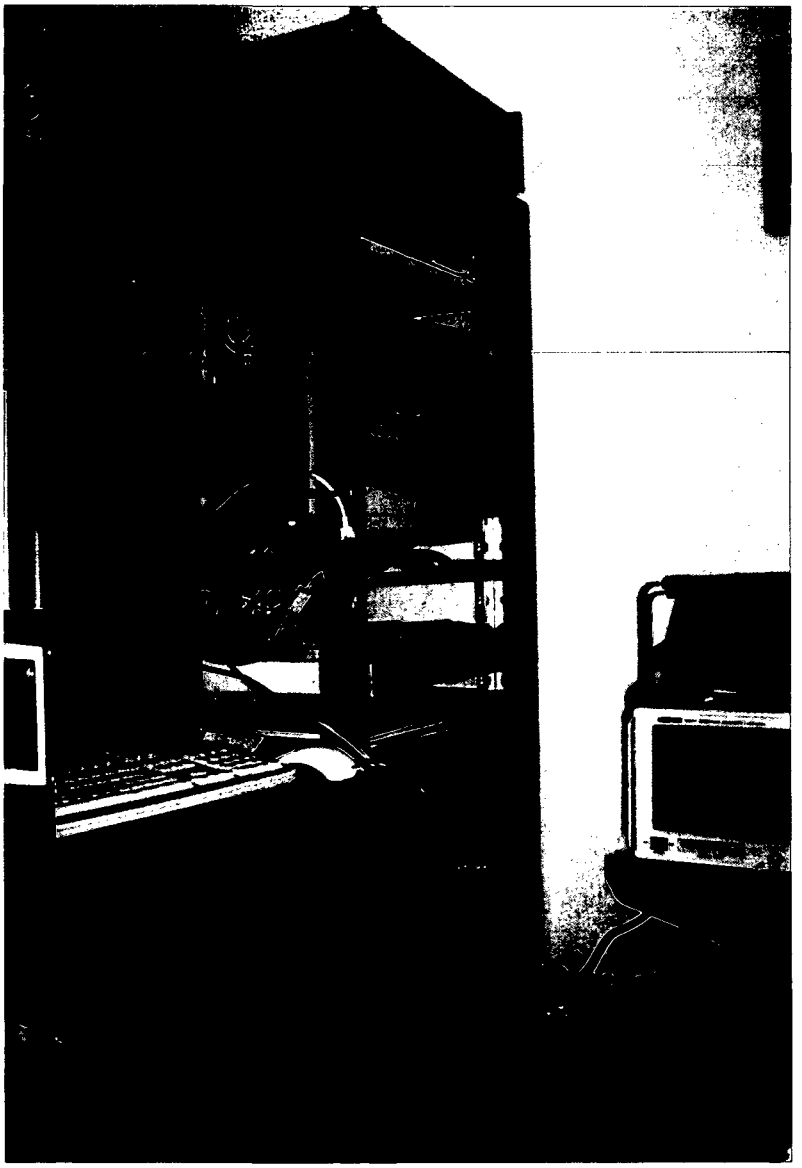

Figure 2.16: Vienna ground station equipment. On the left is the console of the control PC. On the right is a spectrum analyzer. The rack in the middle contains the remaining parts of the ground station equipment. From top to bottom are following components: rotator controller unit, video observation console, video observation computer, UPS.

Chapter 3

System Performance Verification

In this chapter the measurements done for evaluation of the performance of the ground station are presented.

3.1 Figure of Merit G/T_S

Satellite receiving systems must process very weak signals. If the noise added by the system components is too high the signal will be below the noise floor of the receiver and could not be processed. Device sensitivity is either characterized by the noise figure or alternatively by the effective noise temperature. Due to the small noise figures in satellite receiving systems the noise temperature for the description of the sensitivity is preferred. To ensure that the receiver system has a good quality the sensitivity has to be measured.

This section explains the measurement of the figure of merit G/T_S. The measurement is based on the *Y-factor Method*, also known as the *Hot/Cold Method*. The measurement set up is presented in Figure 3.1 where DUT means Device Under Test.

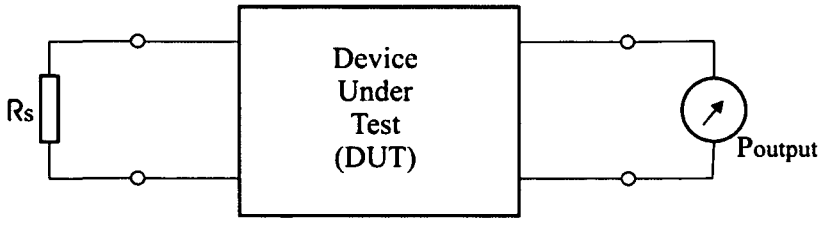

Figure 3.1: General topology for the Y-factor method

The "Y-factor" noise figure measurement technique uses two noise sources at two different temperatures to determine the noise temperature T_{dut} of the DUT. With each noise source R_s connected to the DUT (see Figure 3.1), the output power

corresponding to the different temperatures T_{hot} and T_{cold} is measured. The output power is termed according to the temperature as P_{hot} and P_{cold}. The Y-factor is defined as the ratio of these power measurements

$$Y = \frac{P_{hot}}{P_{cold}}. \tag{3.1}$$

If the DUT has a gain of $G = 1$, a bandwidth B, and if it is assumed that there is no loss resulting from cables and matching, then based on $N = GkTB$, P_{hot} and P_{cold} are

$$P_{hot} = k(T_{hot} + T_{dut})B \tag{3.2}$$

$$P_{cold} = k(T_{cold} + T_{dut})B \tag{3.3}$$

By substituting Equation (3.2) and Equation (3.7) in Equation (3.1), the bandwidth B and Boltzmann's constant k will drop out. Then Y becomes

$$Y = \frac{T_{hot} + T_{dut}}{T_{cold} + T_{dut}}. \tag{3.4}$$

Calculating T_{dut} from Equation 3.4 yields

$$T_{dut} = \frac{T_{hot} - YT_{cold}}{Y - 1}. \tag{3.5}$$

When the temperatures T_{hot} and T_{cold} are known, and Y is measured, the noise temperature T_{dut} can be obtained from Equation (3.5).

For satellite communication the performance of the receiving system is commonly defined through the figure of merit G/T_s where $T_s = T_A + T_{comp}$. T_A is the noise temperature of the receive antenna, G the gain of the receive antenna, and T_{comp} is composite noise temperature of the receiving system.

To obtain G/T_s one could determine G and T_s separately but this requires elaborate measurements. Instead we obtain the ratio G/T_s by a single measurement based on the Sun as a noise signal source. For the measurement of Y the Sun is used as source for T_{hot} and the cold sky is used as source for T_{cold}.

The principle behind the determination of G/T_s is to measure the increase in noise power when the antenna first is pointed to a cold region of the sky and then moved to a strong source of known flux density - usually the Sun. In this case, the Y-factor is

$$Y = \frac{P_{sun}}{P_{coldsky}}. \tag{3.6}$$

The measured power consists of two components: the power generated by the receiving system itself (kT_sB) and the power coming from the external radio source. In case of the cold sky the flux density can be considered as very low or zero because of the low temperature of around 10 K. As the contribution of the external source is negligible, the measured power $P_{coldsky}$ can be expressed as

$$P_{coldsky} = kT_sB. \tag{3.7}$$

When the antenna is pointed to the Sun the received power P_{sun} is

$$P_{sun} = kT_sB + F_{sun}A_eBL_B \tag{3.8}$$

where ($F_{sun}A_eBL$) is the noise power resulting from Solar radiation. In Equation (3.8) F_{sun} is the Solar flux density at the measurement frequency f and is expressed in (W/m^2Hz), L_B is the beamsize correction factor, B is the bandwidth of the system and A_e is the antenna's effective area (see Equation 2.30).

Since the Solar radiation is randomly polarized, half power is in each polarization state ($F_{sun.singlepol} = F_{sun}/2$). For a single polarization state the measured power P_{sun} will be

$$P_{sun} = kT_sB + \frac{F_{sun}}{2}A_eBL_B. \tag{3.9}$$

Substituting Equation (3.9) and Equation (3.7) into Equation (3.8) yields

$$Y = \frac{P_{sun}}{P_{coldsky}} = \frac{kT_sB + (F_{sun}/2)A_eBL}{kT_sB} \tag{3.10}$$

and further

$$Y = 1 + \frac{F_{sun}A_eBL_B}{2kT_sB}. \tag{3.11}$$

With the antenna effective aperture $A_e = \lambda^2 G/4\pi$ Equation (3.11) gives

$$Y = 1 + \frac{F_{sun}\lambda^2 G L_B}{8\pi k T_s} \tag{3.12}$$

Solving Equation (3.12) by (G/T_s), leads to the figure of merit of the receiving system

$$\frac{G}{T_s} = \frac{8\pi k}{F_{sun} L_B \lambda^2}(Y - 1) \tag{3.13}$$

For Equation (3.13) the value of Y will be obtained by measurement. To be able to calculate the figure of merit, the beamsize correction factor and the flux density of the Sun are needed.

The beamsize correction factor L is expressed by [Flagg]

$$L_B = 1 + 0.38\left(\frac{\theta_{sun}}{\theta_A}^2\right) \tag{3.14}$$

where θ_{sun} is the diameter of the sun as radio source at frequency f and θ_A is the full 3 dB beamwidth of the antenna.

The diameter of the Sun θ_{sun} is frequency dependent. Table 3.1 shows the diameter of the Sun for different frequencies [Flagg].

f	400MHz	1420MHz	$\geq$ 3000MHz
θ_{sun}	0.7°	0.6°	0.5°

Table 3.1: Sun diameter table as seen from Earth for different frequencies.

Further the solar flux density F_{sun} at the measurement frequency is needed. The USAF (United States Air Force) Space Command runs a worldwide solar monitoring network and measures the solar flux density at following nine frequencies: 245 MHz, 410 MHz, 610 MHz, 1415 MHz, 2695 MHz, 2800 MHz 4995 MHz, 8800 MHz and 15400 MHz. If the operating frequency does not fit with one of these frequencies the flux value can be calculated by interpolation.

The accuracy of the determination of G/T_s is dependent on the accurate measurement of Y. The easiest measurement technique is to use a power meter connected to the receiver's intermediate frequency. For this measurement the receiver must be operating in a linear region.

Measurement

The measurement presented below was done on January 24, 2004. Further measurements on different days were also performed with identical results for the figure of merit G/T_S. The measurement was done without polarization recovery unit. As power meter a spectrum analyzer connected to the intermediate frequency output of the downconverter was used. Figure 3.2 shows the measurement setup of the figure of merit measurement.

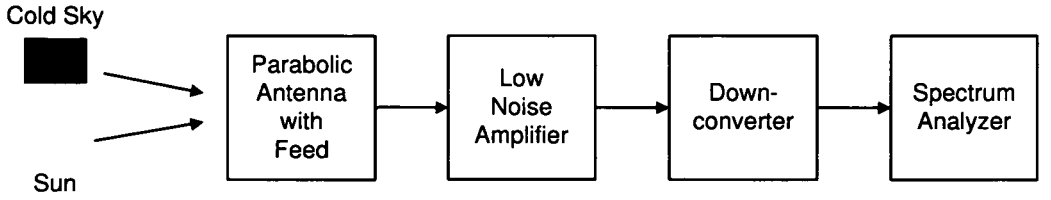

Figure 3.2: Figure of merit measurement setup. First the noise power of the Sun and then the noise power of the cold sky was measured. The noise power levels were measured by a spectrum analyzer.

The measurement result of P_{sun} and $P_{coldsky}$ is presented in Figure 3.3.

In Figure 3.3 RBW is the Resolution Bandwidth, VBW the Video Bandwidth, and SWP the Sweep Time.

In Figure 3.3, the signal at the bottom represents the noise power density when the antenna was pointed to the cold sky. The upper signal shows the noise power when the antenna points to the Sun. These two traces are used for the calculation of the figure of merit.

An accurate measurement of the difference of the measured noise power pointing to the cold sky and the sun gives a difference of

$$Y(dB) = \frac{P_{sun}}{P_{coldsky}} = 11.5dB.$$

For calculation of the figure of merit also the solar flux density is needed. A linear interpolation of the solar solar flux density measurements provided from Learmonth Observatory for the date of January 24, 2004 is presented in Figure 3.4.
The downlink frequency of MOST satellite system is $f_D = 2232\,MHz$. From Figure 3.4 we get a solar flux density for the downlink frequency of

$$F_{sun} = 91{\cdot}10^{-22}\,W/m^2Hz.$$

Equation (3.13) with $\lambda = c/f$ yields

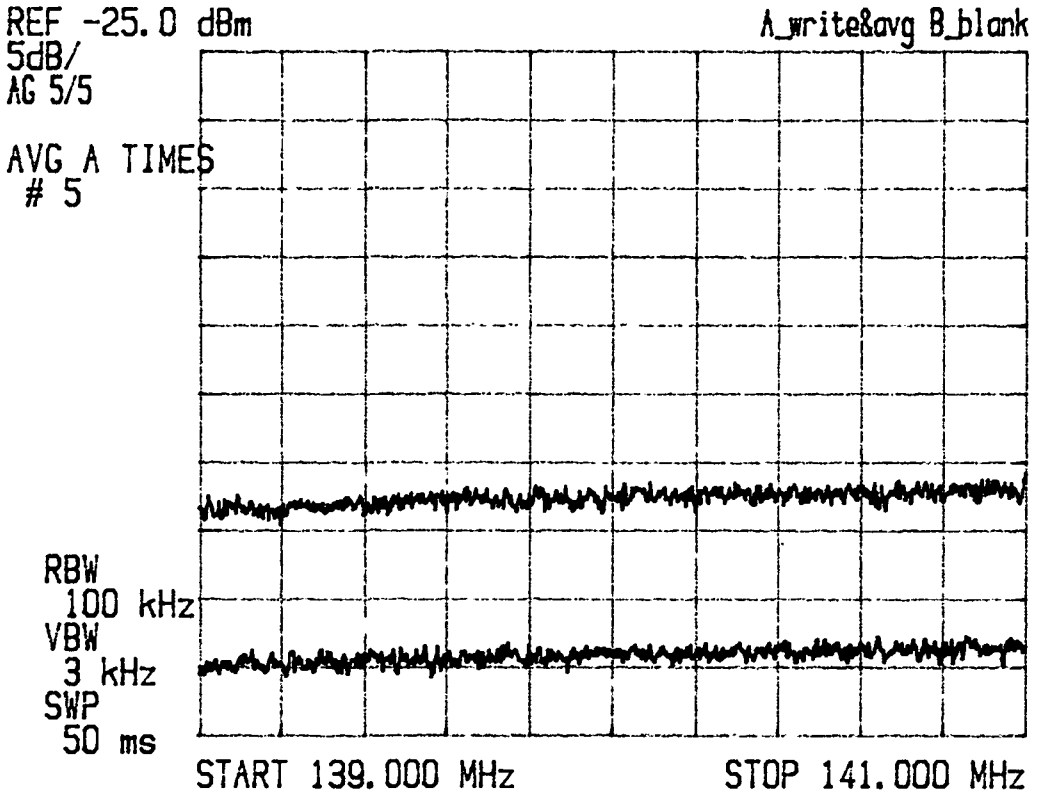

Figure 3.3: P_{Sun} and $P_{coldsky}$ measurement result. The upper curve is the Sun noise power and the lower curve is the noise power of the cold sky. The difference between the two curves is 11.5 dB.

$$\frac{G}{T_s} = \frac{8\pi k f^2}{F_{sun} L_B c^2}(Y-1). \tag{3.15}$$

To solve Equation (3.15) the beamsize correction factor has to be calculated. With Equation (3.14), the diameter of the sun of about $\theta_{sun} = 0.5°$ for $f = 2232\,MHz$, and the 3 dB beamwidth of the receive antenna of $\theta_A = 3.2°$, the beamsize correction factor is

$$L_B = 1.01$$

Now, with Boltzmann's constant $k = 1.38{\cdot}10^{-23} W/HzK$, the downlink frequency, and the speed of light of $c = 3{\cdot}10^8 m/s$, the figure of merit is

$$G/T_s = 14.4dB. \tag{3.16}$$

The value from link budget calculation is $13.3dB$. The result of the measurement

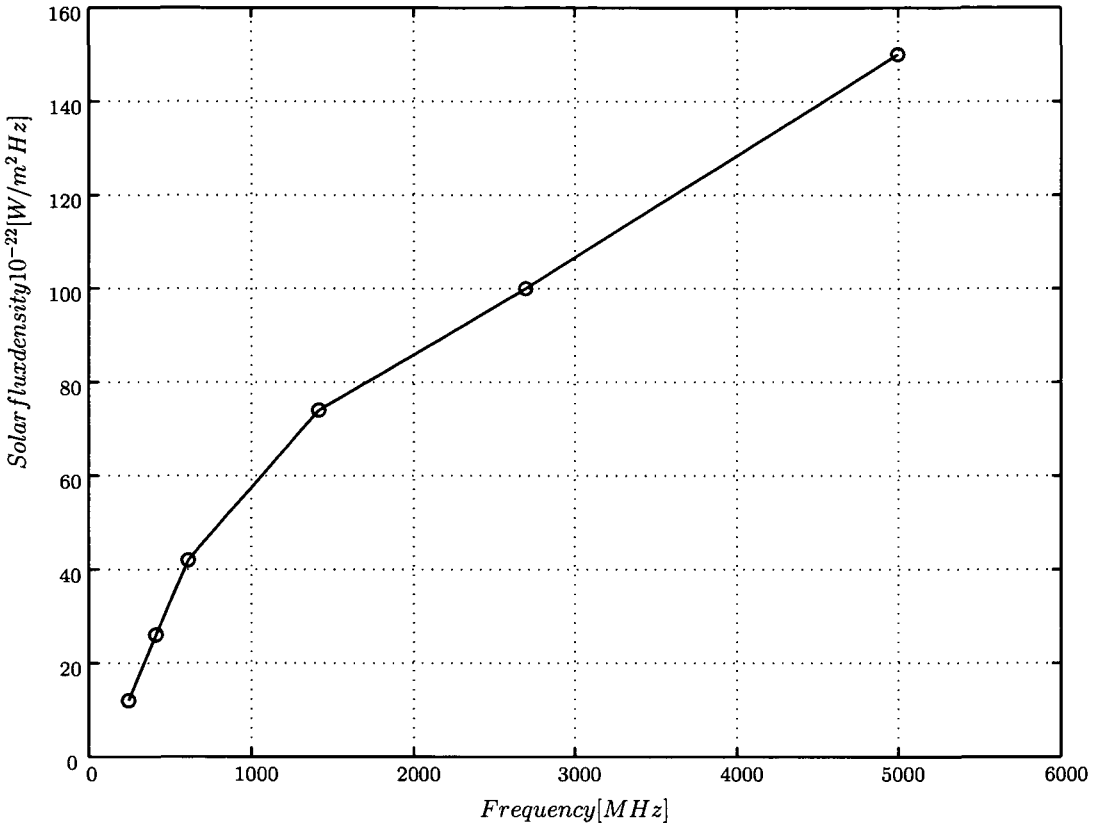

Figure 3.4: Solar flux density provided from Learmonth Observatory.

is $14.4dB$. The measurement was done on a sunny day with clear sky, and the link budget value was assumed for the worst case of a rainy day. The measured result coincides with the theory within 1 dB, which is on the order of the atmospheric loss.

3.2 Intermodulation

The Vienna ground station is optimized to achieve best downlink sensitivity. To achieve good sensitivity no frequency filtering is used in front of the first stages of the LNAs. Therefore intermodulation resulting from the presence of GSM (Global System for Mobile communication) and UMTS (Universal Mobile Telecommunications System) signals and the permanently transmitting uplink had to be carefully assessed.

Intermodulation products are multi-tone distortion products that result when two or more signals at frequencies f_1, f_2 ...f_n are present at the input of a non-linear device. The spurious products which are generated due to the non-linearity

of a device are related to the original input signal frequencies. Analysis and measurements in practice are most frequently done with two input frequencies (also termed "tones").

The frequencies of the two-tone intermodulation products are

$$Mf_1 \pm Nf_2 \, M, N = 0, 1, 2, 3,$$

The order of the intermodulation product is given by the sum of $M + N$. The second order intermodulation products of two signals at f_1 and f_2 would occur at $f_1 + f_2$, $f_2 - f_1$, $2f_1$ and $2f_2$. The third order intermodulation products of the two signals at f_1 and f_2 would be $2f_1 + f_2$, $2f_1 - f_2$, $f_1 + 2f_2$,$f_1 - 2f_2$, $3f_1$ and $3f_2$.

Mathematically the $f_2 - 2f_1$ and $f_1 - 2f_2$ intermodulation product calculation could result in a "negative" frequency. However, it is the absolute value of these calculations that is of concern for measurement. The absolute value of $f_1 - 2f_2$ is the same as the absolute value of $2f_2 - f_1$. It is common to talk about the third order intermodulation products as being $2f_1 \pm f_2$ and $2f_2 \pm f_1$.

The most interfering products are the third order intermodulation products because they fall near to the receive frequency as can be seen in Figure 3.5. If the two input frequencies are close to each other the third order intermodulation products can fall into the receive passband and interfere the receive signal.

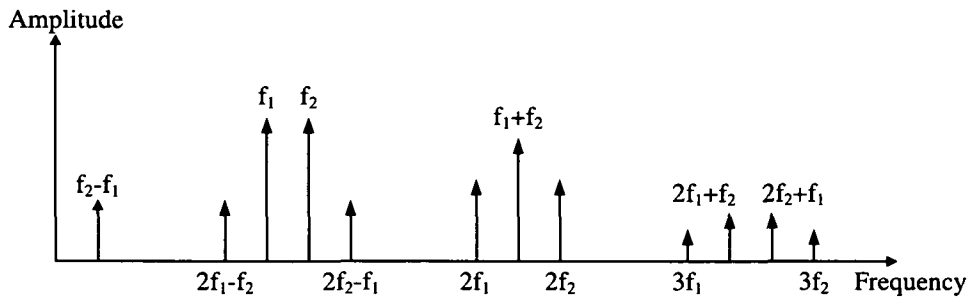

Figure 3.5: Second and third order intermodulation distortion of two input tones f_1 and f_2. The third order intermodulation products fall near to the receive frequency.

The power level of these products is a function of the received power and the linearity of the receiver/preamplifier. All semiconductors inherently exhibit a degree of non-linearity.

Due to full duplex operation of the MOST communication system the uplink

signal with a carrier frequency of 2055 MHz is permanently present. Also GSM 1800MHz, and UMTS downlink signals are present.

The intermodulation measurement setup is shown in Figure 3.6. For the measurement of the intermodulation products the ground station transmitter was turned on. The intermodulation products generated at the low noise amplifier were measured with a spectrum analyzer.

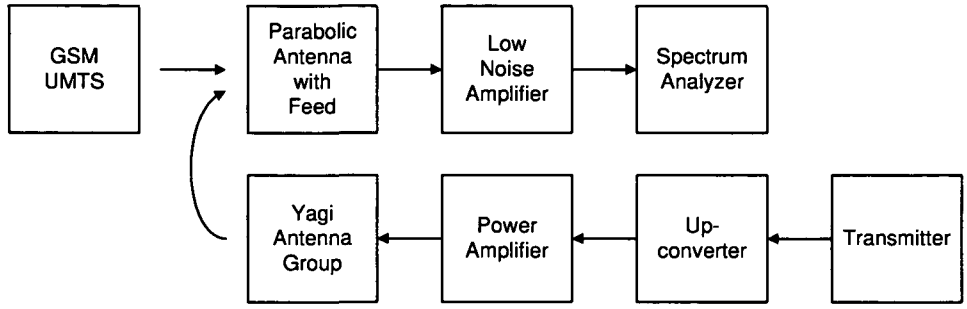

Figure 3.6: Intermodulation distortion measurement setup. For the measurement the uplink signal was turned on and the intermodulation products originating from GSM 1800MHz and UMTS were measured.

In order to see if communication without a filter in front of the low noise amplifier is possible in case of intermodulation an analysis to check if the third order intermodulation products will fall onto the receive frequencies has to be performed.

At first only intermodulation from GSM1800 is considered. The UMTS intermodulation products will be analyzed separately. Only third order products from the GSM1800 downlink will fall into the receiver passband. Outgoing from the information about the GSM frequency allocation the frequencies for GSM1800 were calculated. The frequencies and the corresponding service providers are listed in Appendix A.

GSM uplink is the communication direction from the mobile phone to the base station and downlink is the direction from the base station to the mobile phone. Based on [Bgbl. FNV 03] the frequency band for GSM1800 mobile systems is from 1710 MHz to 1785 MHz for the uplink and from 1805 MHz to 1880 MHz for the downlink. From 1876.4 MHz to 1880 MHz is a guard band to avoid cross interference between DECT (Digital Enhanced Cordless Telephone System) and GSM 1800. From 1880 MHz to 1900 MHz the frequency band for DECT is located.

Figure 3.7 shows the GSM1800 frequency band and the uplink carrier which are present at the input of the low noise amplifier.

As mentioned above only third order intermodulation products originating from

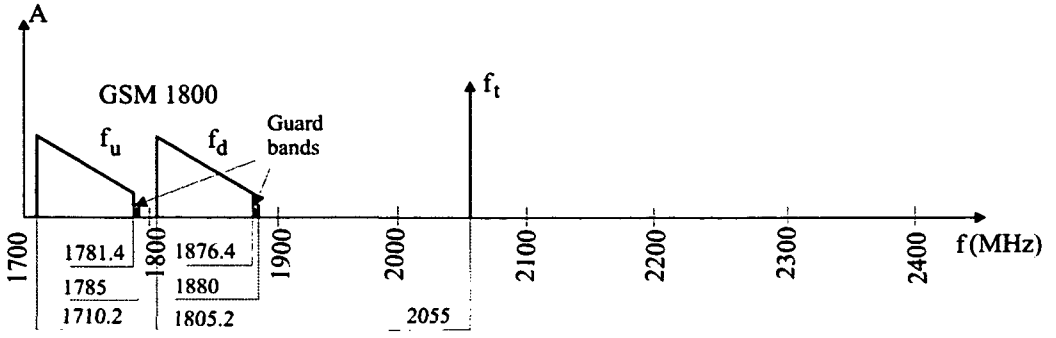

Figure 3.7: GSM 1800 Signals at the frontend of the low noise amplifier.

the uplink and the GSM1800 downlink signals will fall near the passband of the receiver. In particular the product $2f_t - f_d$ is of interest. These intermodulation products which appear at the output of the preamplifier from 2233.6 MHz to 2304.8 MHz.
The output of the preamplifier in the frequency domain is presented in Figure 3.8. The intermodulation products originating from GSM1800 downlink and the receive frequency is shown. The dotted line is the filter curve of the filter between low noise amplifier and downconverter.

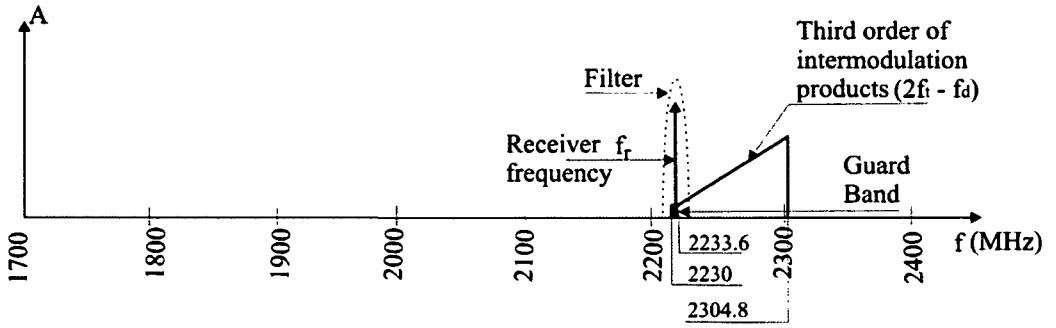

Figure 3.8: Preamplifier output. The intermodulation products and the receive frequency are shown. The dotted line is the filter curve of the filter between low noise amplifier and downconverter.

These signals now will be filtered before they are fed into the downconverter. The situation behind the filter and in front of the downconverter is presented in Figure 3.9.

The local oscillator frequency of the downconverter is $f_{LO} = 2372MHz$. The local oscillator frequency is above the receive frequency and therefore the signals at the intermediate frequency are mirrored. The intermediate frequency spectrum is shown in Figure 3.10.

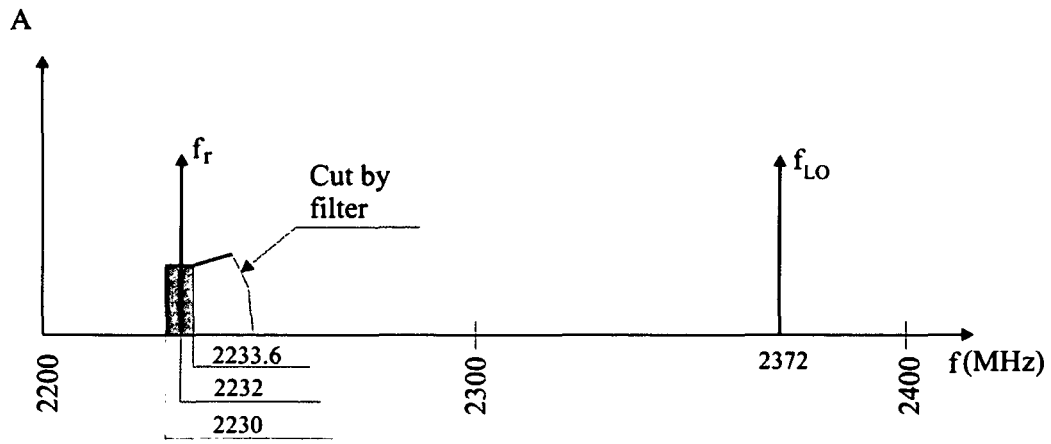

Figure 3.9: Receive signal and intermodulation products after the filter. Also the local oscillator of the downconverter is shown.

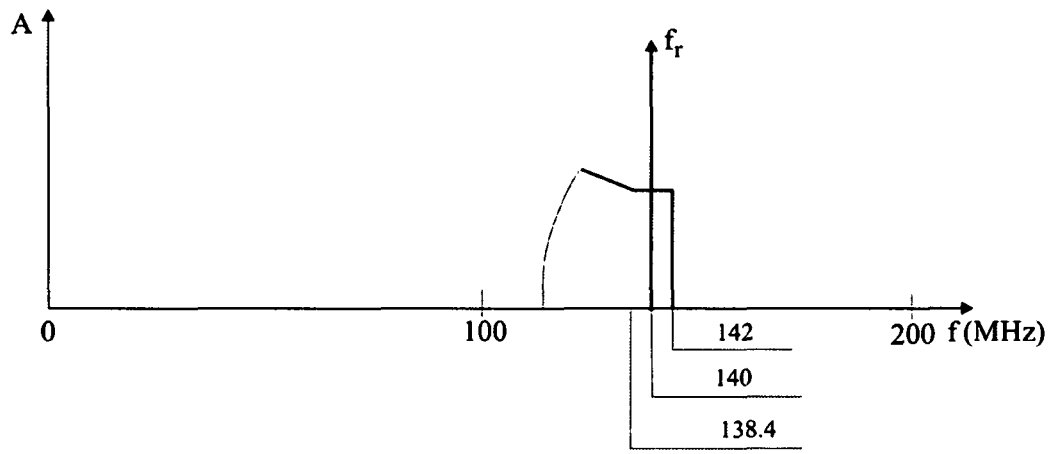

Figure 3.10: Output of the downconverter. Because the local oscillator of the downconverter is higher than the receive frequency the intermodulation products and the downlink signal appear mirrored in the spectrum. It can be seen that the receive frequency lies in the middle of the guard band between DECT and GSM1800.

From Figure 3.10 it is obvious that intermodulation products are present at at the output of the downconverter. Further Figure 3.10 shows that the receive frequency is in the middle of the GSM1800-DECT guard band.

Also intermodulation products originating from UMTS and the permanently present uplink carrier are possible. In the following the UMTS third order intermodulation products will be considered. The frequency range which could produce intermodulation products falling into the passband of the receiver is the UMTS-FDD downlink frequency range. In Appendix A a list of the UMTS-

FDD frequencies and the corresponding service provider [RTR] is presented.

Based on [Bgbl. FNV 03], the frequency band for UMTS-FDD mobile systems is 1920 MHz to 1980 MHz for the uplink and 2210 MHz to 2170 MHz for the downlink. Figure 3.11 shows the UMTS-FDD signals and the uplink signal that are present at the input of the low noise amplifiers.

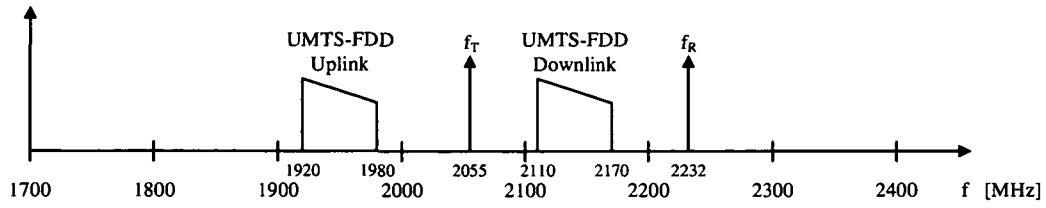

Figure 3.11: UMTS-FDD, uplink and downlink signals at the frontend of the preamplifier.

In particular the product from $2f_d - f_t$ is of interest. These intermodulation products which appear at the output of the preamplifier, are presented in Table A.4 in Appendix A.

The output of the low noise amplifier in the frequency domain is shown in Figure 3.12.

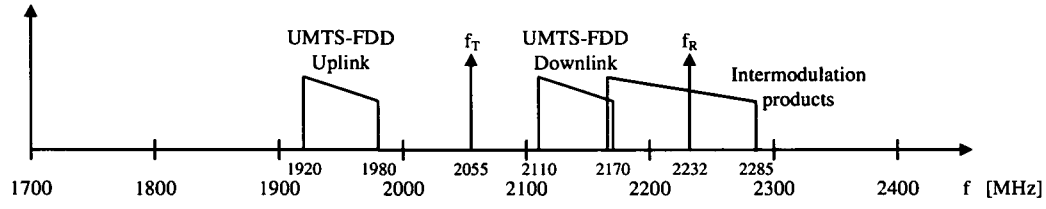

Figure 3.12: Preamplifier output spectrum. Intermodulation products, UMTS uplink and downlink as well as transmit and receive frequency are shown.

Figure 3.12 shows that if intermodulation products from UMTS-FDD and the permanently present uplink signal are present they will fall onto the receive frequency. In this case a filter in front of the low noise amplifier is needed to guarantee communication without distortion with the satellite. If a filter with an insertion loss of 0.5 dB is used the system noise temperature will be increased by 46 K and the downlink margin will decrease by 1.3 dB.

At the time of planning the station, no UMTS service was available in Vienna. Also a rapid increase of UMTS during the duration of the mission was not in

sight. It was checked if intermodulation products originating from UMTS were present and only if there had been an interference a filter would been installed. The connection between low noise amplifier and feed was designed in a way that a filter can be inserted if necessary.

Measurements have been performed to see whether intermodulation is present. Figure 3.13 gives a screen shot of the spectrum analyzer display from the output of the low noise amplifiers. GSM1800 base station carriers can be seen. Since the overall amplifier gain at this frequency is some 40 dB lower than at the MOST downlink frequency the GSM carriers appear weaker than the UMTS carriers at around 2100 MHz. Intermodulation products originating from GSM and the uplink transmit signal at 2055 MHz are present from 2235 MHz upwards. They fall close to but not onto the receiving channel.

Figure 3.14 shows the frequency spectrum at the output of the downconverter. It can be seen that intermodulation products from GSM1800 are present. Further it can be seen that there are no intermodulation products originating from UMTS. In the center of the picture the downlink signal can be seen.

The measurement of the intermodulation products has shown that the intermodulation products from GSM1800 and the uplink carrier do not interfere with the satellite downlink signal. Intermodulation products from UMTS and the uplink carrier are not detectable.

3.3 Desensibilization

Strong signals near the pass band of the LNA can reduce the sensitivity of the LNA and consequently the sensitivity of the entire receiving system. Therefore it was checked if the sensitivity of the receiving system is reduced by the presence of the uplink and the mobile radio signals. The experimental set up is shown in Figure 3.15.

The principle of the desensibilization measurement is the following. The antenna is first pointed to the Sun with the transmitter turned off to determine the Sun noise power. Then the transmitter was turned on and the Sun noise power was measured again. If there is no change in sensitivity of the receiver the power levels must be identical.

Figure 3.16 shows the result of the desensibilization measurement. The red curve is the Sun noise power with transmitter turned on and the green curve is the Sun noise power with the transmitter turned off. The measurement was repeated many times and all curves are plotted into the same diagram.
In Figure 3.16 shows that the red curve where the transmitter is turned on and the green curve where the transmitter is turned off are identical. This means that

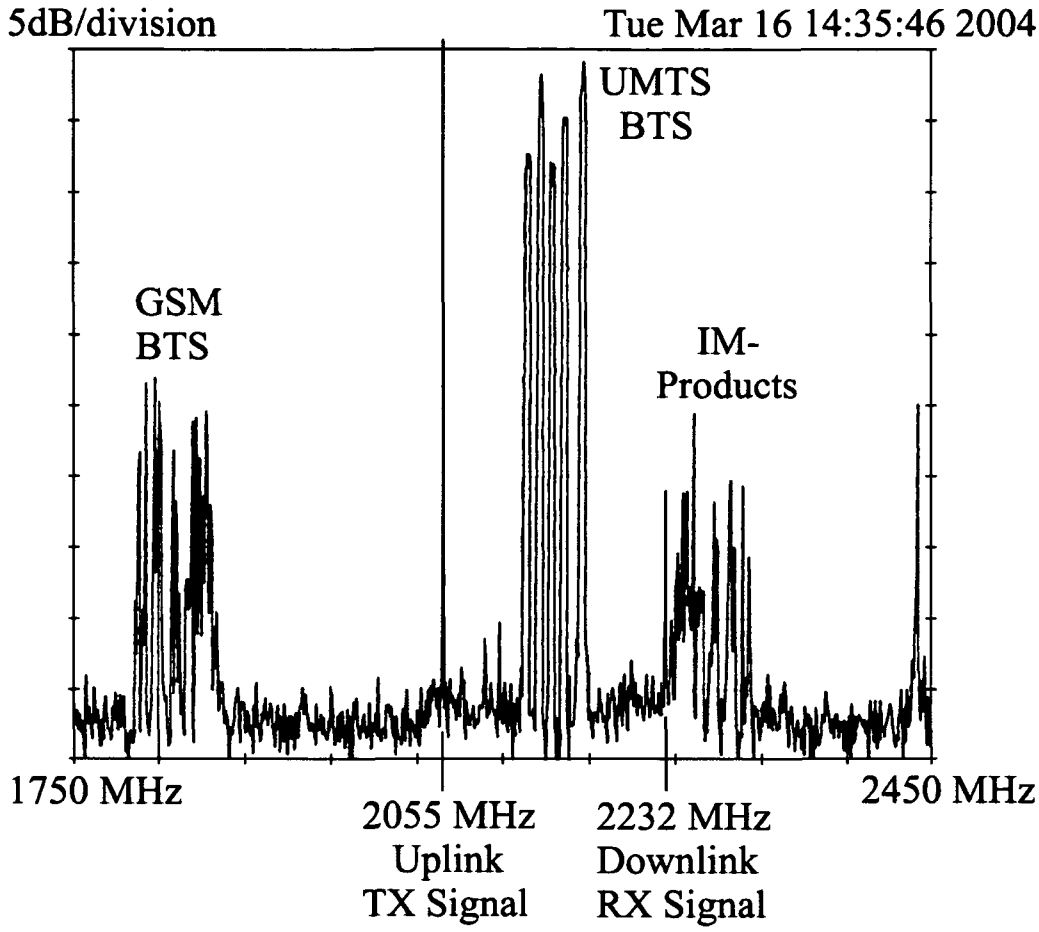

Figure 3.13: Intermodulation spectrum at the output of the low noise amplifier. GSM1800 and UMTS downlink signals are present. Near the receive frequency intermodulation products from the uplink carrier and GSM1800 downlink can be seen. The intermodulation products originating from UMTS downlink are buried into the noise.

there is no desensibilization due to the mobile radio services, the uplink, and the intermodulation products. Therefore no filters in front of the low noise amplifiers are foreseen to keep the best possible sensitivity of the receiving system.

3.4 RSSI/Uplink Performance

For evaluation of the uplink signal strength, we use telemetry data from the RSSI (Receive Signal Strength Indicator) onboard the satellite. In Figure 3.17 such a data set can be seen for a full day of recording, with the RSSI value given in mV. Data for three passes over Vienna in the morning and four passes in the evening are displayed. The RSSI values has to exceed 1000 mV for proper uplink

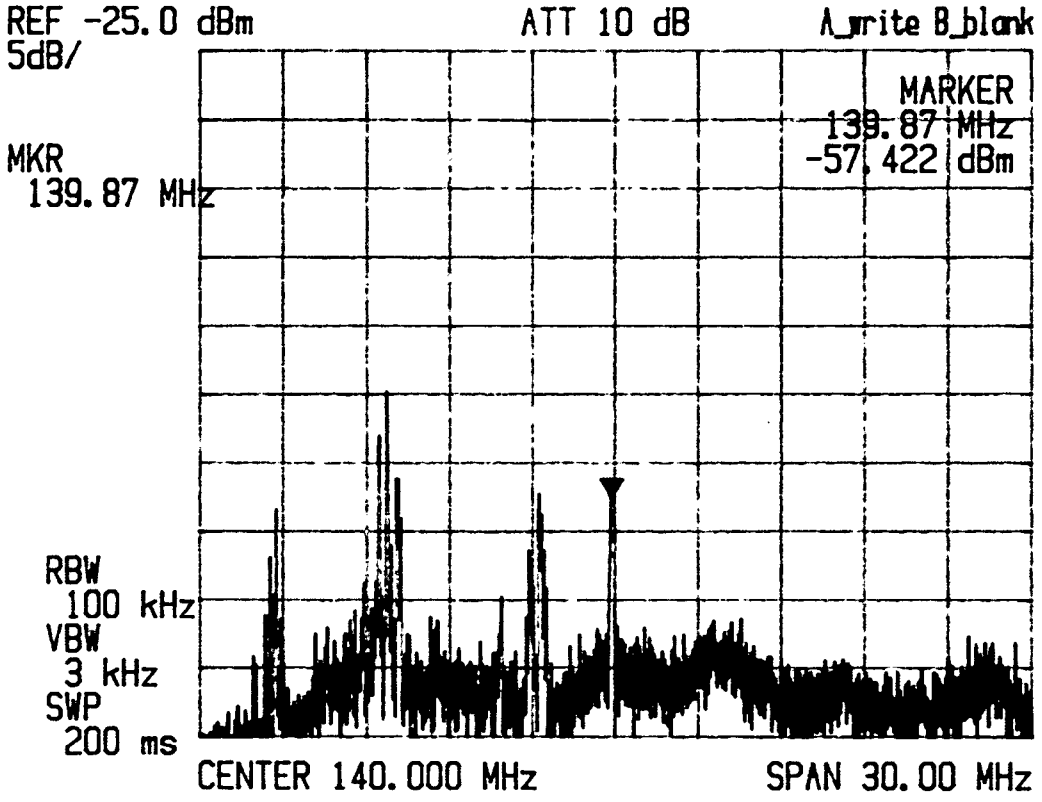

Figure 3.14: Intermodulation spectrum at intermediate frequency. The intermodulation product fall near but not onto the receiver passband.

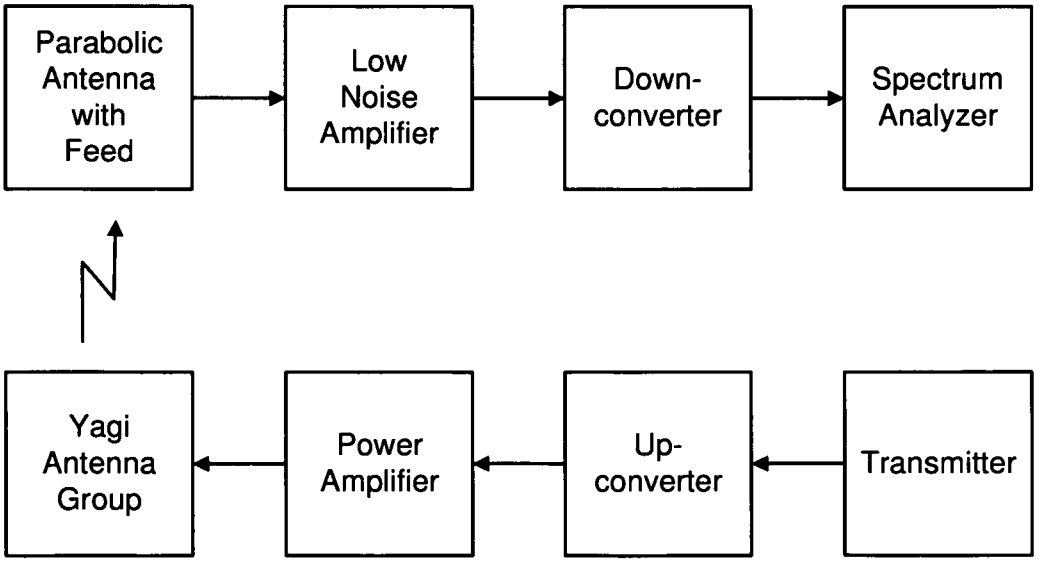

Figure 3.15: Desensibilization measurement set up

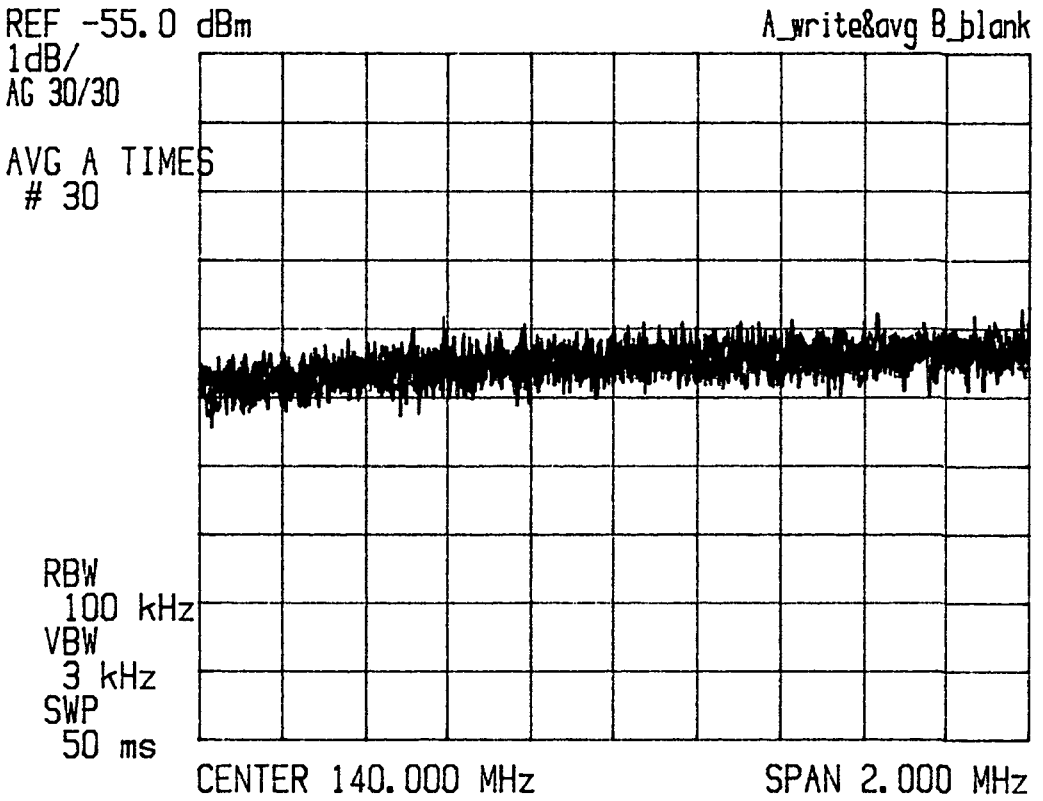

Figure 3.16: Desensibilization measurement result. The red trace is the Sun noise power with transmitter turned on and the green curve is the Sun noise power with the transmitter turned off. Within the measurement accuracy of 0.5 dB no desensibilization was measured.

performance. From Figure 3.17 it can be seen that the uplink signal of the Vienna ground station is sufficiently strong to guarantee the required communication quality.

3.5 Downlink Signal

To see if the signal received from the satellite is sufficiently strong for demodulation, it was measured with a spectrum analyzer. Figure 3.18 shows a spectrum analyzer display from the receive signal.

Expressed in terms of energy per bit E_b and noise power spectral density N_0 from Figure 3.18 one can deduce an E_b/N_0 of roughly 14 dB. This is a very good receive signal with a bit error ratio below 10^{-12}. The design goals of the downlink are obviously met.

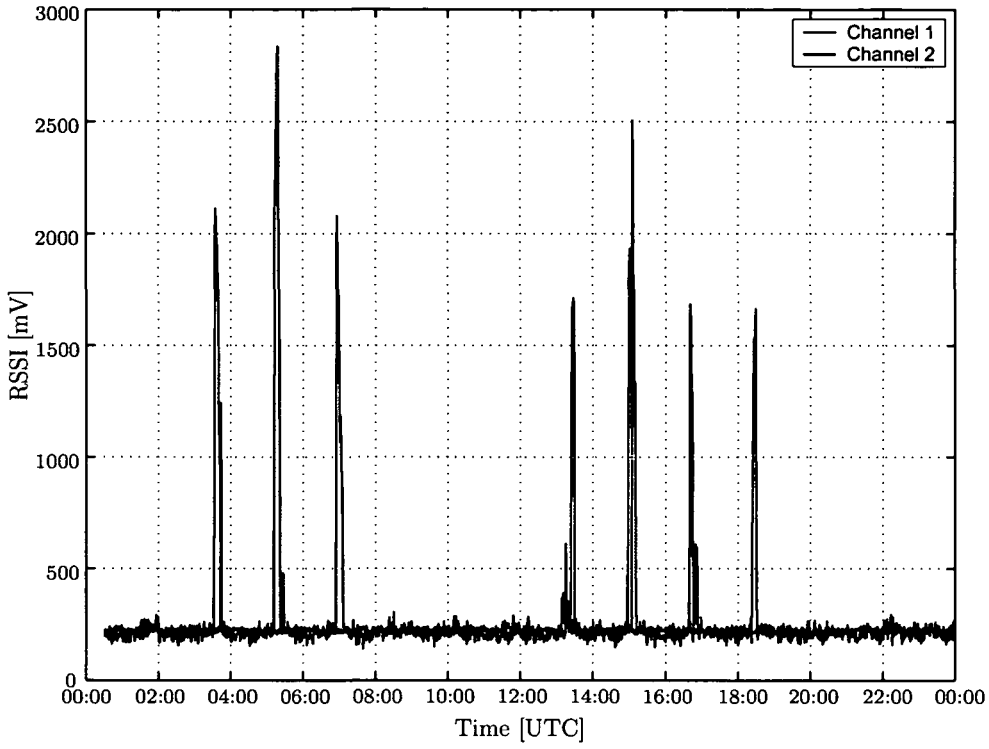

Figure 3.17: Radio Signal Strength Indicator for a whole day. Three passes at dawn and four passes at dusk are shown. Each signal above 1000 mV is sufficiently strong for the required communication quality.

3.6 Antenna Characteristic

To do a careful verification of the design of the antenna feed combination a thorough measurement of the antenna main lobe was done. To measure the beam width of the parabolic antenna the Sun was taken as signal source. The measurement set up is shown in Figure 3.19.

The trajectory of the Sun was calculated with the tracking software NOVA. The antenna pointing position was chosen in a way that the Sun travels trough the center of the main lobe. The position of the Sun and the noise power level of the Sun was measured automatically by the use of the demodulator and the ground station status recording software. In the course of the measurement it was inspected by eye that the shadow of the Sun travels through the center of the dish.

The full width half maximum antenna beam width of a parabolic antenna can be calculated with the empirical relation from [Rothammel 03]

$$\Delta\phi = \Delta\vartheta = \frac{21.3}{Df} \tag{3.17}$$

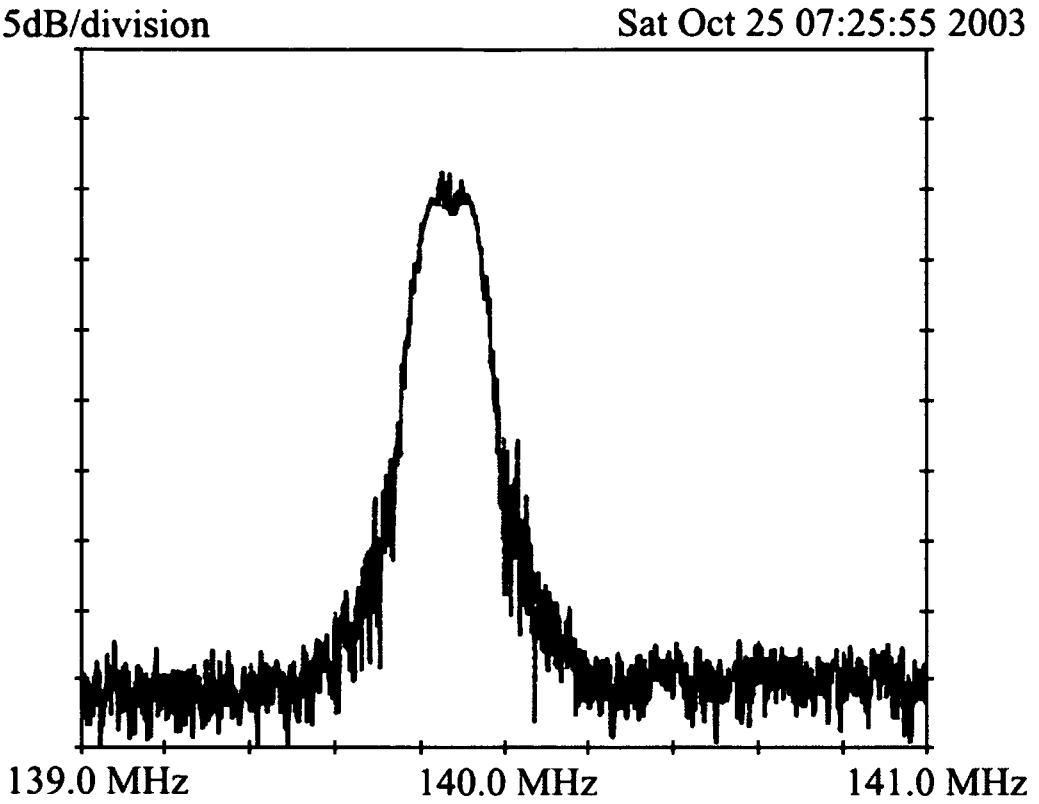

Figure 3.18: Spectrum analyzer display of the receive signal spectrum.

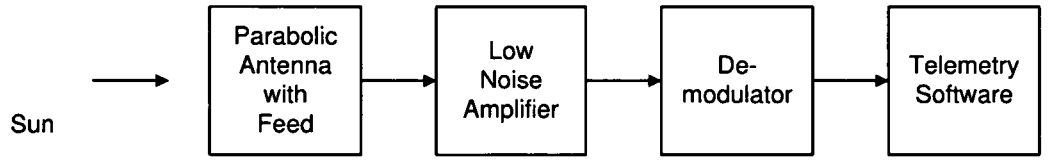

Figure 3.19: Antenna characteristic measurement set up. The Sun is taken as signal source for the antenna characteristic measurement.

where D is the diameter in meter of the antenna and f is the frequency in GHz. For our antenna (parameter see Section 2.3.2) we obtain a full beam width of 3.2°

For the beam width measurement the path of the Sun should move linearly through the main lobe. As can be seen in Figure 3.20 this is approximated very well for the beam width to be checked. The pointing position of the antenna is marked with a red circle. It can be seen that the path is sufficiently linear for a valid measurement.

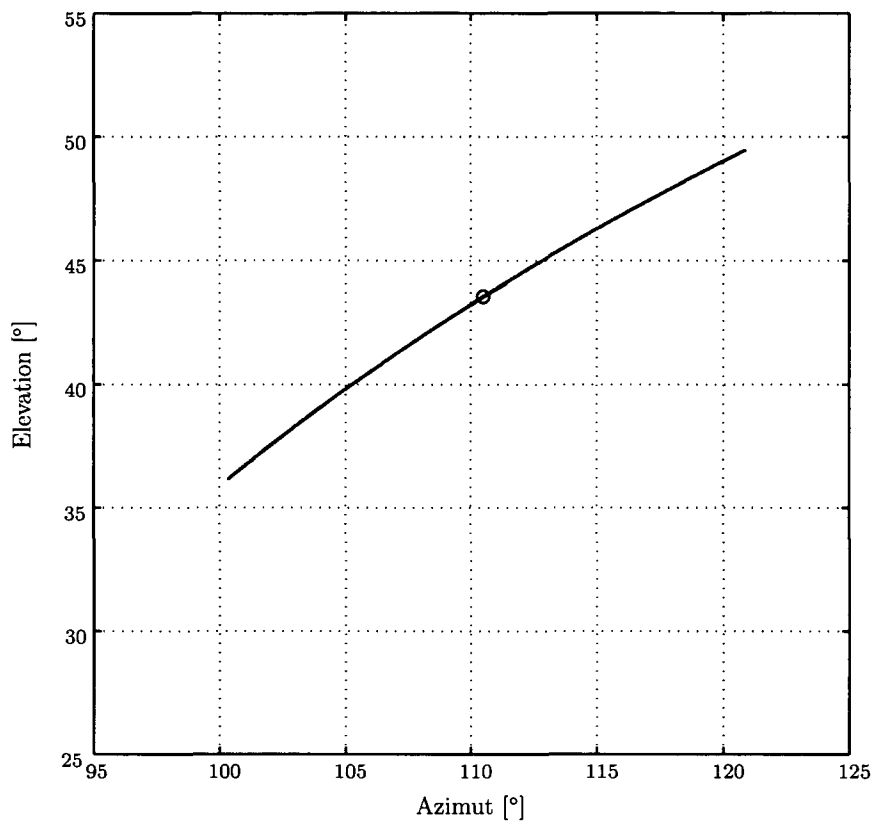

Figure 3.20: Sun path through the main lobe of the parabolic antenna. For the beam width measurement the path of the Sun should move linearly through the main lobe, which is approximated very well.

Figure 3.21 shows the measured antenna beam width of the parabolic antenna. The full 3 dB beam width measured from Figure 3.21 is 3.6 ° with a precision of the measurement of 0.5 °. This is in good agreement with the design target of 3.2°.

3.7 Man Made Noise

At very low elevation angles the communication with the satellite can be disturbed by man made noise. Measurements with a setup according to Figure 3.22 have been performed quantitative analysis of this noise contribution.

In azimuth range from 0° to 360° in steps of 5 ° the noise power was measured at elevation angles ranging from 0° to 3°. The measured noise power was averaged by the spectrum analyzer. The measurement result for the mean man made noise power for vertical polarization is shown in Figure 3.23.

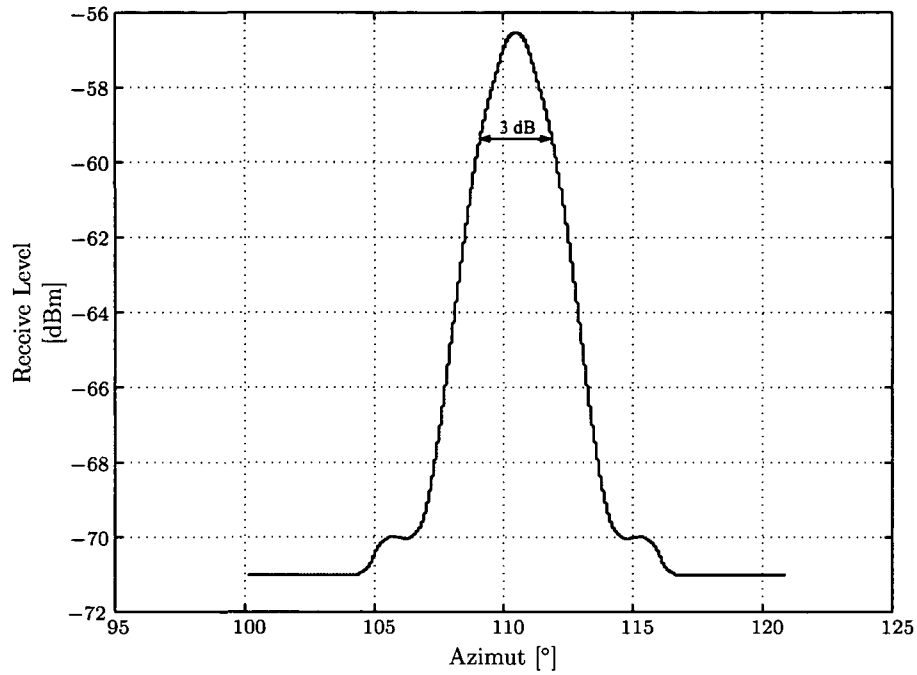

Figure 3.21: Parabolic antenna beam width.

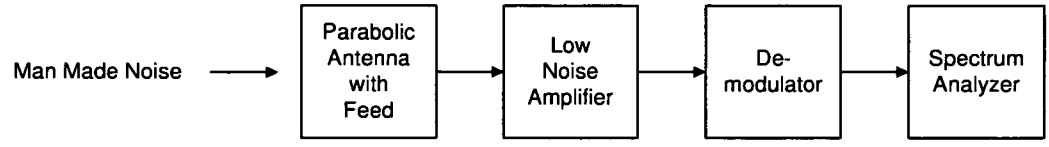

Figure 3.22: Man made noise power measurement setup. In the azimuth range from 0° to 360° at elevation angles ranging from 0° to 3° the noise contribution of man made noise was measured by a spectrum analyzer.

In Figure 3.23 the man made noise for different elevation angles can be seen. Figure 3.23 shows that the noise is very strong if the antenna is pointing to the densely populated inner regions of Vienna. From this picture it is obvious that in the direction of the city no communication below 3° is possible. With increasing elevation angle man made noise decreases. Above an elevation angle of 4° the influence of man made noise to the communication is negligible.

Man made noise has been investigated for the four polarization states vertical polarization, horizontal polarization, left hand circular polarization and right hand circular polarization. Figure 3.24 shows the man made noise in dependence of the polarization state. The measurement has shown that the man made noise at a frequency of 2232 MHz is randomly polarized.

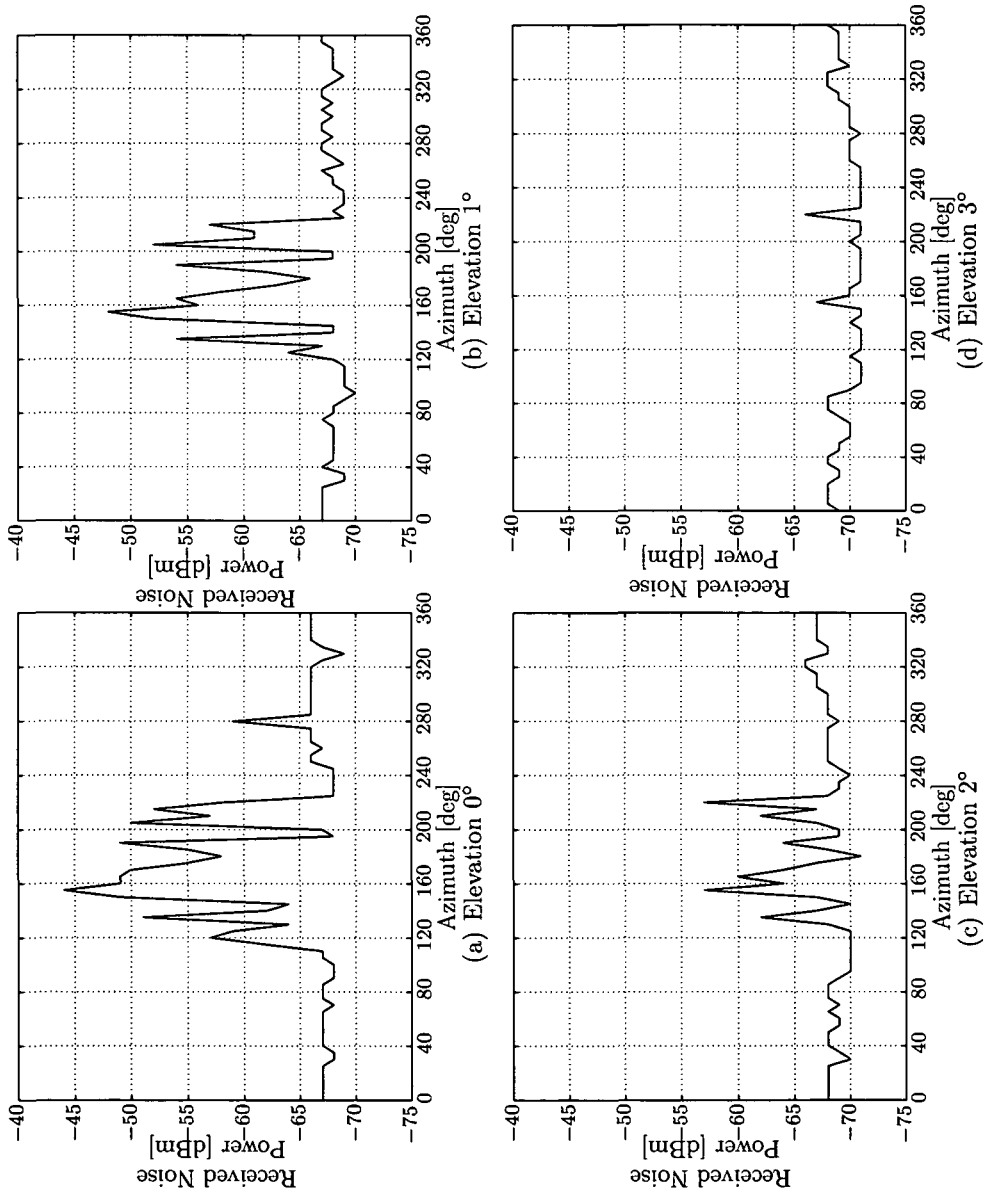

Figure 3.23: Man made noise receive power level.

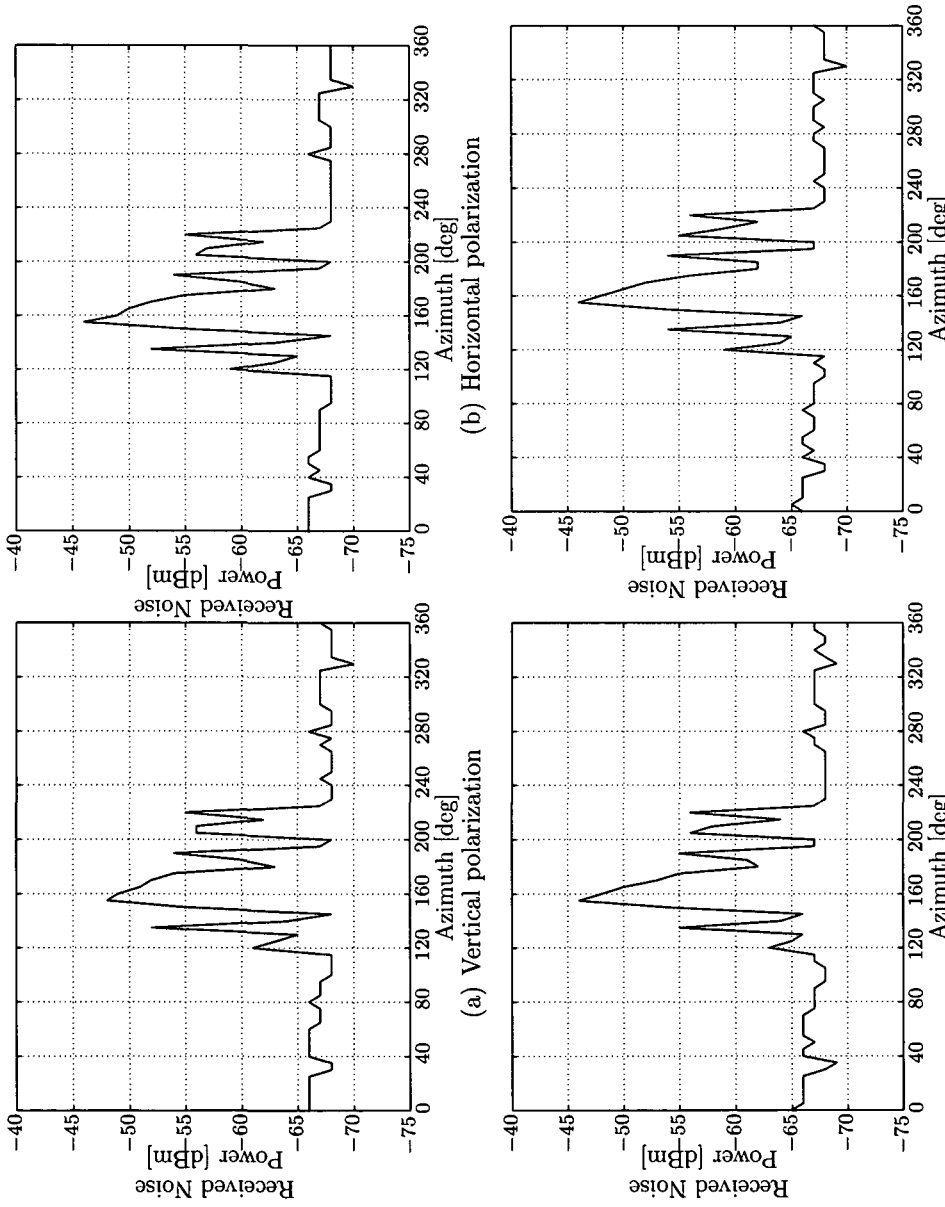

Figure 3.24: Man made noise receive power level at elevation 0° in dependence of the polarization state. The measurement shows that man made noise is randomly polarized.

3.8 Radio Horizon

At each pass of the satellite, parameters of important ground station systems are recorded. From these recorded data the real radio horizon is extracted. From each recorded data set the azimuth and elevation values of the first contact and the last contact are taken. Then the mean elevation value for each azimuth value was calculated. More than 1000 passes of the satellite are used to extract the real radio horizon of the Vienna ground station. The real radio horizon of the Vienna ground station is shown in Figure 3.25.

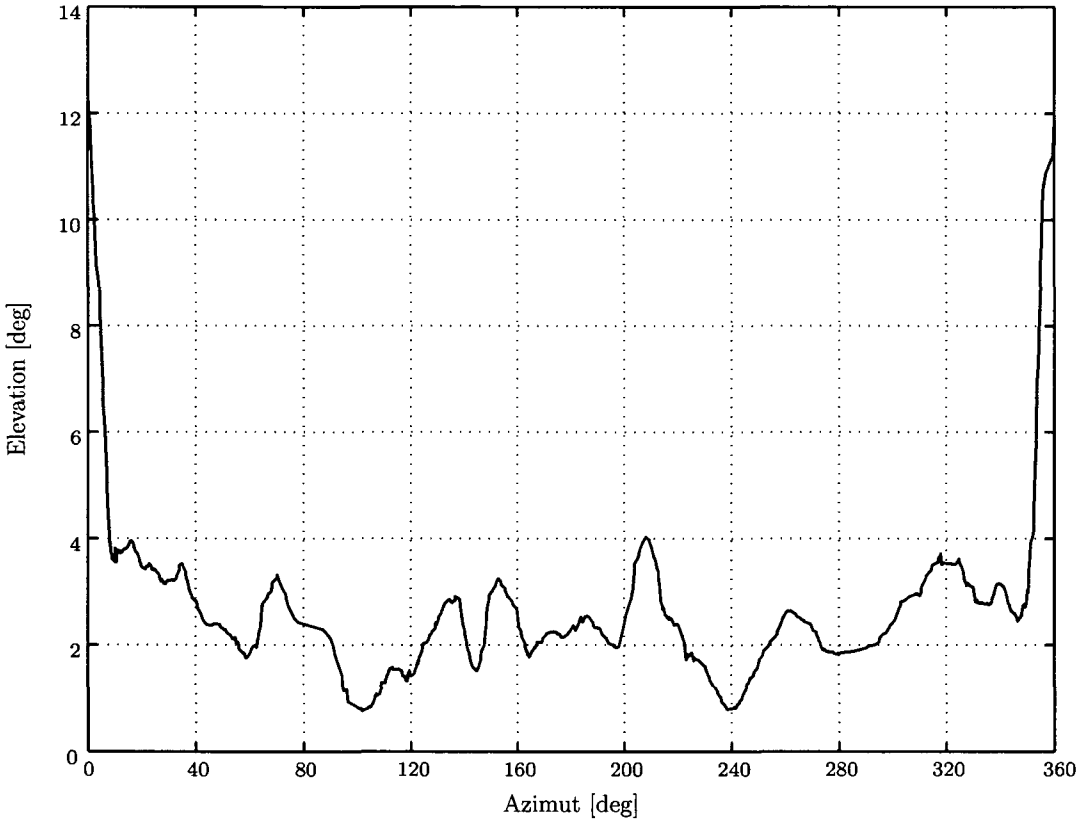

Figure 3.25: Radio horizon calculated from about 1000 overpasses. In the north the dome of the Instiute of Astronomy hinders communication below 12°.

The cardinal point north is at an azimuth angle of 0°. In the north the dome of Institute of Astronomy hinders communication below 12° elevation. Due to natural barriers in the northeast, and from the southwest to north communication below 3° elevation is not possible. From the northeast to the southeast man made noise hinders and not listed natural barriers in the topographic map like trees hinder communication below an elevation angle of 2°.

3.9 Ground Station Performance

To show the performance of the ground station during a whole pass of the satellite two typical cases of an overpass are shown. Most of the passes have a maximum elevation between 20° and 50°. Also approximately one third of all passes are below 10°.

Figure 3.26 shows a first example for one pass of the satellite above the Vienna ground station. The maximum elevation of this pass is 45°. The pass begins in the south, goes over west, and ends in the north. Further parameters of the pass can be seen also in Figure 3.26.

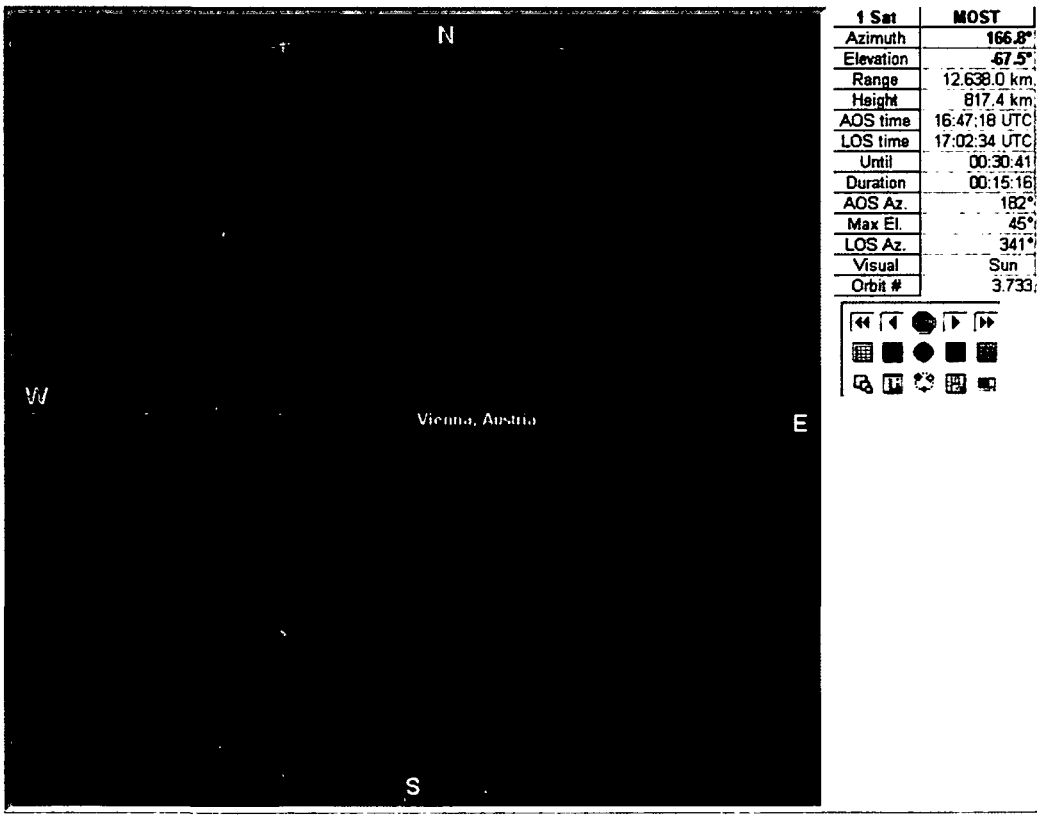

Figure 3.26: Nova screen shot of the MOST Orbit 3733 over Vienna.

The following figures show ground station status data. Figure 3.27 shows the elevation of the pass shown in Figure 3.26 versus time. Figure 3.28 shows the according receive level at the demodulator input. The receive level is highest when the maximum elevation is reached, where the distance to the satellite is smallest. Figure 3.29 shows the E_b/N_0 of the pass versus time. Together with Figure 3.27 one can see that above an elevation of 5° the satellite can be received with an excellent E_b/N_0 of around 15 dB. Above an E_b/N_0 of 8 dB the bit error ratio is

below 10^{-12}. In Figure 3.30 the Doppler shift of the overpass is shown. When the satellite rises above the horizon the Doppler shift is around +50 kHz. At the end of the pass the Doppler shift is around -50 kHz. The values for the Doppler shift are shown in Figure 3.30.

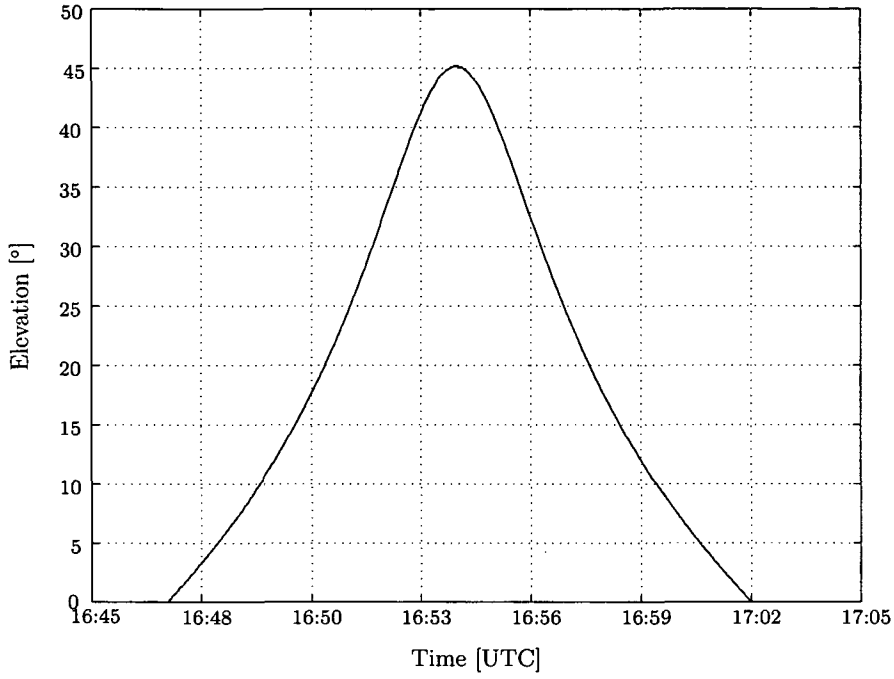

Figure 3.27: Recorded ground station data for the elevation versus time of satellite orbit 3733. The maximum elevation of this orbit is 45°.

The ground station has also a good performance at very low elevation angles. A second example for a pass with a maximum elevation angle of $\theta = 3.5\,°$ is shown. Figure 3.31 shows the path of the satellite over the ground station. If the path of the satellite is compared to the measured radio horizon in Figure 3.25 it can be seen that there is a window where communication to the satellite should be theoretically possible.

Figure 3.32 shows the elevation angle over the time in UTC. According to the elevation angle in Figure 3.32, Figure 3.33 shows the receive power level at the input of the demodulator and Figure 3.34 shows the E_b/N_0 versus time. It can be seen that as soon as a line of sight contact without interference of the town is possible, a strong signal of the satellite will be received. Figure 3.35 shows the Doppler shift.

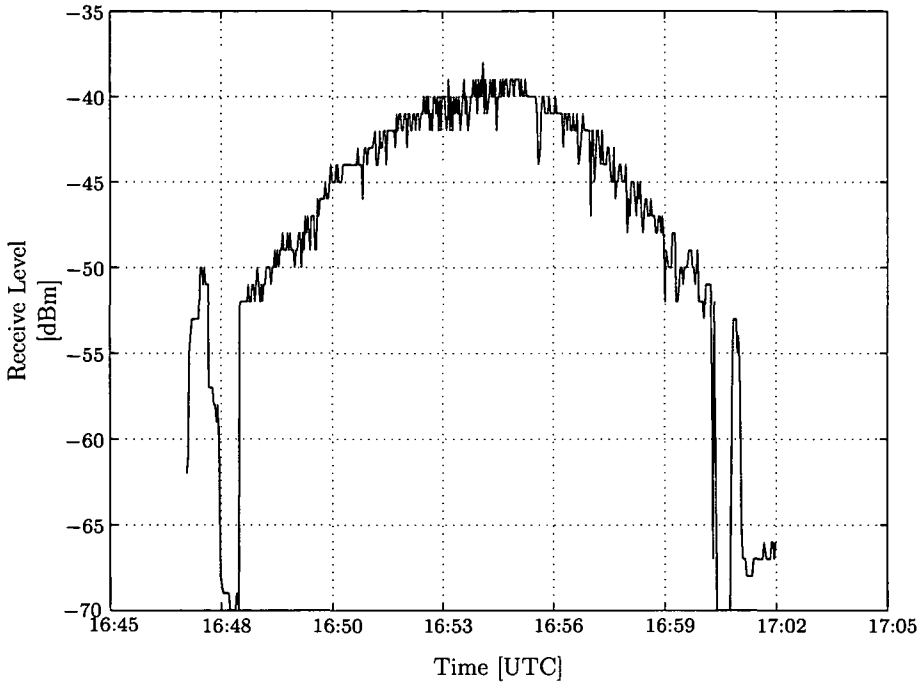

Figure 3.28: Recorded ground station data for the receive level. The receive level is highest where the distance to the satellite is smallest.

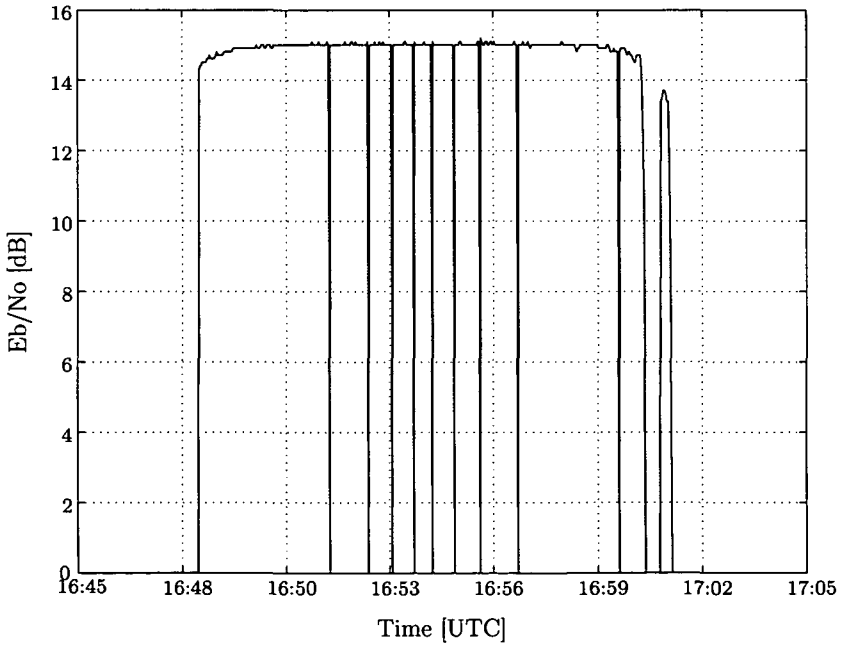

Figure 3.29: Recorded ground station data for the Eb/No. Above an elevation angle of 5° the E_b/N_0 is above 14 dB.

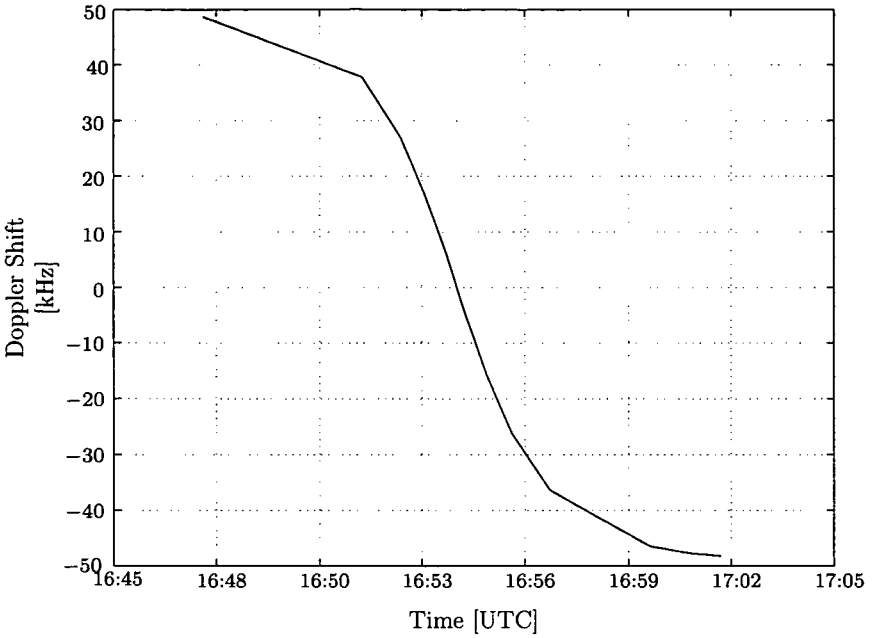

Figure 3.30: Recorded ground station data for the Doppler shift. When the satellite rises the Doppler shift is about +50 kHz, and when the satellite leaves the Doppler shift is about -50 kHz.

If the results of this measurements are compared to the noise power level of the Sun (see Figure 3.3) we can see that in the direction of the main parts of the city the man made noise is stronger than the noise received when the antenna is pointing to the Sun.

3.10 Reliability

An important issue was the reliability of the Vienna ground station. The goal was to reach a successful operation during at least 95 % of the total pass time. The remaining 5 % it was assumed that the station will be offline due to strong winds.

For the calculation of the reliability of the station ground station status data of all recorded passes were used. All recorded passes of the satellite were used for the calculation. The criterion for the reliability calculation were the following: Only passes which have an elevation angle higher than 4 ° were used for the analysis. The 4 ° border was used because below this value communication is not possible in all directions. All passes with a successful communication were marked as good and all others as bad. Also the number of passes below 4 ° was counted.

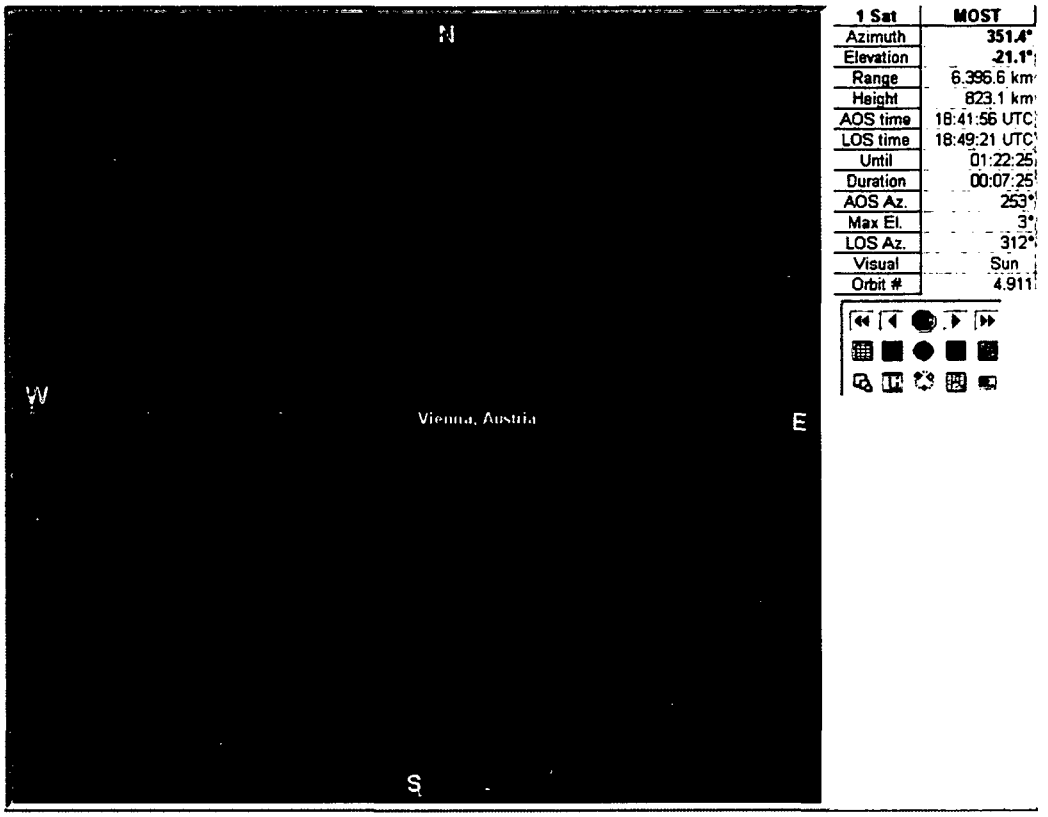

Figure 3.31: Nova screen shot of the MOST Orbit 4911 over Vienna.

The result of the reliability analysis was that in 98 % of the passes successful data download from the satellite was done. Only in 2 % of the overpasses no communication to the satellite could be established. The reason of the overpasses with no communication were strong winds over Vienna so that the antenna was in parking position. Until now no overpasses were lost due to hardware failures.

Also the number of passes with an elevation angle below 4 ° were counted. The result was that one third of all passes over Vienna is below 4 °. Due to the orbit many passes of them are below 1 °. In directions were communication with the satellite is possible a reliable connection to the satellite was established.

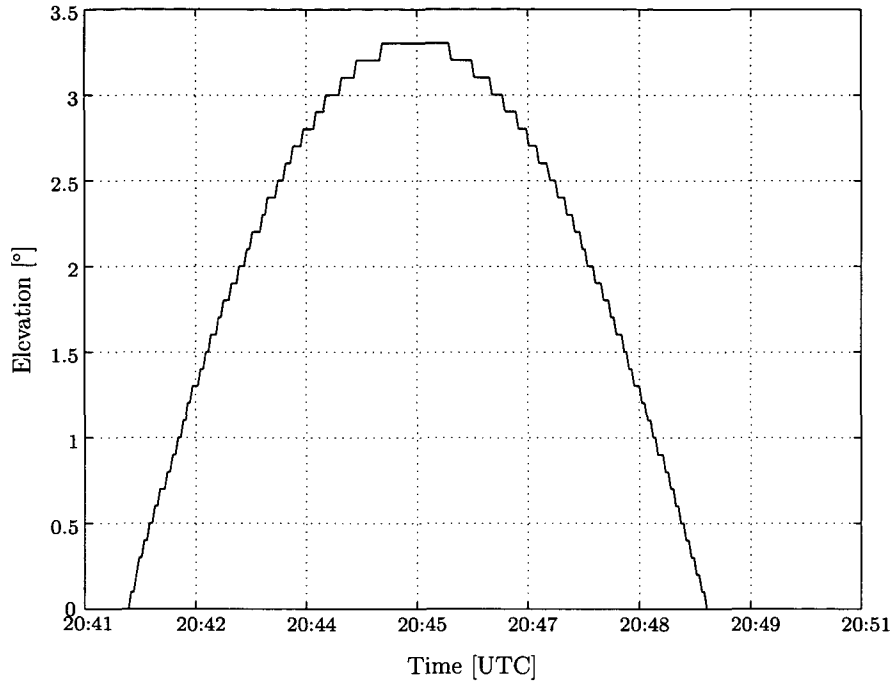

Figure 3.32: Recorded ground station data for the elevation versus time of satellite orbit 4911. The maximum elevation of this orbit is 3.4°.

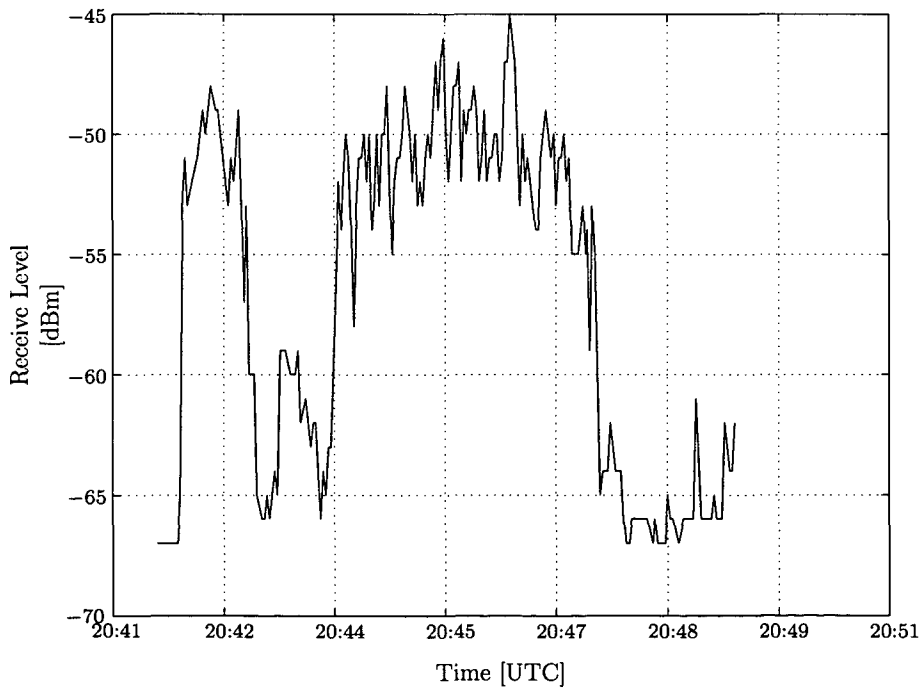

Figure 3.33: Recorded ground station data for the receive level. Due to man made noise and the low elevation angles only slightly changes in the receive power level can be seen.

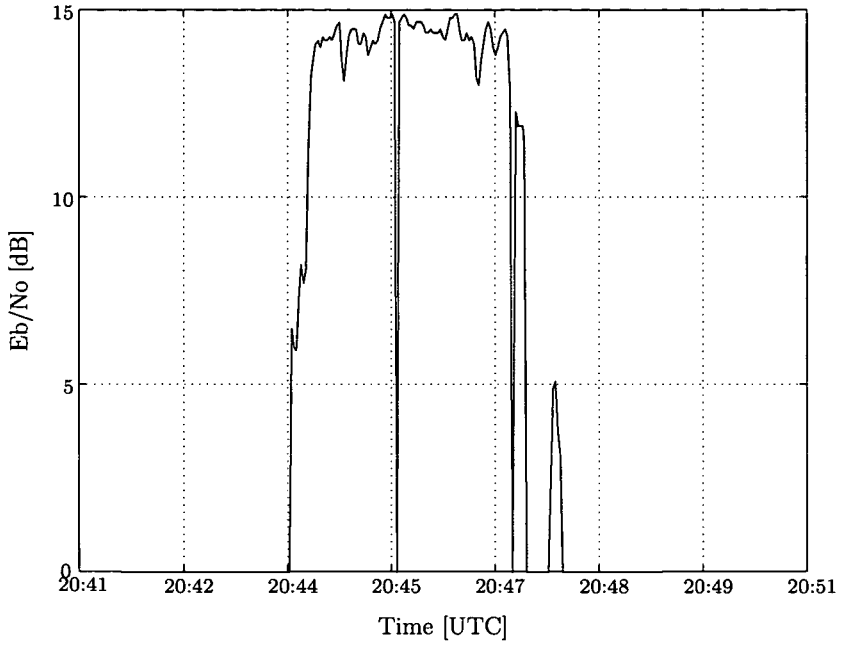

Figure 3.34: Recorded ground station data for the Eb/No. It can be seen that in directions where communication below 4° is possible an excellent E_b/N_0 can be achieved.

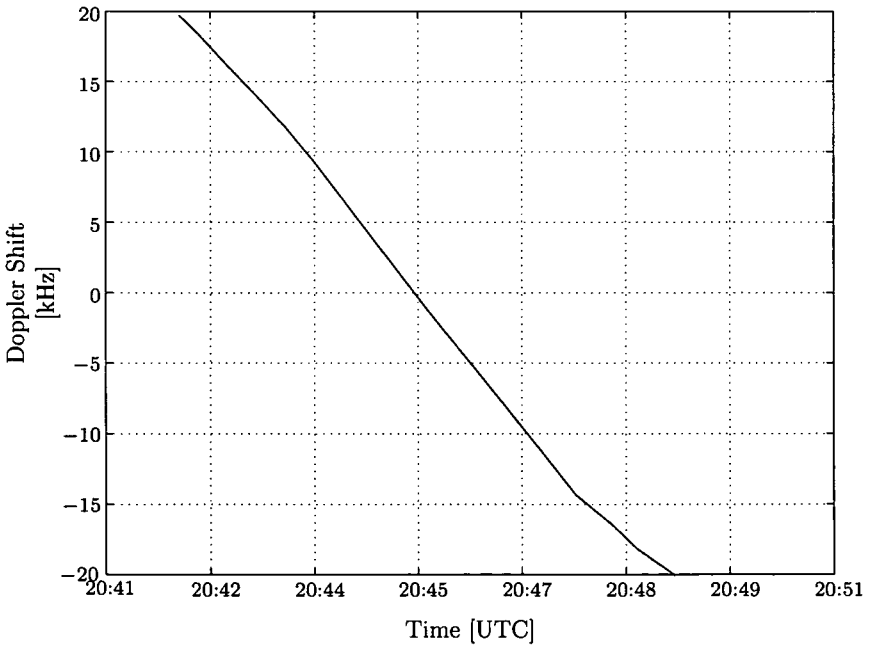

Figure 3.35: Recorded ground station data for the Doppler shift. When the satellite rises the Doppler shift is about +20 kHz, and when the satellite leaves the Doppler shift is about -20 kHz.

Chapter 4

Ground Station Operation

In the previous chapter the design of the station was described. Also measurements done to check the performance are described. This chapter describes the operation of the Vienna ground station.

4.1 Principle of Operation Strategy

The Vienna ground station is one of three ground stations of the project MOST. It was chosen that Toronto will be the control station for coordinating the satellite access. All three ground stations are linked together via Internet. When the satellite is above the station, data communication with the satellite is initiated from the control station. All data will be transferred to the control station. The received data will then be sent to all other ground station sites and stored.

4.2 Operation

For operation of the Vienna ground station two computers are used, one control PC which controls the ground station equipment and the data communication with the satellite, and one for the video observation of the antenna structure. Externalization of video observation on a separate computer has two reasons, first a reduction of data traffic at the control PC, and second safety reasons. Video observation is still possible if a crash of the control computer occurs. This is important for the operator to see the position of the ground station antennas.

The control PC is connected to the Internet as well as to the ground station equipment. All housekeeping functions are controlled locally. Also the tracking of the satellite by the antennas, and Doppler shift correction is controlled locally. Only the data communication of the ground station to the satellite is controlled by the control station in Toronto via Internet. In case of an interruption of the Internet link to the control station only telemetry data can be received from the satellite.

The position of the satellite is determined from it's Keplerian elements. With these elements the position of the satellite for each time instant can be calculated. Because the Keplerian laws are valid only for the idealistic assumption of homogenous gravity, no residual atmosphere, etc., the element set must be updated periodically. All tracking software programs use the NASA two line orbital element set format. The position of all space objects in the Earth orbit are determined by NORAD (North American Aerospace Defense Command) and the orbital elements of most of the satellites can be downloaded at the Celestrak web site [Celestrak]. The NASA two line element set contains the satellite name and the orbital element set. The element set contains information like mean motion, epoch time, inclination, eccentricity, etc. An example for the two line orbital element set for the MOST satellite is:

```
MOST
1 27843U 03031D   03221.95551155  .00000012  00000-0 26139-4 0   332
2 27843  98.7216 228.2890 0009910 184.4683 175.6411 14.19923368 5717
```

A more detailed description of the two line orbital element set format is given in Appendix B.

At the Vienna ground station the program NOVA from Northern Light Software Associates is used for tracking of the satellite. NOVA is familiar with most of the antenna rotator controller units which allows a straightforward setup of tracking. With the NASA two line element set as input the actual position of the satellite and the time of a pass is predicted. A screen shot of NOVA is presented in Figure 4.1.

On the left is the sphere around the ground station antenna. The circles are circles of constant elevation where the mid point stands for an elevation of 90° and the outermost circle stands for an elevation of 0°. The lines from the mid point to the outermost circle are the four cardinal points north, east, south and west. The text column on the right shows information about the position of the satellite. There we can find the height of the satellite above the earth surface, the time until the next contact, the duration of the next pass, the maximum elevation of the next pass, the orbit number of the satellite, the azimuth angle of acquisition of signal (AOS) and loss of signal (LOS), the range to the satellite from the ground station, and the azimuth and elevation angle for pointing to the satellite. This program also controls the tracking of the antennas via the rotator controller unit. Further information about the position of the satellite is provided to the data communication program MUXLocal. After a pass the tracking program moves the antenna into the safe parking position.

The program MUXLocal is responsible for control of the data communication. This program acts as interface between the control station and our ground station. MUXLocal is connected to the communication equipment of the ground station (FM modulator, BPSK demodulator, TNC) as well as to the tracking program.

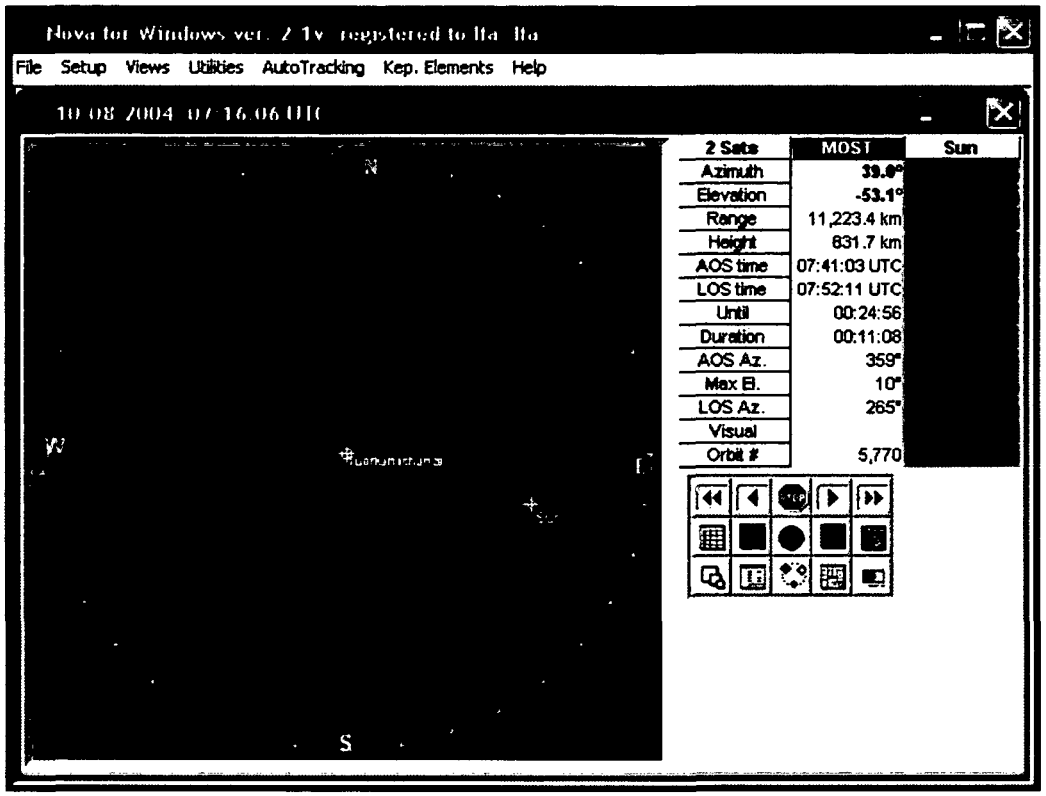

Figure 4.1: Screen shot of tracking software NOVA. On the left the path of the satellite for the next or ongoing overpass is shown. On the right the different parameters of all chosen satellites and celestial objects are shown.

If NOVA reports to MUXLocal that the satellite rises above the horizon the communication to the satellite is initiated. The transmitter will be turned on and data communication is started. The data downloaded from the satellite are received by MUXLocal and immediately transmitted via Internet to the ground station. Also an upload of an upgraded satellite software from the control station to the satellite is possible via MUXLocal. Figure 4.2 shows a screenshot of MUXLocal. The text box on the top shows all modules which are connected to the ground station. In the example shown two local modules and two modules from the control station are connected to MUXLocal. The text box below displays the data downloaded from the satellite. The third text box shows the data uploaded to the satellite (in most cases acknowledgment of correct received data packets). Below the text boxes buttons for connecting the communication equipment to MUXLocal can be seen. For MUXLocal two external modules exist, one monitor software called MUXMonitor and one control software called MUXControl.

MUXMonitor allows observation of the data communication and the status of the communication equipment via Internet. Figure 4.3 shows a screen shot of

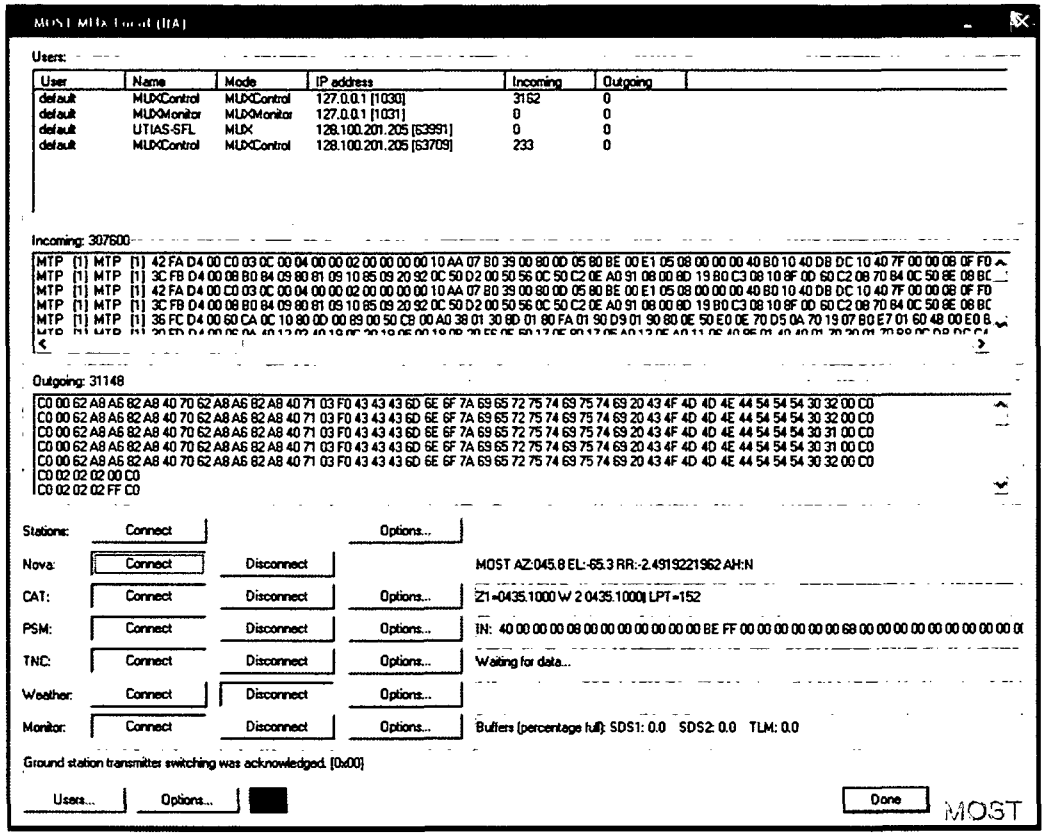

Figure 4.2: Screen shot of MUXLocal. The top text box shows the connected modules, the middle text box the downloaded data and the bottom text box the uploaded data. Below the text boxes buttons for connecting the communication equipment can be seen.

MUXMonitor.

The list box on the left shows the data downloaded from the satellite. The text box on the right shows the data uploaded to the satellite. At the tabs below information about the status of transmitter and receiver is presented. Also the satellite access strategy as well as the information provided by NOVA is displayed. With MUXMonitor only observation and no change of any parameter of the communication system is possible.

With MUXControl the strategy of the data communication is set. It can be chosen if a software to the satellite is uploaded or if observed data stored on the satellite are downloaded. Further the selection of the communication channel is done. The program offers the possibility to select either channel A or channel B or both channels simultaneously as well as an automatic selection of the communication channel. Figure 4.4 shows a screen shot of the MUXControl.

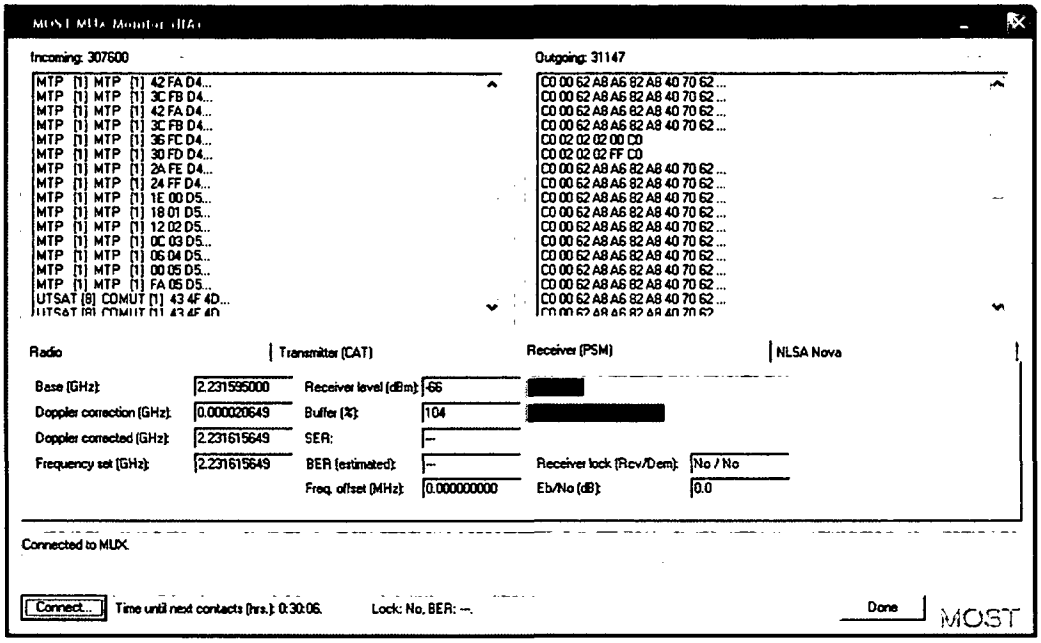

Figure 4.3: Screen shot of MUXMonitor. On the left text box the downloaded data and on the right text box the uploaded data can be seen. The tabs below provide information about the status of transmitter receiver, the satellite access strategy and displays information provided by NOVA.

In the frame V53 the communication mode (software upload or data download) can be chosen. The frame TNC allows to turn on, turn off or automatically operate the TNC relay. The TNC relay is used to turn on and off the power supply for the power amplifier. With the frame CAT the transmitter can be turned on or off or automatically selected. The ground station frame enables or disables tracking of the satellite. The frame Radio allows a selection of the communication channel.

All status data of the demodulator as well as the data provided from NOVA and the wind speed are recorded by a so called ground station telemetry program. These data are used to check the health and the performance of the Vienna ground station. Also long term statistics about the performance of the station is possible with the recorded data. A Matlab script allows a fast visualization and analysis of the recorded status data.

Remote control of the Vienna ground station is also possible. For remote access to the ground station computer the program tightvnc is used. This program shows the desktop of the ground station computer on each computer which is running a VNCViewer client program independent from the operating system. In the desktop of the ground station computer shown, all commands can be done in the same way as if sitting at the console of the ground station computer.

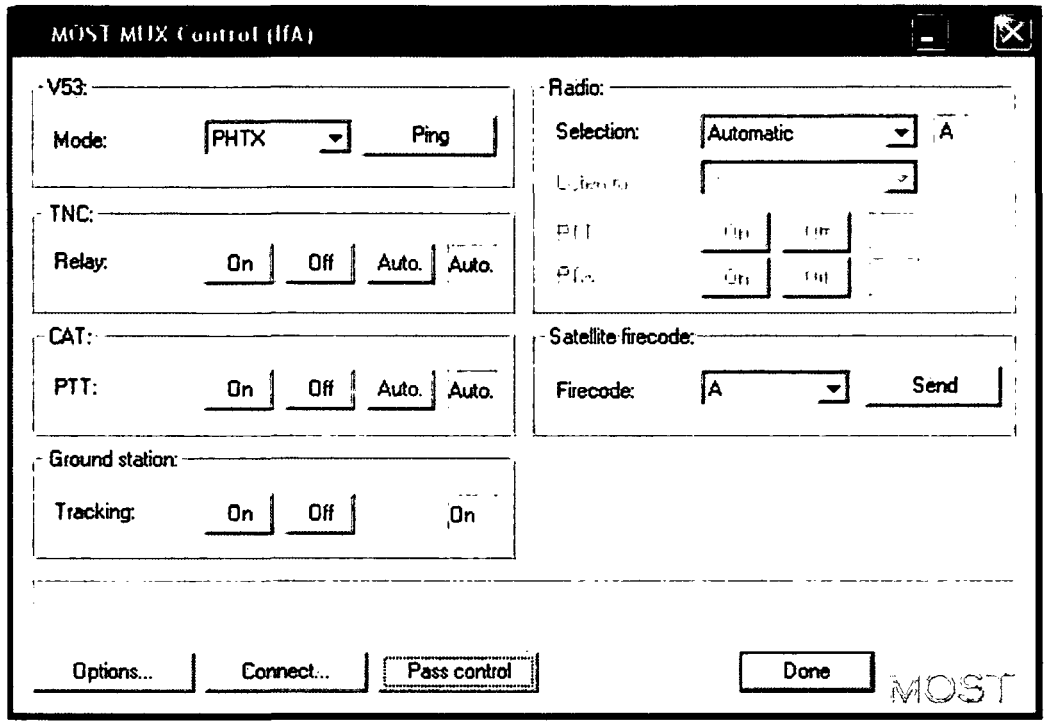

Figure 4.4: Screen shot of MUXControl. Different parameters like software upload or data download, channel selection, turning on and off the transmitter and the power amplifier, and enable or disable tracking can be selected.

A firewall at the control computer as well as on the video observation computer ensures that only authorized operators have access.

The ground station operates fully automated. The clock of the computer and the two line orbital elements are updated weekly by the tracking program NOVA. Three minutes before a satellite pass the tracking program moves the antenna to the predicted position where the satellite will rise above the horizon. During the pass the antenna will track the satellite. If the satellite overpass is done the antenna will be moved into the safe parking position. To save power, the communication system of the satellite is in a stand-by mode if no contact with a ground station is possible. At the beginning of a satellite pass the communication system of the satellite will be activated by the ground station. Then the data collected by the satellite will be downloaded.

If the wind speed exceeds 50 km/h the antenna will be moved into or kept in the safe parking position. If the wind speed falls below 20 km/h the antenna pointing system is re-enabled.

The MOST satellite detects luminosity variations of stars. Dependent on the brightness of the observed star the exposure time of the CCD (Charged Coupled Device) is varied. The largest gap in communication between the ground stations is about three hours. In the case that the exposure time is 30 s, there are 21.610 data sets in the memory of the satellite waiting for download. Such a data set contains one picture of the main target which is spread by a Fabry lens over a larger number of pixels. Further several secondary targets are on the picture. The first picture of the MOST satellite received by the Vienna ground station is shown in 4.5.

One primary target with the form of a doughnut, and five secondary targets can be seen. As it can be seen in Figure 4.5 only a square which contains the target and is a little bit larger than the target is stored due to limited memory reasons. The secondary targets are observed in the open field of the science CCD detector. Due to the tracking jitter the target is smeared over a few pixels. The primary target has the shape of a doughnut. This shape of the doughnut is the image of the telescope entrance pupil focused on the science detector by the Fabry lenses.

From the downloaded data sets one target is chosen and all pictures of this target are combined to a so called light curve. A light curve shows the variations of brightness of a star versus time. With Fourier analysis the spectrum of the light curve is calculated. From this spectrum predictions about the inner structure and the age of a star are done by the use of Asteroseismology. The longer the observation time, the more accurate predictions of the parameters of the star can be done. As an example the light curve of an observed star is presented in Figure 4.6.

As an example for a spectrum calculated from a light curve the pulsating spectrum of our Sun is presented in Figure 4.7.

The analysis of the first observed star *Procyon* results in a discussion between the experts in the field of Asteroseismology. It was assumed that Procyon is a Sun-like star with a pulsation period of 15 min. With the MOST satellite no pulsations of Procyon were detected. This findings were published in the journal *Nature*.

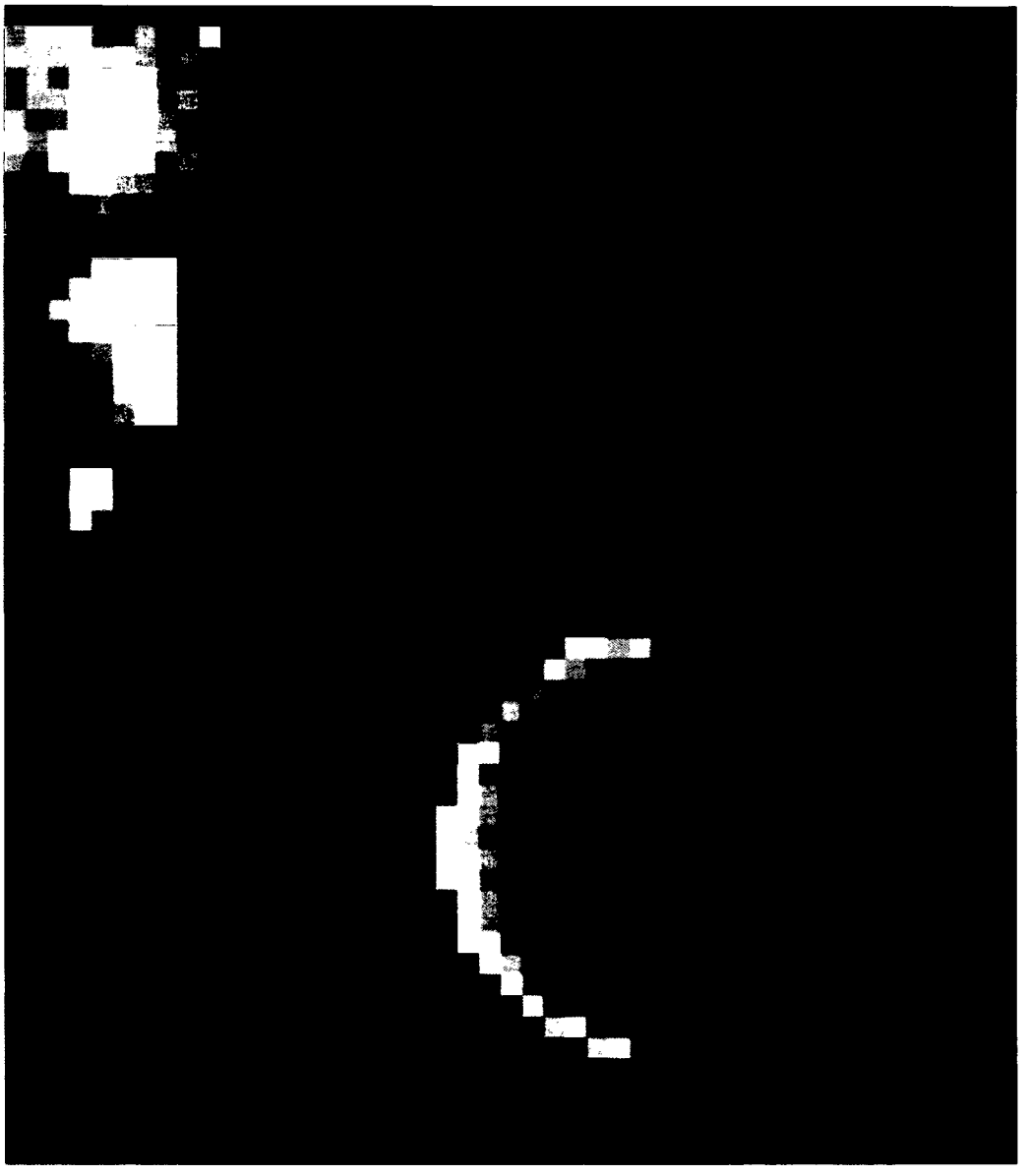

Figure 4.5: First picture recorded by MOST. On the left five directly detected secondary targets can be seen. On the lower right the primary target is shown. A Fabry lens spreads the light of the primary target over a larger number of pixels.

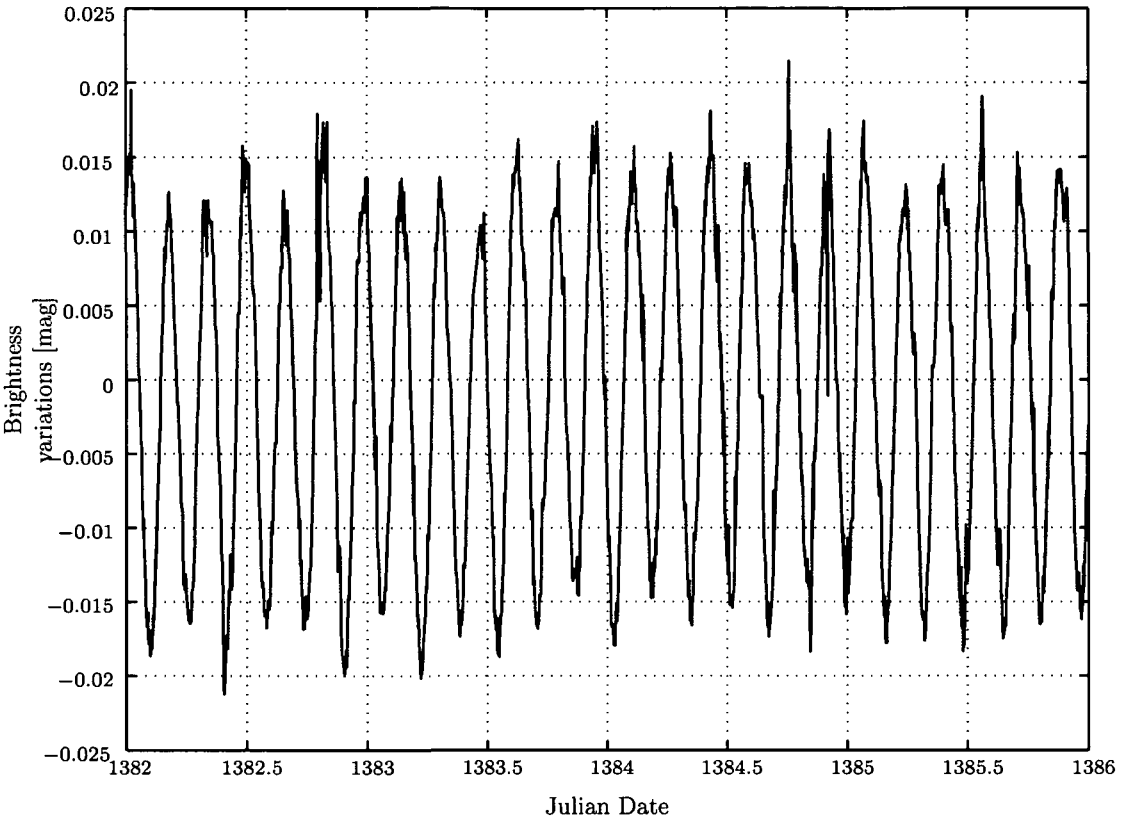

Figure 4.6: Light curve of a pulsating star. A light curve shows the brightness variations of a star versus time.

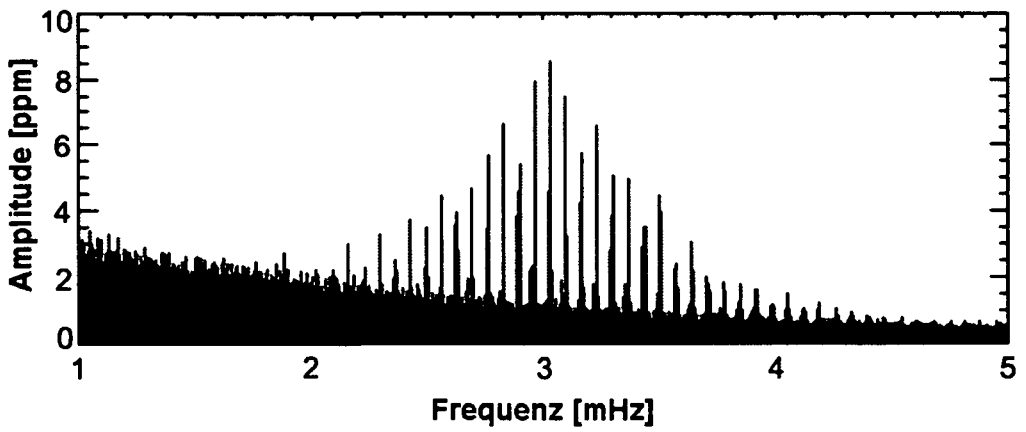

Figure 4.7: Pulsating spectrum of our Sun. Our Sun pulsates with a period of 5 min.

Summary and Conclusions

The goal of this work was to answer the following questions: Is it possible to build a fully automated ground station in urban environment at costs affordable for Universities? Will possible intermodulation products due to mobile radio services interfere with the receive signal? How strong is the impact of man made noise to the receive system?

The design, setting up and operating of a fully automated satellite ground station in urban environment was described. Measurements documenting the quality of the communication link between ground station and satellite and the reliability of the ground station were presented.

The measurements show that the intermodulation products fall near but not onto the receive frequency and do not hinder proper communication. Further it was shown that man made noise at the receive frequency and very low elevation angles can reach a higher level than the noise power received of the Sun, when the antenna is directed to the Sun. In the azimuth range pointing to the inner city communication is not possible for elevation angles below 3 ° due to the interference from man made noise.

Since September 2003 the ground station downloads data from the satellite. From January 2004 on the station works in an unmanned autonomous mode. The Keplerian elements necessary for antenna pointing are regularly updated automatically from Celestrak via the Internet. Monitoring equipment was provided to ensure a safe operation of the ground station. Remote access enables the change of ground station parameters manually.

The reliability of the ground station was analyzed considering all recorded satellite passes over Vienna. In 98 % of the satellite passes successful data download from the satellite was done. At the remaining 2 % the operation of the ground station was not possible due to strong winds.

In summary it has been shown that setting up and operating of a fully automated ground station in an urban environment with a budget of 50.000 Euro is possible. The communication system of the ground station works with excellent performance.

Appendix A

Mobile Radio Frequencies

In this Appendix the frequencies and the corresping service providers are listed for GSM1800 and UMTS [RTR]. Also the intermodulation products are listed.

The frequencies and the corresponding service providers for GSM1800 are listed in table A.1, where f_u is the uplink frequency and f_d is the downlink frequency.

The third order intermodulation products originated from the ground station uplink and the GSM1800 downlink signals will fall near the passband of the receiver. In particular the product $2f_t - f_d$ is of interest. These intermodulation products are listed in Table A.2.

The UMTS-FDD frequencies with the corresponding service provider [RTR] are listed in Table A.3.

In particular the product from $2f_d - f_t$ is of interest. These intermodulation products which appear at the output of the preamplifier, are presented in Table A.4.

Channel	f_u	f_d	Provider
512	1710.2MHz	1805.2MHz	TMA(T-Mobile Austria)
521	1712.0MHz	1807.0MHz	TMA
523	1712.4MHz	1807.4MHz	Mobilkom
573	1722.4MHz	1817.4MHz	Mobilkom
575	1722.8MHz	1817.8MHz	Free
584	1724.6MHz	1819.6MHz	Free
586	1725.0MHz	1820.0MHz	Telering
617	1731.2MHz	1826.2MHz	Telering
619	1731.6MHz	1828.8MHz	Mobilkom
630	1733.8MHz	1828.8MHz	Mobilkom
632	1734.2MHz	1829.2MHz	One
659	1739.6MHz	1834.6MHz	One
661	1740.0MHz	1835.0MHz	TMA
666	1741.0MHz	1836.0MHz	TMA
668	1741.4MHz	1836.4MHz	Mobilkom
673	1742.4MHz	1837.4MHz	Mobilkom
675	1742.8MHz	1837.8MHz	TMA
680	1743.8MHz	1838.8MHz	TMA
682	1744.2MHz	1839.2MHz	Telering
699	1747.6MHz	1842.6MHz	Telering
701	1748.0MHz	1843.0MHz	TMA
712	1750.2MHz	1845.2MHz	TMA
714	1750.6MHz	1845.6MHz	Telering
736	1755.0MHz	1850.0MHz	Telering
738	1755.0MHz	1850.4MHz	Mobilkom
743	1756.4MHz	1851.4MHz	Mobilkom
745	1756.8MHz	1851.8MHz	TMA
750	1717.8MHz	1812.8MHz	TMA
752	1718.2MHz	1813.2MHz	One
868	1781.4MHz	1876.4MHz	One

Table A.1: Frequency allocation table of GSM1800.

f_t	f_d	$2f_t - f_d$
2055 MHz	1805.2 MHz	2304.8 MHz
2055 MHz	1807.0 MHz	2293.0 MHz
2055 MHz	1807.4 MHz	2292.6 MHz
2055 MHz	1817.4 MHz	2282.6 MHz
2055 MHz	1817.8 MHz	2292.2 MHz
2055 MHz	1819.6 MHz	2290.4 MHz
2055 MHz	1820.0 MHz	2290.0 MHz
2055 MHz	1826.2 MHz	2283.8 MHz
2055 MHz	1828.8 MHz	2283.4 MHz
2055 MHz	1828.8 MHz	2281.2 MHz
2055 MHz	1829.2 MHz	2280.8 MHz
2055 MHz	1834.6 MHz	2275.4 MHz
2055 MHz	1835.0 MHz	2275.0 MHz
2055 MHz	1836.0 MHz	2274.0 MHz
2055 MHz	1836.4 MHz	2273.6 MHz
2055 MHz	1837.4 MHz	2272.6 MHz
2055 MHz	1837.8 MHz	2272.2 MHz
2055 MHz	1838.8 MHz	2271.2 MHz
2055 MHz	1839.2 MHz	2270.8 MHz
2055 MHz	1842.6 MHz	2267.4 MHz
2055 MHz	1843.0 MHz	2267.0 MHz
2055 MHz	1845.2 MHz	2264.8 MHz
2055 MHz	1845.6 MHz	2264.4 MHz
2055 MHz	1850.0 MHz	2260.0 MHz
2055 MHz	1850.4 MHz	2259.6 MHz
2055 MHz	1851.4 MHz	2258.6 MHz
2055 MHz	1851.8 MHz	2258.2 MHz
2055 MHz	1812.8 MHz	2297.2 MHz
2055 MHz	1813.2 MHz	2296.8 MHz
2055 MHz	1876.4 MHz	2233.6 MHz

Table A.2: Third order intermodulation products originating from ground station uplink and GSM1800 downlink.

Provider	f_u	f_d
Mobilkom	1922.8 MHz	2112.8 MHz
Mobilkom	1927.6 MHz	2117.6 MHz
Hutchison	1932.6 MHz	2122.6 MHz
Hutchison	1937.4 MHz	2127.4 MHz
TRA3G	1942.4 MHz	2132.4 MHz
TRA3G	1947.2 MHz	2137.2 MHz
One	1952.2 MHz	2142.2 MHz
One	1957.2 MHz	2147.2 MHz
Mobilkom	1962.2 MHz	2152.2 MHz
TMA	1967.2 MHz	2157.2 MHz
TMA	1972.2 MHz	2162.2 MHz
TMA	1977.2 MHz	2167.2 MHz

Table A.3: UMTS frequency allocation table.

f_t	f_d	$2f_d - f_t$
2055 MHz	2112.8 MHz	2170.6 MHz
2055 MHz	2117.6 MHz	2180.2 MHz
2055 MHz	2122.6 MHz	2190.2 MHz
2055 MHz	2127.4 MHz	2199.4 MHz
2055 MHz	2132.4 MHz	2209.8 MHz
2055 MHz	2137.2 MHz	2219.4 MHz
2055 MHz	2142.2 MHz	2229.4 MHz
2055 MHz	2147.2 MHz	2239.4 MHz
2055 MHz	2152.2 MHz	2249.4 MHz
2055 MHz	2157.2 MHz	2259.4 MHz
2055 MHz	2162.2 MHz	2262.4 MHz
2055 MHz	2167.2 MHz	2279.4 MHz

Table A.4: Third order intermodulation products origination from ground station uplink and UMTS-FDD downlink.

Appendix B

NASA Two-Line Element Set

The current position of the satellite is determined from the control computer by the Keplerian element set. The Keplerian element set is given in the NASA two-line element set. An example for the two-line element set is:

```
MOST
1 27843U 03031D   03221.95551155  .00000012  00000-0 26139-4 0   332
2 27843  98.7216 228.2890 0009910 184.4683 175.6411 14.19923368 5717
```

The title line contains the satellite name which can have the length of eleven characters. The following two lines contains the orbital parameters of the satellite. Following the parameters of the two lines are explained [Celestrak].

Line 1

Column	Meaning
01	Line Number of Element Data
03-07	Satellite Number
08	Classification (U=Unclassified)
10-11	International Designator (Last two digits of launch year)
12-14	International Designator (Launch number of the year)
15-17	International Designator (Piece of the launch)
19-20	Epoch Year (Last two digits of year)
21-32	Epoch (Day of the year and fractional portion of the day)
34-43	First Time Derivative of the Mean Motion
45-52	Second Time Derivative of Mean Motion (decimal point assumed)
54-61	BSTAR drag term (decimal point assumed)
63	Ephemeris type
65-68	Element number
69	Checksum (Modulo 10) (Letters, blanks, periods, plus signs = 0; minus signs = 1)

Line 2

Column	Meaning
01	Line Number of Element Data
03-07	Satellite Number
09-16	Inclination [Degrees]
18-25	Right Ascension of the Ascending Node [Degrees]
27-33	Eccentricity (decimal point assumed)
35-42	Argument of Perigee [Degrees]
44-51	Mean Anomaly [Degrees]
53-63	Mean Motion [Revolutions per day]
64-68	Revolution number at epoch [Revolutions]
69	Checksum (Modulo 10)

The parameters of the two lines are identical for the NASA and the NORAD two-line element set. NORAD maintains general perturbation element sets on all resident space objects. These element sets are periodically refined so as to maintain a reasonable prediction capability on all space objects.

The NORAD element sets are "mean" values obtained by removing periodic variations in a particular way. In order to obtain good predictions, these periodic variations must be reconstructed (by the prediction model) in exactly the same way they were removed by NORAD.

All space objects are classified by NORAD as near-Earth or deep-space. A object is classified as near-Earth if the orbit period is less then 225 min, otherwise it is classified as deep-space. Depending on the period, the NORAD element sets are automatically generated with the near-Earth or deep-space model.

Five mathematically models for prediction of satellite position and velocity are available for the two-line element set. For near-Earth objects following models can be used: SGP, SGP4 and SGP8. For deep-space objects the models SDP4 and SDP8 can be used. A detailed description of the models can be found in [Hoots 80].

At the Vienna ground station the program NOVA from Northern Light Software Associate is used for prediction of the satellite position and velocity. The input for the prediction is the NASA two-line element set. For the prediction the SGP4 model is used.

Acknowledgement

I want to express my special thanks to Prof. Werner W. Weiss from the Institute of Astronomy, who initiated and supported this project.

Also I want to thank the Austrian Space Agency for funding this project.

Thanks also to Viktor Kudielka for his valuable advice and his help during the integration phase. Also I want to thank him for frequently manning the ground station in the first phase of the ground station operation.

Further I thank Christian Praxmarer, Shkelzen Cakaj, and Peter Rieger for their valuable contributions during the integration and the early operation phase of the ground station.

I would like to take this opportunity to thank my parents and Silvia who helped me in any situation during my studies.

Bibliography

[Bohrmann 66] A. Bohrmann, *Bahnen künstlicher Satelliten*, Bibliographisches Institut AG, Mannheim, 2. Auflage, 1966

[Bgbl. FNV 03] Bundesgesetzblatt für die Republik Österreich, *457. Verordnung: Frequenznutzungsverordnung - FNV*, Teil II, 30. September 2003.

[Cakaj 04] S. Cakaj, *Vienna Satellite Ground Station*, Master Thesis, Vienna, 2004.

[Celestrak] T.S. Kelso, *CelesTrack*, Homepage for satellite tracking and satellite orbit elements, www.celestrak.com

[Dissanayake 02] A. Dissanayake, J. Allnutt, F. Haidara, *A Prediction Model that Combines Rain Attenuation and Other Propagation Impairments Along Earth-Satellite Paths*, Online Journal of Space Communication, Issue No. 2, Fall 2002.

[Eurockot 03] Eurockot, *Eurockot Press Release CD*, July 2003.

[FCC 97] Federal Communication Commission, *Millimeter Wave Propagation: Spectrum Managment Implications*, Bulletin Number 70, July 1997.

[Flagg] R. Flagg, *Determination of G/T_S*, SETI Publications Department, http://www.setileague.org/articles/g-t.htm.

[Grocott 03] S.C.G. Grocott, R.E. Zee, J. Matthews, *Exploring the Mysteries of the Cosmos on the MOST Microsatellite Mission*, 17^{th} Annual AIAA/USU Conference on Small Satellites, Logan, Utah, August 2003.

[Hoots 80] F.R. Hoots, R.L. Roehrich, *Models for Propagation of NORAD Element Sets*, Spacetrack Report No. 3, 31. December 1980.

[ITU P.618 97] International Telecommuniction Union, *ITU-R Recommondation P.618-5: Propagation data and prediction methods required for the design of Earth-space telecommunication systems*, Geneva, 1997.

[ITU P.676 97] International Telecommuniction Union, *ITU-R Recommondation P.676-3: Attenuation by atmospheric gases*, Geneva, 1997.

[ITU P.838 92] International Telecommuniction Union, *ITU-R Recommondation 838: Specific attenuation model for rain for use in prediction methods*, Geneva, 1992.

[Keim 04] W. Keim, V. Kudielka, A.L. Scholtz, *A Scientific Satellite Ground Station for an Urban Environment*, Proceedings of the IAESTED International Conference Communication Systems and Networks 2004, pp. 280-284, ACTA Press 2004, ISBN: 0-88986-450-0

[Rieger 02] P. Rieger, *Antenna Control Equipment for the "MOST" Vienna Groundstation*, Diplomarbeit, Wien, 2002.

[RTR] Rundfunk & Telekom Regulierungs-GmbH, Homepage, http://www.rtr.at

[Rothammel 03] A. Krischke, K. Rothammel, *Rothammels Antennenbuch*, DARC Verlag, 12. Auflage.

[Saunders 99] S.R. Saunders, *Antennas and Propagation for wireless communication systems*, John Wiley & Sons, LTD, 1999.

[Sklar 01] B. Sklar, *Digital Communications Fundamentals and Applications*, Prentice Hall, Inc., Second Edition, 2001.

[Stibrany 01] P. Stibrany, K.A. Caroll, *The Microsat Way in Canada*, 11^{th} CASI (Canadian Aeronautics and Space Institute) Conference on Aeronautics, November 2001.

[UBC] University of British Columbia, *The Project MOST*, Mission homepage, http://www.astro.ubc.ca/MOST

[Walker 03] G. Walker, J. Matthews et al., *The MOST Asteroseismology Mission: Ultraprecise Photometry from Space*, The Astronomical Society of the Pacific, University of Chicago, Vol. 115, No. 811, pp 1023-1035, September 2003.

[Zee 01] R.E. Zee, P. Stibrany, *Canada's First Microsatellite - An Enabling Low-Cost Technology for Future Space Science and Technology Missions*, 11^{th} CASI (Canadian Aeronautics and Space Institute) Conferene on Aeronautics, November 2001.

[Zee 02] R.E. Zee, S.C.O. Grocott, J. Matthews, *The MOST Microsatellite Mission: All Systems Go for Launch*, 12^{th} CASI (Canadian Aeronautics and Space Institute) Conference on Aeronautics, November 2002.

Curriculum Vitae

Personal

Name and Surname	Werner Keim
Address	A-2305 Eckartsau, Obere Hauptstrasse 23
Date of birth	June 26, 1974
Place of birth	Vienna, Austria
Nationality	Austria

Education

June 1993	Technical High School Wien Donaustadt, Option: Communications and Information Engineering
1994 - 2001	Dipl.-Ing. Studies, Electrical Engineering, Option: Communication Engineering
2001 - 2004	PhD Studies, Electrical Engineering

Experience

July 1990	Industrial practice Siemens AG
July 1991	Industrial practice Siemens AG
July 1992	Industrial practice Siemens AG
September 1993 - April 1994	Military service
July 2000 - August 2000	Industrial practice Siemens AG
October 2001 - September 2004	Project assistant at the Institute for Astronomy, University of Vienna